

Geological Survey of Finland

Bulletin 382

Relationship of granitoids, structures and metamorphism at the eastern margin of the Central Finland Granitoid Complex

Edited by
Pentti Hölttä

Geological Survey of Finland
Espoo 1995



Geological Survey of Finland, Bulletin 382

RELATIONSHIP OF GRANITOIDS, STRUCTURES AND
METAMORPHISM AT THE EASTERN MARGIN OF THE CENTRAL
FINLAND GRANITOID COMPLEX

Edited by
PENTTI HÖLTTÄ

with 41 figures, 13 tables and 4 appendices

GEOLOGICAL SURVEY OF FINLAND
ESPOO 1995

Hölttä, P. (ed.) 1995. Relationship of granitoids, structures and metamorphism at the eastern margin of the Central Finland Granitoid Complex. *Geological Survey of Finland, Bulletin* 382. 115 pages, 41 figures, 13 tables and 4 appendices.

This Bulletin presents a selection of articles that have been prepared in connection with the Global Geoscience Transect (GGT) project at the Geological Survey of Finland. The papers particularly emphasize on the relationship between granitoids, deformation and metamorphism.

Coarse grained orthopyroxene-bearing granitoids represent a distinctive rock type, which occur especially in the Raahe-Ladoga zone along the Archean craton margin, although they are also present to a limited extent within the Central Finland granitoid complex. They are normally undeformed, being evidently late-kinematic as regards to deformation. Most of these pyroxene granitoids are dated at ca.1885 Ma. When intruded into suitable lithologies, they have well developed granulite facies contact aureoles.

The first three papers in this volume present case studies from a pyroxene granitoid, which is located near the village of Vaaraslahti in the Pielavesi district, Central Finland. This pluton was intruded into pelitic sequence, and its thermal aureole is very well developed. Seppo Lahti describes the petrology of the intrusion, Pentti Hölttä presents data on the contact metamorphism and Ueli Haudenschild Rb-Sr and K-Ar age dating of the intrusion and its country rock. The authors have used the term pyroxene granitoid instead of charnockite for the sake of accuracy because, following the classifications of Streckeisen and LeMaitre, charnockitic igneous rocks *sensu stricto* should contain more than 5% orthopyroxene, and in these rocks the amount of orthopyroxene is commonly considerably less.

The fourth paper, by Mikko Nironen, deals with structures and granite emplacement at the boundary (shear zone) between two blocks of different metamorphic grade, that were probably also metamorphosed at different times. His study area is located close to Mikkeli in SE Finland, and includes the Sulkava complex in the east, which is characterized by turbidite sequences and well developed metamorphic zoning, and a western domain which consists mainly of granitoids, metatexites and diatexites.

Key words (GeoRef, Thesaurus AGI): granites, charnockite, granulites, mineralogy, geochemistry, contact metamorphism, deformation, structural geology, absolute age, Proterozoic, Central Finland

Pentti Hölttä, Geological Survey of Finland, FIN-02150 ESPOO, FINLAND

ISBN 951-690-603-6
ISSN 0367-522X

CONTENTS

Abbreviations.....	4
Mineralogy and geochemistry of the Vaaraslahti pyroxene granitoid in Pielavesi, Finland <i>Seppo I. Lahti</i>	5
Contact metamorphism of the Vaaraslahti pyroxene granitoid intrusion in Pielavesi, Central Finland <i>Pentti Hölttä</i>	27
The Vaaraslahti pyroxene granitoid intrusion and its contact aureole: isotope geology <i>Ueli Haudenschild</i>	81
Block boundary at the southeastern margin of the Paleoproterozoic Central Finland Granitoid Complex <i>Mikko Nironen</i>	91

ABBREVIATIONS

Abbreviations to the text by Pentti Hölttä (p. 27). Abbreviations used in the text follow the usage of Kretz (1983).

als	Al ₂ SiO ₅ mineral
and	andalusite
bt	biotite
crd	cordierite
cpx	clinopyroxene
cum	cummingtonite
diat	diatexite
ep	epidote
gph	graphite
grt	garnet
hbl	hornblende
hc	hercynite
ilm	ilmenite
kfs	potassium feldspar
ky	kyanite
ms	muscovite
opx	orthopyroxene
pl	plagioclase
po	pyrrhotite
qtz	quartz
sil	sillimanite
spl	spinel
st	staurolite
stic	stictolite
ttn	titanite

MINERALOGY AND GEOCHEMISTRY OF THE VAARASLAHTI PYROXENE GRANITOID IN PIELAVESI, FINLAND

by

SEPPO I. LAHTI

Lahti, S. I. 1995. Mineralogy and geochemistry of the Vaaraslahti pyroxene granitoid in Pielavesi, Finland. *Geological Survey of Finland, Bulletin 382*, 5–25. 10 figures and 5 tables.

The Paleoproterozoic Vaaraslahti pyroxene granitoid intrusion is situated in the Pielavesi district, Central Finland, near the Archaean - Proterozoic boundary. The stock is roughly rectangular with dimensions 3.5x2 km, and it contains xenoliths of surrounding Svecokarelian gneisses and plutonic rocks. The U/Pb age of 1.884 Ga is typical for synkinematic Svecokarelian intrusive rocks. The high emplacement temperature of the granitoid magma produced a wide thermometamorphic aureole around the stock.

Two intrusive phases have been recognized in the stock, an older quartz syenitic and a younger granitic phase with quartz syenite also present as breccia fragments of varying size in the granite. Both rock types are coarse grained and porphyritic. The main minerals are K-feldspar, oligoclase-andesine, quartz, biotite, orthopyroxene and locally hornblende. K-feldspar is usually intermediate microcline, but its structure vary largely between maximum microcline and orthoclase. Orthopyroxene, biotite and hornblende are all iron-rich varieties.

Mineralogically and geochemically the intrusion shows I-type characteristics, with an A/CNK ratio of 1.0 - 1.1, initial $^{87}\text{Sr}/^{86}\text{Sr}$ 0.7048 and $\delta^{18}\text{O}$ of 7.1, all of which are rather low. An earlier isotope geological study shows that the initial ϵ_{Nd} value of -0.6 does not deviate from values reported for other syntectonic Svecokarelian granitoids. The rocks of the Vaaraslahti intrusion, especially the quartz syenitic intrusion phase, are exceptionally enriched in iron, potassium and barium, and in this respect differs from most other Svecokarelian granitoids.

Key words (GeoRef, Thesaurus AGI): granites, pyroxene group, quartz syenite, quartz monzonite, mineralogy, geochemistry, Paleoproterozoic, Pielavesi, Central Finland

Seppo I. Lahti, Geological Survey of Finland, FIN-02150 ESPOO, FINLAND

INTRODUCTION

The Vaaraslahti porphyritic pyroxene granitoid intrusion is situated in Central Finland, about 15 km north of Pielavesi church village (Fig 1). This area is close to the boundary between Archaean and Proterozoic rocks, and lies within so called Raahe-Ladoga suture zone. The rocks around the Vaaraslahti intrusion are typical Proterozoic Svecokarelian pelitic-semipelitic schists and gneisses with volcanic rock intercalations. Irregular tonalite-granodiorite, diorite-gabbro and granite intrusions are also characteristic of the area. Granites are often porphyritic and locally orthopyroxene-bearing.

The Vaaraslahti pyroxene-bearing granitoid stock is situated in the NW part of the 3314

Pielavesi map sheet (Salli 1977), and the petrography of the rocks has been described in the accompanying explanatory notes (Salli 1983). The studies by Marttila (1976,1977, 1981) also contain detailed geological information about the region and a short petrographical outline of the pyroxene granitoids in the neighbouring Kiuruvesi district.

The tonalitic intrusions of the Pielavesi-Kiuruvesi area are often foliated and gneissose, but the pyroxene granitoids do not show any tectonic fabric. The xenoliths found in the Vaaraslahti granite indicate that it is younger than the surrounding granodiorites, tonalites, schists and gneisses. The U-Pb zircon age from the Vaaraslahti granite is 1.884 Ga (Salli

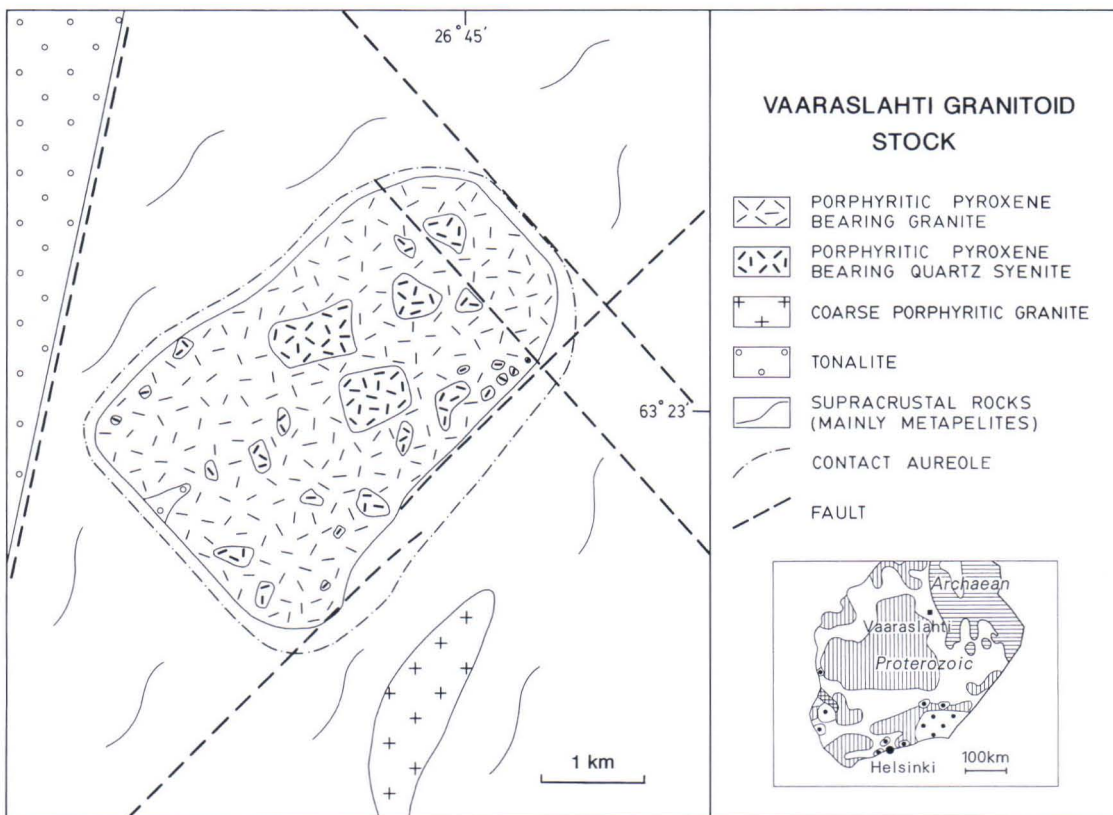


Fig. 1. Geological map of the Vaaraslahti pyroxene granitoid stock.

1983), and the rocks can be therefore classified as belonging to the synkinematic group of Svecokarelian igneous rocks.

The temperature of the pyroxene granite magma during intrusion was so high that a contact aureole developed around the stock. The grade of metamorphism of the surrounding rocks varies between amphibolite and granulite facies. Numerous faults, however, later divided the area into several blocks differing in metamorphic grade. The general tectonometamorphic evolution of the Raahe-Ladoga zone has been discussed by Korsman et al. (1984) and Korsman et al. (1988), while metamorphism in the Pielavesi area was studied by Hölttä (1988).

A U/Pb isotope study of the rocks surrounding the Vaaraslahti intrusion was published by Vaasjoki and Sakko (1988). Subsequently, Haudenschild (1995) studied the Rb-Sr, K-Ar and oxygen isotope chemistry of the rocks and discussed the cooling history of the intrusion.

The larger quartz syenitic fragments are clearly discernible on the aeromagnetic low-altitude maps, because the magnetic susceptibility of the quartz syenite ($1000-8000 \times 10^{-6}$ SI units) is usually much higher than that of granite ($100-800 \times 10^{-6}$ SI units). The magnetic anomalies form angular patterns on the aeromagnetic maps, reflecting the breccia structure of the intrusion. Both rock types show exceptionally low susceptibility values in the northern part of the stock, which indicates that the magnetite content of the quartz syenite is higher in the southern part, as a result of variation in crystallization conditions within the intrusion.

GENERAL DESCRIPTION OF THE GRANITOID STOCK

The Vaaraslahti granitoid intrusion is a rectangular stock measuring 3.5 km x 2 km. The SW and SE contacts between the intrusion and the surrounding gneisses are exposed; elsewhere, the margin of the stock is obscured by erosional valleys and filled with glacial overburden. These valleys follow linear NW-SE and NE-SW trending fractures, which are characteristic of the region. Because the granitic rocks have been more resistant to erosion than the schists, the stock tends to form hilly terrain and represents an elevated area in the local topography.

The low-altitude airborne magnetic maps produced by the Geological Survey of Finland (total intensity, sheet 3314 09 Tommonmäki and 3314 08 Vaaraslahti, scale 1: 20 000) indicate internal heterogeneity within the Vaaraslahti granitoid stock, reflected by slightly magnetic and less-magnetic varieties. Detailed field studies and mapping of these rock types, sampling, petrographical studies, chemical analyses and petrophysical measurements of the rocks have confirmed the composite nature of the intrusion.

The stock is mainly composed of coarse-grained granite, which brecciates the older quartz syenitic - monzonitic phase. These two main rock types nevertheless often closely resemble each other in mineralogy and fabric so that their recognition in the field may be difficult.

The most significant differences is that the granitic varieties are richer in quartz and often slightly coarser in grain size than the syenitic ones. The quartz syenite-monzonite fragments are randomly distributed throughout the whole stock. Their size generally varies from several square metres to several hectares, but several larger homogeneous quartz syenite areas are also present. The contact between the granite and the syenite is usually sharp, as indicated in Fig. 2.

Both granite and quartz syenite contain small amounts of xenoliths; most typically these are roundish fragments of mica schist and various gneisses; medium-grained enclaves of tonalite or granodiorite are also present (Fig. 3). The

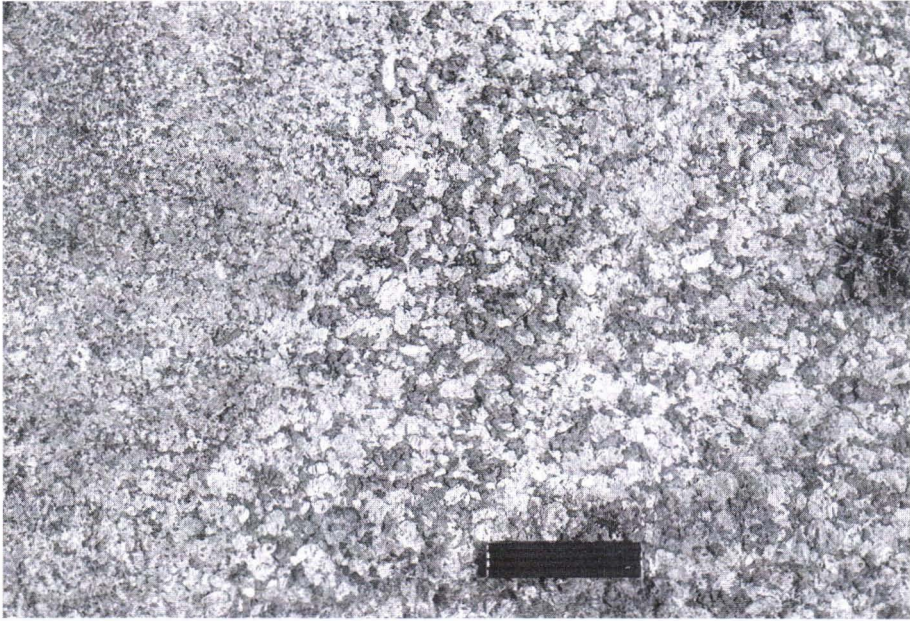


Fig. 2. Contact between a coarse-grained orthopyroxene-bearing granite (at right) and quartz monzonitic enclave at the hill Särkimäki, near the SE contact of the Vaaraslahti intrusion. Scale bar is 10 cm long.



Fig. 3. Small roundish tonalite xenolith in a granite to the north of the central part of the intrusion (north of Honkavuori). The length of the xenolith is about 10 cm.

xenoliths and enclaves are most common near the contacts of the intrusion, but rare in the middle of the stock. Most of them are very small, several centimetres or occasionally some decimetres in diameter and are sparsely distributed throughout the rock. Near the south-western contact of the intrusion, between the hills Pirttilänvuori and Hirvivuori there is large tonalite fragment at least several tens of square meters in extent, although its exact size and contact relations have not been fully established. Large schist xenoliths are also present along the SE contact of the intrusion between the hills Honkavaara and Yijäkönmäki.

Distinctive fine-grained black graphite-bearing inclusions, five to fifteen centimetres long and composed mainly of normal granitic minerals are locally abundant, and they occur in both the granitic and quartz syenitic varieties. The carbon isotope composition of one such graphite accumulation (containing 3.7% carbon) taken from the northern part of the stock gave a $\delta^{13}\text{C}$ value of 23‰ (PDB), which does not deviate markedly from the mean isotopic composition of organic carbon in sedimentary rocks. This indicates that the graphite-bearing inclusions are restitic after almost totally remelted graphite-bearing schist inclusions.

CLASSIFICATION OF GRANITOID TYPES

The rocks comprising the Vaaraslahti intrusion are so coarse-grained that point counting of minerals in thin section does not give statistically reliable modal compositions. Therefore, rock names were defined using the Q'-ANOR classification based on normative mineral abundances computed from the total rock analyses (see Streckeisen & Le Maitre 1979). The CIPW weight norms were computed from X-ray fluorescence analyses of the rocks and plotted on the Q'-ANOR classification diagram (Fig. 4). The total iron from the X-ray

fluorescence data was divided before the norm computation into FeO and Fe_2O_3 using the equation given for plutonic rocks by LeMaitre (1976). As Fig. 4 indicates, the data plot in four compositional fields: syenogranite, monzogranite, quartz syenite and quartz monzonite. The data points are not randomly scattered, but form two clearly defined groups. The term quartz syenite is used in this study for rocks that plot in both the quartz syenite and quartz monzonite fields.

PETROGRAPHY AND MINERALOGY OF THE GRANITOIDS

Fresh rock surface is greenish or gray, but weathered surface of both the granite and the quartz syenite is brown. The outcrops are locally, especially on the lee side of hills, covered by a soft preglacial saprolite (grus) layer, which may be several decimetres thick. The soft weathered rock contains large potassium feldspar crystal fragments embedded in clay mineral-bearing sandy or silty matrix (Lahti 1985). Tors and separate strongly weathered boulders are also common.

The two main rock types are coarse-grained

and often slightly porphyritic. The quartz and plagioclase grains in the groundmass are 1-5 mm in diameter, but the K-feldspar phenocrysts are larger, 1-3 cm in length. Coarser varieties with less-developed porphyritic texture are known from the northeastern corner of the intrusion. Only one thin granite pegmatite dyke, which is very simple in mineralogy, was found to cut the coarse biotite granite in the northeastern part of the intrusion (at the hill Yijäkönmäki).

There are only slight mineralogical differ-

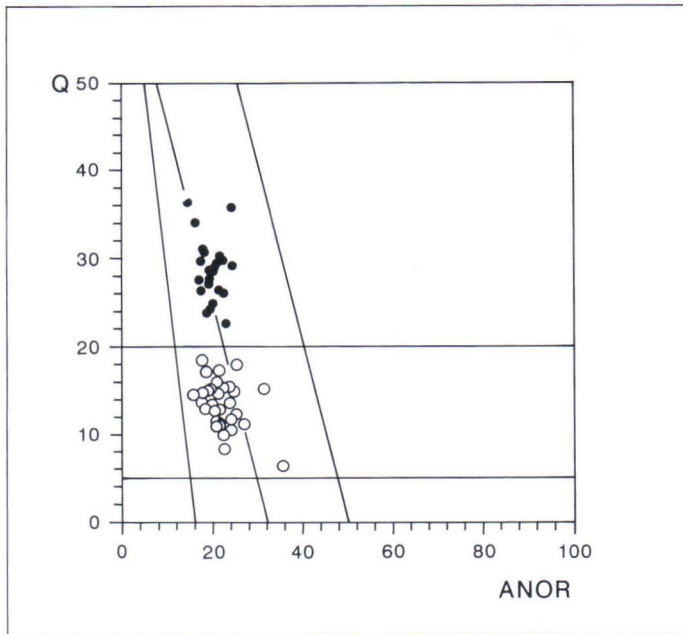


Fig. 4. Q'-ANOR classification of the rocks from the Vaaraslahti intrusion. A data plot in the monzogranite - syenogranite field (dots) and quartz syenite - quartz monzonite field (circles).

ences between the granite and the quartz syenite. The main minerals in the quartz syenite are K-feldspar, plagioclase, quartz, biotite, orthopyroxene, and locally hornblende. The granite is similar in mineralogy except it is richer in quartz and contains less mafic constituents and potassium feldspar than the quartz syenite. Myrmekitic quartz-alkali feldspar textures are typical in the granite, but not in the quartz syenite (Fig. 5).

The rocks usually contain both biotite and orthopyroxene as major mafic constituents. The amount of orthopyroxene is always less than that of biotite and biotite is the only mafic mineral in some varieties of granite. Minute amounts of hornblende may occur as an alteration product after orthopyroxene. For example, coarse biotite granite is dominant in the eastern corner of the intrusion at Yijäkönmäki. Altered orthopyroxene is brown, and

therefore easy to observe on the rock surface.

K-feldspar is translucent, and greenish or greyish in colour. It mainly occurs as phenocrysts 1-3 cm in length. Thin section and X-ray diffraction studies show that the mineral is usually cryptoperthitic or microperthitic intermediate microcline (Fig. 6). Tartan-twinned domains are characteristic in the K-feldspar phenocrysts especially in quartz- and biotite-rich granite varieties in which orthopyroxene is rare or absent. Zoned microcline crystals are common. Small myrmekitic alkali-feldspar quartz grains of later generation are typical between the K-feldspar phenocrysts in the granites.

Microprobe analyses of the K-feldspars are given in Table 1. Chemical analyses show that K-feldspar is exceptionally enriched in barium. The Ba concentration of the K-feldspar increases sympathetically with increasing Ba

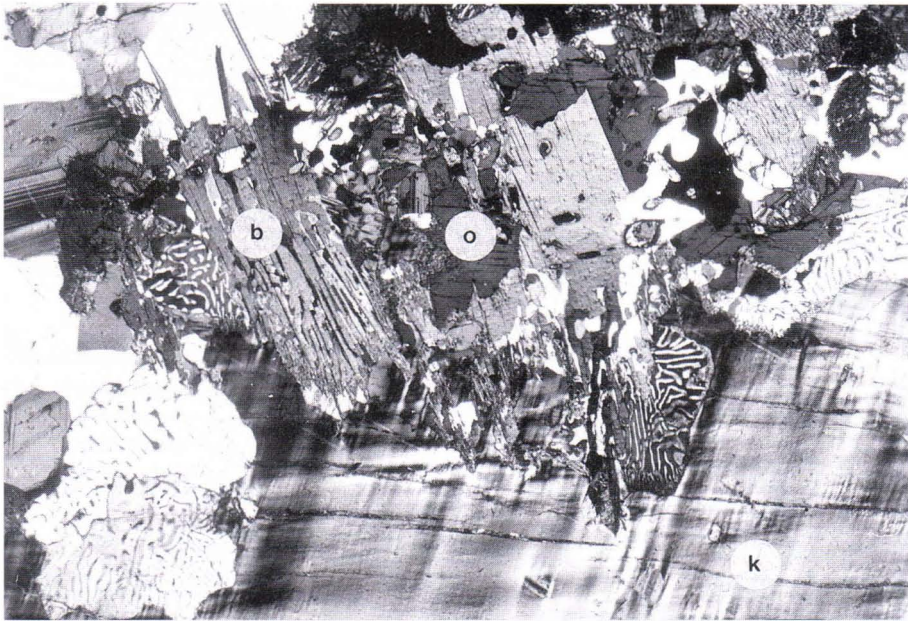


Fig. 5. Photomicrograph of porphyritic pyroxene-bearing granite. K-feldspar phenocrysts (lower right) often show tartan twinned domains (k). Myrmekitic texture is common at rims of the feldspar crystals. Orthopyroxene (o) occurs typically inside the biotite (b) aggregates. Biotite and quartz may also occur as myrmekite-like intergrowths (left of middle).

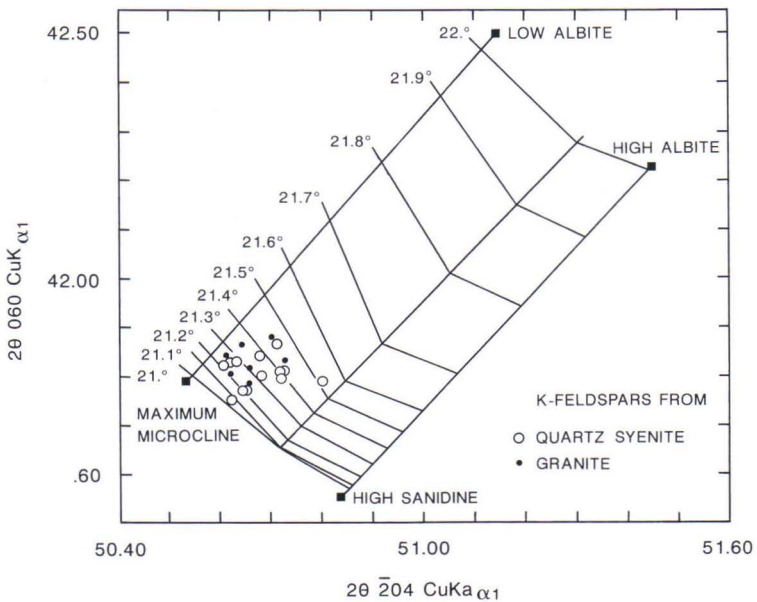


Fig. 6. The structural state of alkali feldspar from quartz syenite and granite samples. The $2\theta_{060}$ and $2\theta_{204}$ reflections ($\text{CuK}\alpha_1$ -peaks) were measured from the X-ray powder diffractograms and plotted on the diagram of Wright (1968).

Table 1. Microprobe analyses from K-feldspar and plagioclase samples. Successive K-feldspar and plagioclase analyses are from the neighbouring crystals. Chemical analyses by Bo Johanson. Jeol Superprobe 733 and natural mineral standards were used in the determinations.

	1	2	3	4	5	6	7	8	9	10	11	12	13	14	15	16
SiO ₂	64.15	60.08	63.22	57.38	65.44	57.27	64.31	58.94	63.58	60.43	65.16	61.15	65.18	60.74	65.83	61.72
TiO ₂	0.00	0.01	0.01	0.00	0.03	0.01	0.04	0.00	0.03	0.00	0.00	0.00	0.02	0.01	0.00	0.00
Al ₂ O ₃	18.09	23.99	18.01	25.09	18.37	24.75	18.38	24.80	17.90	24.84	17.97	23.88	18.28	24.51	18.53	24.11
FeOtot.	0.00	0.05	0.02	0.03	0.00	0.05	0.00	0.04	0.02	0.01	0.00	0.04	0.01	0.07	0.03	0.06
K ₂ O	14.49	0.40	14.17	0.25	13.51	0.24	12.39	0.35	13.78	0.29	13.23	0.39	14.23	0.35	12.94	0.24
Na ₂ O	1.38	8.18	1.68	7.24	1.92	7.38	2.55	7.33	1.64	8.25	1.79	8.02	1.54	7.85	2.54	8.29
CaO	0.03	5.82	0.03	7.45	0.05	7.27	0.20	7.09	0.02	6.27	0.02	5.56	0.06	6.30	0.09	5.74
BaO	0.25	0.04	0.55	0.08	0.49	0.04	0.62	0.00	0.50	0.00	0.16	0.02	0.40	0.01	0.22	0.00
Sum	98.40	98.57	97.68	97.53	99.80	97.01	98.49	98.55	97.48	100.09	98.34	99.08	99.71	99.83	100.17	100.16

atoms based on 8 oxygens/ formula

Si	3.00	2.71	2.99	2.63	3.01	2.64	3.00	2.67	3.00	2.69	3.03	2.74	3.00	2.71	3.01	2.74
Ti	0.00	0.00	0.00	0.00	0.00	0.00	0.00	0.00	0.00	0.00	0.00	0.00	0.00	0.00	0.00	0.00
Al	1.00	1.28	1.00	1.36	1.00	1.35	1.01	1.32	1.00	1.30	0.98	1.26	0.99	1.28	1.00	1.26
Fe	0.00	0.00	0.00	0.00	0.00	0.00	0.00	0.00	0.00	0.00	0.00	0.00	0.00	0.00	0.00	0.00
K	0.87	0.02	0.66	0.01	0.79	0.01	0.74	0.02	0.84	0.02	0.78	0.02	0.84	0.02	0.75	0.01
Na	0.12	0.72	0.16	0.64	0.17	0.66	0.23	0.64	0.15	0.71	0.16	0.70	0.14	0.68	0.22	0.71
Ca	0.00	0.28	0.00	0.37	0.00	0.35	0.01	0.34	0.00	0.30	0.00	0.27	0.00	0.30	0.00	0.27
Ba	0.00	0.00	0.00	0.00	0.01	0.00	0.01	0.00	0.01	0.00	0.00	0.00	0.01	0.00	0.00	0.00

1 = K-feldspar, 374-SIL-85, in quartz syenite
 2 = Plagioclase, 374-SIL-85, in quartz syenite
 3 = K-feldspar, 451-SIL-85, in quartz syenite
 4 = Plagioclase, 451-SIL-85, in quartz syenite
 5 = K-feldspar, 455-SIL-85, in quartz syenite
 6 = Plagioclase, 455-SIL-85, in quartz syenite
 7 = K-feldspar, 471-SIL-85, in quartz syenite
 8 = Plagioclase, 471-SIL-85, in quartz syenite

9 = K-feldspar, 615-SIL-83, in quartz monzonite
 10 = Plagioclase, 615-SIL-83, in quartz monzonite
 11 = K-feldspar, 462-SIL-85, in granite
 12 = Plagioclase, 462-SIL-85, in granite
 13 = K-feldspar, 464-SIL-85, in granite
 14 = Plagioclase, 464-SIL-85, in granite
 15 = K-feldspar, 465-SIL-85, in granite
 16 = Plagioclase, 465-SIL-85, in granite

in the whole rock. The K-feldspar samples derived from the quartz syenites usually contain 0.4 - 0.6 wt% BaO, whereas the concentrations are slightly lower in feldspars from the granitic rocks.

Plagioclase is dark grey in colour. Microprobe analyses indicate that the composition varies from oligoclase to andesine (Table 1 and Table 5). Granitic varieties always contain oligoclase with an anorthite content between 25 and 30 mol.%, whereas in the quartz syenitic parts the anorthite content varies between 25 and 37 mol.%. The crystals are often zoned and the compositional variation may be substantial even within a single crystal. Thin section studies show that the crystal laths are often curved.

Quartz is grey or bluish, and usually occurs as large anhedral crystals between the feldspars. In some varieties the crystals are broken, and undulating extinction shows that the grains have been strained.

Biotite flaky aggregates occur between the feldspar and quartz crystals. Myrmekite-like intergrowths between biotite and quartz are locally common. The mineral is dark brown in thin section. Microprobe analyses indicate that the mineral is always rich in iron and poor in octahedral aluminium, thus corresponding to a very annite rich variety. Some representative microprobe analyses are given in Table 2. The Mg/Fe+Mg ratio of biotite is between 0.15 and 0.35, and the iron content of the biotite increases as Fe in the whole rock

increases.

Orthopyroxene occurs as subhedral to anhedral prismatic crystals or crystal aggregates, commonly associated with biotite or hornblende. In thin section the mineral is light brown with a violet tint and is strongly pleochroic. The results of the microprobe analyses show that the mineral is rich in iron (Table 3), having 70-80 mol.% ferrosilite in the granites and 78-83 mol.% in the syenites. Green hornblende often occurs as an alteration product around orthopyroxene crystal laths.

Dark green hornblende is a major ferromagnesian mineral in some granite varieties. It occurs as separate crystals often associated with biotite flakes or as an alteration product after orthopyroxene. Chemical analyses indicate that the mineral is rich in iron, and corresponds to ferroedenite in composition (Table 3).

Accessory minerals identified during mineral separation and microscopic studies include: ilmenite, magnetite, zircon, monazite, apatite, garnet, anatase, pyrite, molybdenite, and chalcopyrite. Zircon occurs as long, prismatic needles with well-developed pyramidal surfaces. The crystals may contain small biotite inclusions. Small garnet crystals were observed in granite types rich in schist xenoliths. Anatase seems to be an alteration product and replaces ilmenite. The heavy mineral concentrates are mainly composed of ilmenite and magnetite, with sulfide minerals being relatively rare.

GEOCHEMISTRY

About sixty rock samples from various parts of the intrusion were analysed for major elements and some rare elements using diamond drill core samples. A Minidrill diamond drill was used for sampling, and core samples were

usually about 30 cm long. Samples selected for chemical analyses were as fresh as possible, and strongly weathered samples were rejected. About 0.5 to 1.0 kg of core material were crushed on average for each analysis.

Table 2. Microprobe analyses for biotite from various rock types of the Vaaraslahti intrusion. n.d. = not determined. Chemical analyses by Bo Johanson. Jeol Superprobe 733 and natural mineral standards were used in the determinations.

	1	2	3	4	5	6	7
SiO ₂	34.73	33.03	34.97	34.62	35.57	35.75	35.87
TiO ₂	4.41	4.22	4.71	4.34	4.42	4.35	4.37
Al ₂ O ₃	14.28	13.75	13.88	14.55	14.17	14.10	13.84
Cr ₂ O ₃	0.01	0.01	0.02	n.d.	0.04	0.04	0.02
V ₂ O ₃	0.02	0.08	0.11	0.09	0.07	0.04	0.07
FeOtot.	31.08	30.19	30.18	30.08	27.63	27.25	26.41
MnO	0.14	0.12	0.17	0.14	0.11	0.09	0.11
MgO	3.57	3.54	3.76	4.01	5.63	6.12	6.74
CaO	0.01	0.00	0.04	0.05	0.01	0.03	0.01
BaO	0.22	n.d.	n.d.	n.d.	n.d.	0.17	0.12
K ₂ O	8.90	8.46	8.65	8.72	9.17	8.95	9.22
Na ₂ O	0.14	0.02	0.09	0.09	0.12	0.52	0.07
Sum	97.51	93.41	96.58	96.70	96.93	97.41	96.85
atoms / formula based on 22 oxygens							
Si	5.51	5.46	5.56	5.49	5.56	5.56	5.59
Al(4)	2.48	2.53	2.43	2.50	2.43	2.43	2.40
Al(6)	0.18	0.15	0.16	0.21	0.18	0.15	0.13
Ti	0.52	0.52	0.56	0.51	0.52	0.50	0.51
Cr	0.00	0.00	0.00	n.d.	0.00	0.00	0.00
V	0.00	0.01	0.01	0.01	0.00	0.00	0.00
Fe	4.12	4.18	4.01	3.99	3.61	3.54	3.44
Mn	0.01	0.01	0.02	0.01	0.01	0.01	0.01
Mg	0.84	0.87	0.89	0.94	1.31	1.42	1.56
Ca	0.00	0.00	0.00	0.00	0.00	0.00	0.00
Ba	0.02	n.d.	n.d.	n.d.	n.d.	0.02	0.01
ΣY	5.72	5.76	5.68	5.72	5.66	5.68	5.70
K	1.80	1.78	1.75	1.76	1.83	1.77	1.83
Na	0.04	0.00	0.02	0.02	0.03	0.15	0.02
ΣX	1.84	1.79	1.78	1.79	1.87	1.93	1.86
Fe/Fe+Mg	0.83	0.83	0.82	0.81	0.73	0.71	0.69

1 = Biotite, 615-SIL-83, in quartz monzonite

2 = Biotite, 451-SIL-85, in quartz syenite

3 = Biotite, 458-SIL-85, in quartz syenite

4 = Biotite, 470-SIL-85, in quartz monzonite

5 = Biotite, 465-SIL-85, in granite

6 = Biotite, 645-SIL-83, in granite

7 = Biotite, 641-SIL-83, in granite

Table 3. Microprobe analyses for orthopyroxene and hornblende from various rock types of the Vaaraslahti stock. Chemical analyses by Bo Johanson. Jeol Superprobe 733 and natural mineral standards were used in the determinations.

	1	2	3	4	5	6	7	8	9	10	11	12
SiO ₂	49.15	47.67	48.84	48.09	48.79	47.91	47.96	48.50	42.01	40.89	41.35	40.97
TiO ₂	0.19	0.16	0.13	0.19	0.13	0.17	0.10	0.20	1.72	1.11	2.08	1.14
Al ₂ O ₃	0.59	1.38	0.57	0.46	0.41	0.53	0.00	0.45	10.08	11.51	9.95	10.41
Cr ₂ O ₃	0.01	n.d.	0.00	n.d.	0.01	0.01	0.03	0.01	0.00	0.00	0.03	n.d.
V ₂ O ₃	0.05	0.03	0.02	n.d.	0.03	0.05	0.02	0.05	0.02	0.05	0.09	n.d.
FeOtot.	40.16	40.32	42.54	43.60	44.73	45.12	45.32	44.94	29.35	28.01	27.49	27.00
MnO	0.58	0.66	0.93	0.82	0.95	0.96	0.93	1.00	0.29	0.33	0.24	0.15
MgO	9.11	7.39	7.70	5.52	5.45	5.49	5.28	5.16	2.94	2.99	3.50	3.82
BaO	n.d.	n.d.	0.02	n.d.	0.01	0.00	0.02	0.00	0.00	0.03	0.07	n.d.
CaO	0.91	0.35	0.50	0.95	1.09	0.90	0.77	1.04	9.82	10.24	10.07	10.44
Na ₂ O	0.05	0.02	0.01	0.05	0.03	0.04	0.10	0.06	1.62	1.62	1.87	1.63
K ₂ O	0.00	0.02	0.01	0.01	0.01	0.01	0.03	0.00	1.10	1.38	1.44	1.19
Sum	100.82	97.99	101.27	99.70	101.64	101.19	100.87	101.41	98.95	98.16	98.18	96.75

atoms / formula based on 6 oxygens in orthopyroxene and 23 oxygens in hornblende

Si	1.98	1.98	1.98	2.00	2.00	1.98	1.99	2.00	6.59	6.46	6.53	6.54
Al(4)	0.01	0.01	0.01	0.00	0.00	0.01	0.00	0.00	1.40	1.53	1.46	1.45
Al(6)	0.01	0.05	0.01	0.03	0.02	0.01	0.01	0.02	0.46	0.61	0.39	0.50
Ti	0.00	0.00	0.00	0.00	0.00	0.00	0.00	0.00	0.20	0.13	0.24	0.13
Cr	0.00	n.d.	0.00	n.d.	0.00	0.00	0.00	0.00	0.00	0.00	0.00	n.d.
V	0.00	0.00	0.00	n.d.	0.00	0.00	0.00	0.00	0.00	0.00	0.01	n.d.
Fe	1.35	1.40	1.44	1.52	1.53	1.56	1.57	1.55	3.85	3.70	3.63	3.60
Mn	0.02	0.02	0.03	0.02	0.03	0.03	0.03	0.03	0.03	0.04	0.03	0.02
Mg	0.54	0.45	0.46	0.34	0.33	0.33	0.32	0.31	0.68	0.70	0.82	0.90
Ba	n.d.	n.d.	0.00	n.d.	0.00	0.00	0.00	0.00	0.00	0.00	0.00	n.d.
Ca	0.03	0.01	0.02	0.04	0.04	0.03	0.03	0.04	1.65	1.73	1.70	1.78
Na	0.00	0.00	0.00	0.00	0.00	0.00	0.00	0.00	0.49	0.49	0.57	0.50
K	0.00	0.00	0.00	0.00	0.00	0.00	0.00	0.00	0.22	0.27	0.29	0.24
Fe/Fe+Mg	0.71	0.75	0.75	0.81	0.82	0.82	0.82	0.83	0.84	0.84	0.81	0.79

- 1 = Orthopyroxene, 464-SIL-85, in granite
 2 = Orthopyroxene, 462-SIL-85, in granite
 3 = Orthopyroxene, 641-SIL-83, in granite
 4 = Orthopyroxene, 455-SIL-85, in quartz syenite
 5 = Orthopyroxene, 615-SIL-83, in quartz monzonite
 6 = Orthopyroxene, 637A-SIL-83, in quartz syenite
 7 = Orthopyroxene, 637A-SIL-83, in quartz syenite
 8 = Orthopyroxene, 615-SIL-83, in quartz monzonite
 9 = Hornblende, 615-SIL-83, in quartz monzonite
 10 = Hornblende, 615-SIL-83, in quartz monzonite
 11 = Hornblende, 616-SIL-83, in quartz syenite
 12 = Hornblende, 456-SIL-85, in granite

Major elements

Representative chemical analyses from the various rock types of the intrusion (22 analyses) are given in Table 4. Figure 6 shows variation diagrams for the major elements. The quartz syenites and granites form two homogeneous groups, which are separated by a SiO₂ compositional gap from 66 to 69 weight %. The SiO₂ content of the quartz syenites and monzonites varies between 62 and 66 weight % and that of the granite between 69 and 74 weight %.

In addition to this bimodal distribution of analytical points with respect to SiO₂ content, major element data form a distinct trend decreasing towards the granitic end-member compositions (Fig. 7). The scatter of data is slight-

ly less in the quartz syenite group than in the granite group. The concentration of K and Fe in both the main rock types is exceptionally high. The mean concentrations of K, Ca, Na, Fe and Mn are higher in the quartz syenite, because it contains more feldspars and mafic minerals than the granite. In addition, plagioclase from the quartz syenite has a higher anorthite component, and all mafic minerals (biotite, orthopyroxene and hornblende) analysed from quartz syenites show higher concentrations of iron than those from the granites. The concentrations of Mg and Ti are low (often below 0.5 %), and do not show any remarkable variations.

Minor elements Ba, Sr, Rb, Sc and Zr

X-ray fluorescence analyses of some minor elements of the rocks are given in Table 4 and variation diagrams for Ba, Rb, Sr and Zr in Fig. 8. The chemical analyses indicate that Ba, Sr, Sc and Zr are enriched in quartz syenites, whereas Rb shows nearly similar contents in both granites and quartz syenites, or else is marginally concentrated in granites. Sr values are close to the detection limit in the granite.

The chemical analyses show that the contents of trace elements do not differ significantly from those given previously by Nurmi

(1984) for the various Svecokarelian granitoids. An exception is, however, barium, which seems to be highly enriched in the pyroxene-bearing granitoids. The range of Ba is between 600 and 1600 ppm in the granites and between 1600 and 3400 in the quartz syenites. Ba is almost totally incorporated in K-feldspar and the highest contents are in K-feldspar samples derived from the quartz syenites. Microprobe determinations indicate that K-feldspar has 0.2 - 0.6 wt% Ba, whereas the concentrations of this element are below 0.01 wt% in other minerals.

Rare earth elements

Thirteen quartz syenite and six granite samples were studied and the rare earth elements were found to be preferentially concentrated in the youngest granitic differentiates of the intrusion. A sum of rare earths (9 analysed elements) is between 100 and 200 in quartz syenites and 200 and 500 ppm in granites. The diagram showing the sum of REE:s plotted

against SiO₂ is given in Fig. 9 (lower right part). The data cluster within a restricted area for the quartz syenites, whereas those for granite samples are widely scattered.

The rare earth distribution spectrum for both granite and quartz syenite is given in the upper part of Fig. 9. The curves show the limits of REE variations in the samples stud-

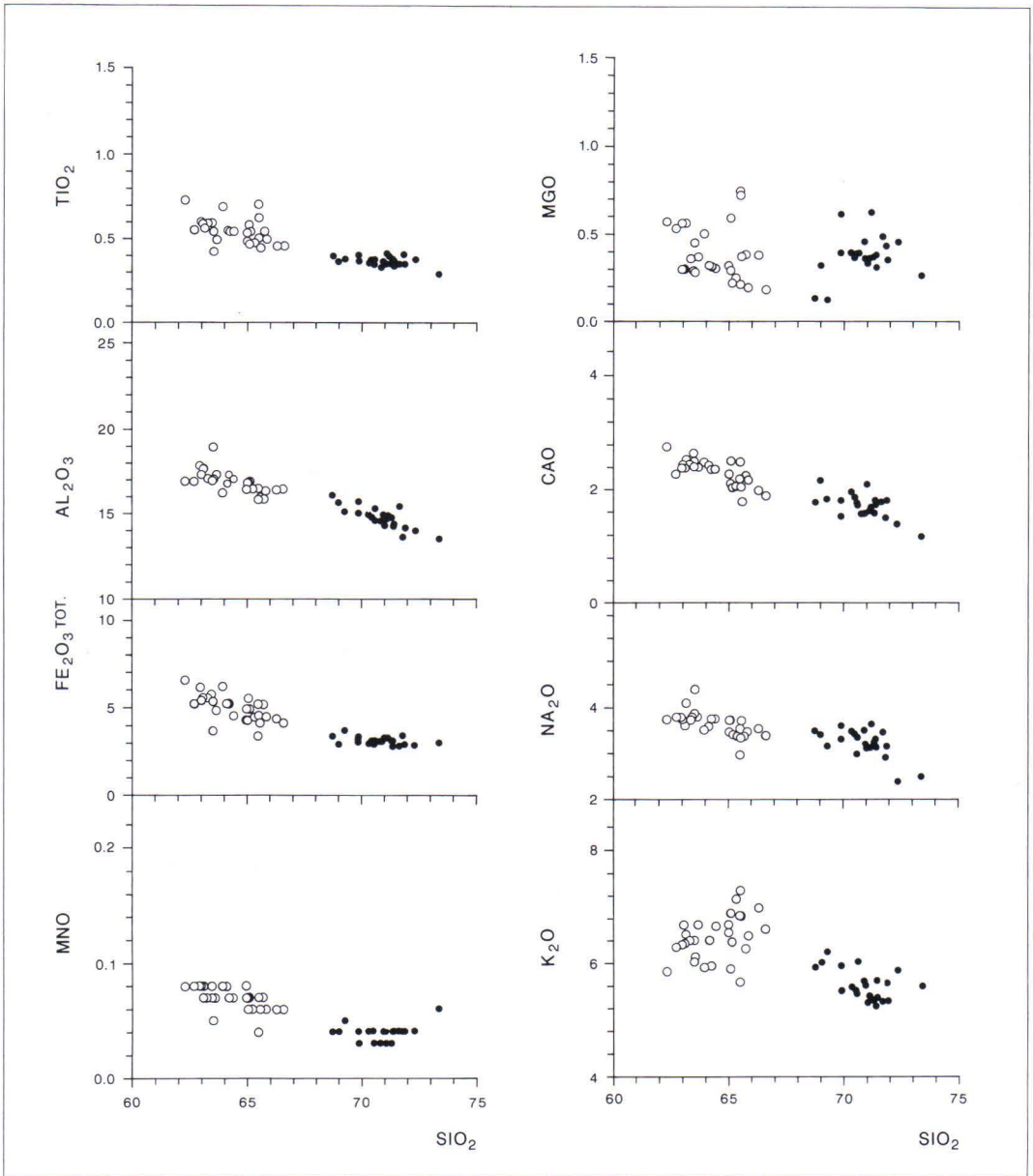


Fig. 7. Variation diagrams for major elements from the Vaaraslahti intrusion. X-ray fluorescence analyses; see Table 4. Circles mark quartz syenites, dots mark granites.

ied. The curve for granite is steeper and shows more variation than that for quartz syenite. The CeN/YbN ratio, which indicates fractionation between heavy and light REE's, is 5-10 in the quartz syenites and 15-40 in the gran-

ites (Fig. 9, lower right part). Moreover, the REE distribution curve for quartz syenite has europium maximum, whereas for the granites the curve has a Eu minimum.

Table 4. Representative analyses of various rock types in the Vaaraslahti intrusion. X-ray fluorescence analyses determined at the Geochemical Laboratory of the Rautaruukki Company. Note: n.d. = element not determined.

	1	2	3	4	5	6	7	8	9	10	11
SiO ₂	63.46	65.50	62.30	63.93	63.52	66.59	65.14	64.23	63.10	62.70	65.57
TiO ₂	0.59	0.62	0.73	0.69	0.42	0.45	0.54	0.54	0.59	0.55	0.44
Al ₂ O ₃	16.94	15.84	16.94	16.21	18.96	16.47	16.94	17.31	17.64	16.92	15.95
Fe ₂ O ₃ tot.	5.73	5.19	6.55	6.18	3.70	4.12	4.90	5.22	5.55	5.20	4.13
MnO	0.08	0.07	0.57	0.50	0.28	0.18	0.22	0.31	0.30	0.53	0.37
CaO	2.66	2.49	2.77	2.50	2.52	1.88	2.02	2.36	2.39	2.28	1.78
Na ₂ O	3.44	3.23	3.308	0.08	0.05	0.06	0.07	0.07	0.07	0.08	0.06
MgO	0.29	0.72	0.9	3.20	3.91	3.09	3.12	3.39	3.27	3.43	3.36
K ₂ O	6.02	5.65	5.85	5.92	6.11	6.59	6.36	5.94	6.35	6.28	6.82
P ₂ O ₅	0.00	0.00	0.00	0.00	0.11	0.11	0.17	0.18	0.19	0.17	0.07
Sum	99.21	99.31	99.18	99.21	99.58	99.54	99.48	99.55	99.45	98.14	98.55
Ba	2590	1620	2490	2510	1860	2140	3050	2530	2880	3370	2150
Sr	140	160	150	140	150	120	140	140	150	190	240
Zr	800	410	800	800	580	630	700	680	790	540	450
Rb	108	113	106	97	127	111	95	81	96	140	190
Sc	23	16	33	24	11	21	21	19	19	19	19
Th	3	12	10	16	5	4	2	3	1	2	5
Co	44	46	36	33	8	5	6	7	6	12	14
Cr	n.d.	146	n.d.	134	n.d.	111	75	112	105	20	20
W	236	213	174	166	22	3	4	4	3	62	82

1 = Quartz monzonite, 15-SIL-86, x= 7032.10, y= 3487.20

2 = Quartz monzonite, 22-SIL-86, x= 7030.00, y= 3486.50

3 = Quartz monzonite, 453-SIL-85, x= 7032.60, y= 3487.30

4 = Quartz monzonite, 468-SIL-85, x= 7031.70, y= 3486.38

5 = Quartz syenite, 374-SIL-85, x= 7031.52, y= 3487.82

6 = Quartz syenite, 377-SIL-85, x= 7029.78, y= 3486.00

7 = Quartz syenite, 382-SIL-85, x= 7031.26, y= 3486.93

8 = Quartz syenite, 384-SIL-85, x= 7031.97, y= 3486.30

9 = Quartz syenite, 380-SIL-85, x= 7031.72, y= 3486.10

10 = Quartz syenite, 636A-SIL-83, x= 7031.10, y= 3486.15

11 = Quartz syenite, 616B-SIL-83, x= 7030.00, y= 3486.05

THERMOMETRY AND BAROMETRY

Two-feldspar geothermometry was applied in estimating crystallization temperature of the intrusion, and calculated using the feldspar analyses and the equation given by Haselton et al. (1983). The two-feldspar thermometer of Haselton et al. (1983) gives highly variable crystallization temperatures from 540° C to 780°C, where the lowest temperatu-

res evidently represent cooling. The pressures obtained using the experimental aluminium-hornblende barometer of Johnson & Rutherford (1989) are 3.9 - 5.3 kbars, and in one aluminous hornblende 5.1 - 6.1 kbars. The empirical hornblende barometers of Hollister et al. (1987) and Hammarstrom & Zen (1986) give pressures which are 1 - 1.7 kbars higher

Table 4 cont.

	12	13	14	15	16	17	18	19	20	21	22
SiO ₂	63.14	66.29	70.56	71.00	70.48	71.36	71.10	71.17	71.66	68.74	69.87
TiO ₂	0.56	0.45	0.34	0.34	0.36	0.37	0.40	0.38	0.34	0.39	0.39
Al ₂ O ₃	17.71	16.42	15.25	14.30	14.76	14.24	14.67	14.80	15.38	16.05	15.70
Fe ₂ O ₃ tot	5.53	4.36	2.87	3.22	3.07	3.09	3.19	3.19	2.77	3.36	3.20
MnO	0.08	0.06	0.03	0.04	0.04	0.04	0.03	0.00	0.04	0.04	0.03
CaO	0.56	0.38	0.38	0.33	0.37	0.37	0.36	0.62	0.48	0.13	0.61
Na ₂ O	2.56	1.98	1.70	2.08	1.84	1.79	1.60	1.68	1.76	1.77	1.51
MgO	3.67	3.22	3.05	2.87	3.10	3.02	2.88	3.28	3.13	3.17	0.26
K ₂ O	6.51	6.97	5.42	5.28	5.49	5.21	5.38	5.31	5.29	5.90	5.48
P ₂ O ₅	0.16	0.09	0.10	0.00	0.00	0.00	0.11	0.11	0.08	0.10	0.08
Sum	100.48	100.22	99.70	99.46	99.51	99.49	99.72	100.54	100.93	99.65	100.13
Ba	3110	2270	927	1240	2730	1110	1070	989	1010	1380	1220
Sr	210	150	110	110	110	100	100	120	180	100	150
Zr	530	450	240	290	280	300	250	190	170	510	210
Rb	90	111	135	n.d.	101	120	127	140	110	118	130
Sc	18	18	8	n.d.	23	9	10	12	8	8	8
Th	3	4	14	n.d.	2	4	8	16	20	14	23
Co	14	19	7	n.d.	33	42	10	18	17	6	19
Cr	19	12	151	170	n.d.	151	n.d.	18	23	n.d.	17
W	76	96	3	n.d.	157	221	34	122	103	23	110

12 = Quartz syenite, 637A-SIL-83, x= 7031.25, y= 3486.20

13 = Quartz syenite, 616-SIL-83, x= 7030.00, y= 3486.05

14 = Monzogranite, 383-SIL-85, x= 7032.16, y= 3486.24

15 = Monzogranite, 469-SIL-85, x= 7031.74, y= 3485.95

16 = Monzogranite, 462-SIL-85, x= 7032.10, y= 3486.28

17 = Monzogranite, 465-SIL-85, x= 7032.10, y= 3486.28

18 = Monzogranite, 372-SIL-85, x= 7031.33, y= 3476.80

19 = Monzogranite, 643A-SIL-83, x= 7031.60, y= 3488.05

20 = Monzogranite, 645-SIL-83, x= 7032.05, y= 3486.90

21 = Syenogranite, 373-SIL-85, x= 7031.76, y= 3487.40

22 = Syenogranite, 641-SIL-83, x= 7030.55, y= 3485.80

than the Johnson & Rutherford pressures, respectively. The Johnson & Rutherford pressures are in good agreement with the pressures obtained for the contact metamorphism of the

country rock using other geobarometric methods (Hölttä 1995). There is no evidence for pressure or temperature differences between granitic and quartz syenitic rock types.

DISCUSSION

On the basis of its 1.884 Ga U/Pb zircon age (Salli 1983), the Vaaraslahti pyroxene-bearing

granite falls to the group of synkinematic Svecokarelian granitoids, which have U/Pb

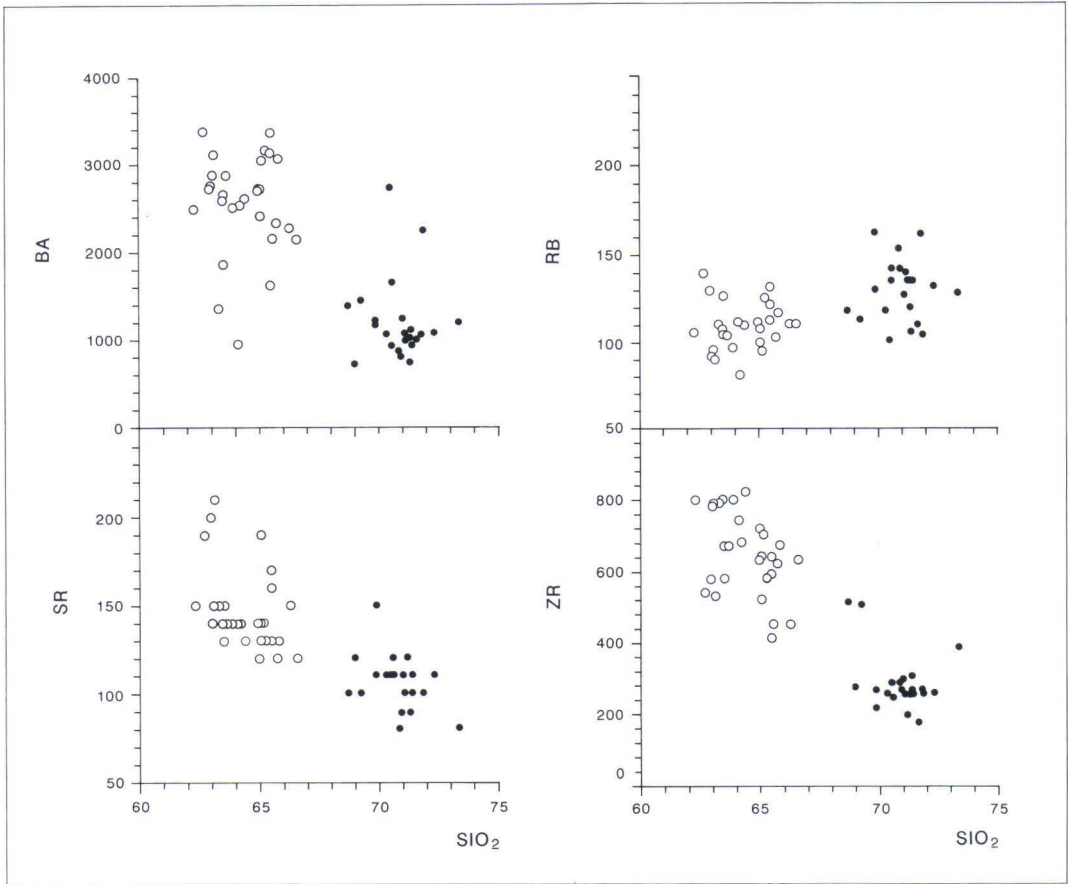


Fig. 8. Variation diagrams for some trace elements from the Vaaraslahti intrusion. X-ray fluorescence analyses. Circles quartz syenites and dots granites. X-ray fluorescence analyses; see Table 4.

ages ranging between 1.8-1.9 Ga (Huhma 1986). Although these rocks are most commonly tonalites and granodiorites in composition, porphyritic granite varieties are also abundant. Wahl (1963) demonstrated that coarse pyroxene granitoids in Finland are closely associated with the Raahe-Ladoga suture zone, but the present author later found porphyritic pyroxene-bearing granitic, quartz syenitic and monzonitic rocks closely resembling those of the Vaaraslahti stock sporadically distributed

throughout the whole Central Finland Granitoid Complex (see Lahti 1985).

The porphyritic pyroxene-bearing granitoids seem to form a geochemically and mineralogically coherent igneous rock group. The radiometric U/Pb ages reported for some of the rocks are also close to each other: An age of 1.887 ± 16 Ga was given by Korsman et al. (1984) for the porphyritic pyroxene bearing granitoids in the Rautalampi area (Haukilampi, Rautalampi), 1.886 ± 3 Ga by Patchett &

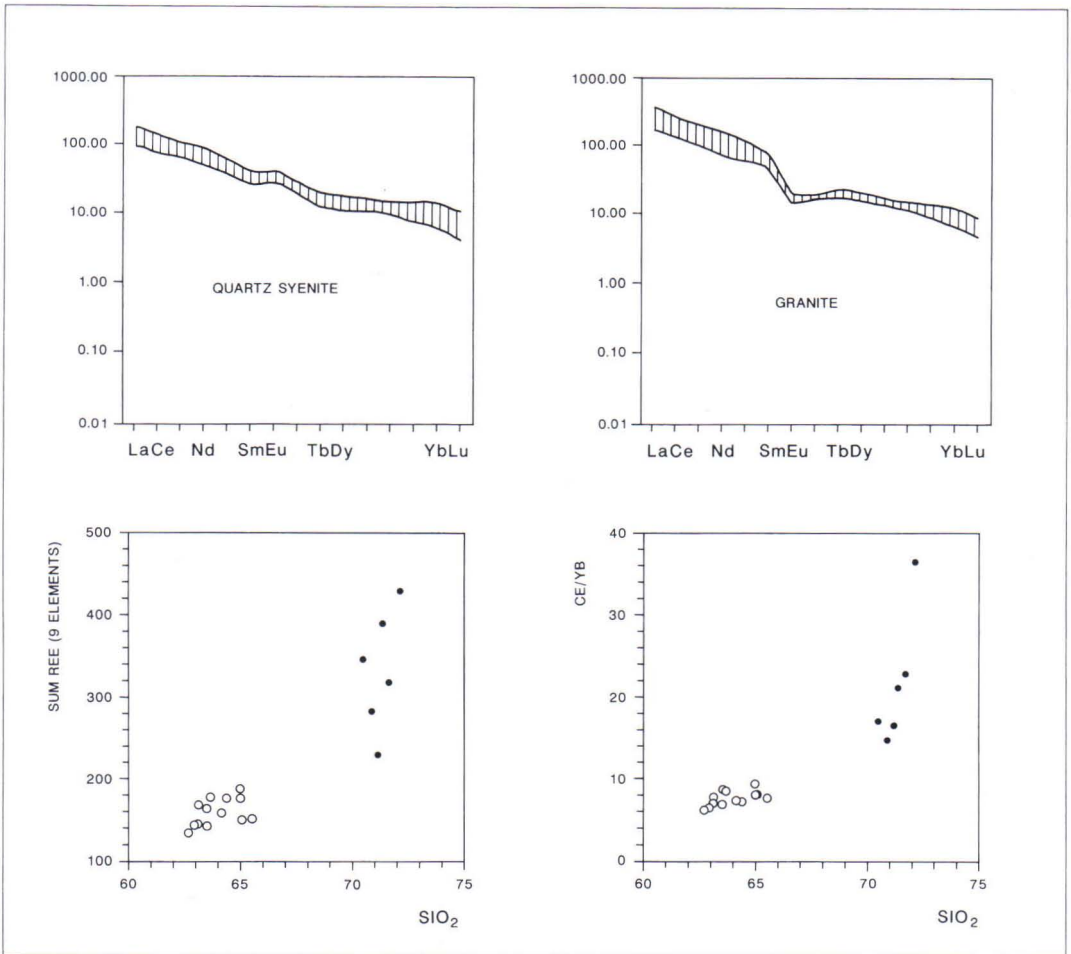


Fig. 9. REE distribution (chondrite normalized values) in thirteen quartz syenite and six granite samples (upper part of the figure) and the sum of nine REE plotted against SiO₂ in quartz syenites (circles) and granites (dots). Neutron activation analyses determined at the Reactor Laboratory of the Technical University of Helsinki.

Kouvo (1986, see also Gaal & Rauhamäki 1971) for the pyroxene granitoids in the Rantasalmi area (Voinsalmi, Rantasalmi), and 1.871 ± 1 Ga by Mäkitie & Lahti (1991) for the pyroxene granitoids in the Ilmajoki-Jalasjärvi area south of the town Seinäjoki in W-Finland.

The 1.884 Ga Vaaraslahti intrusion (Salli 1983) is younger than the local quartz diorite-tonalite-granodiorite intrusions, but the age difference is not drastic. The radiometric U-

Pb age of the Mustikkamäki gneissose quartz diorite southwest from the Vaaraslahti intrusion is around 1.890 Ga (Hölttä 1988). According to Korsman et al. (1988) and Hölttä (1988) the progressive stage of metamorphism in the area was associated with D₁-D₂ deformations, the age of which broadly coincided with the 1.890 Ga granitoids. These studies also suggest that much of the deformation was completed before the emplacement of the younger pyroxene-bearing granites.

Table 5. Crystallization temperatures (T°C) of certain rock types from the Vaaraslahti intrusion computed on the basis of two feldspar thermometry. The mole fractions (X) were computed using the feldspar analyses given in Table 1 (K= K-feldspar, P= plagioclase). The equations given by Haselton et al. (1983) were used in thermometric computations.

Rock	sample no.	T°C	XCaK	XNaK	XKK	XAnP	XAbP	XOrP
Quartz syenite	374-SIL-85	537	0.002	0.126	0.872	0.276	0.701	0.023
Quartz syenite	451-SIL-85	631	0.001	0.152	0.846	0.357	0.628	0.014
Quartz syenite	455-SIL-85	674	0.002	0.177	0.820	0.348	0.638	0.014
Quartz syenite	471-SIL-85	780	0.010	0.236	0.754	0.341	0.639	0.020
Qu.monzonite	615-SIL-83	593	0.001	0.153	0.846	0.291	0.693	0.016
Granite	462-SIL-85	616	0.001	0.170	0.828	0.271	0.707	0.023
Granite	464-SIL-85	576	0.001	0.141	0.856	0.301	0.679	0.020
Granite	465-SIL-85	701	0.003	0.229	0.767	0.273	0.713	0.014

The breccia structure of the Vaaraslahti stock indicates that the melt intruded in two major pulses. First, the quartz syenitic melt ascended and crystallized at an unknown crustal level. Later, the more fractionated granitic phase disrupted the quartz syenitic-monzonitic roof parts of the magma chamber, intruded to higher crustal levels and crystallized soon after the culmination of the progressive metamorphism. Multiphase intrusion of the pyroxene granitoid magma may be connected to the active and long-lived thrusting and shearing of the earth crust in the Raahe-Ladoga suture zone.

The porphyritic pyroxene-bearing granitoid intrusions in central Finland seem to have a prominent thermometamorphic aureole around them caused by the high intrusion temperature of the melt. The Vaaraslahti granitoid stock is surrounded by a rim of completely melted and recrystallized rock and a high grade metamorphic aureole. Quite similar contact phenomena can be detected for example around the Ilmajoki-Jalasjärvi porphyritic pyroxene granitoid (quartz monzonite) intrusion (Lahti & Mäkitie 1990), which is also slightly younger (about ten million years) than the other synorogenic rocks of the surrounding area (Mäkitie & Lahti 1991).

In the Vaaraslahti intrusion the contact meta-

morphic reactions of minerals can be traced far from the contact of the stock as demonstrated by Hölttä (1995) in his detailed studies. The crystallization temperatures of the rocks determined using two feldspar thermometry show variation from 540° to 780°C (see Table 5). The large range of values obviously indicates slow cooling processes of the feldspars and the intrusion itself. The observation is in good agreement with the mineralogical studies, which indicate that K-feldspar is always very heterogeneous.

The X-ray diffraction determinations show that K-feldspar is usually intermediate microcline, but the range of the structural varieties is large, from triclinic maximum microcline to nearly monoclinic orthoclase (Fig. 6). The thin section studies show that the crystals are often zoned and the twinned triclinic domains are common in untwinned phases (Fig 5). The small myrmekitic alkali feldspar-quartz grains of the later generation, crystallized very late, possibly in subsolidus conditions.

Geochemically the Svecokarelian synkinematic granitoids are usually calc-alkaline and show I-type characteristics (Front & Nurmi 1987). The rocks of the Vaaraslahti intrusion, especially the quartz syenitic intrusion phase, are exceptionally enriched in iron, potassium and barium, and in this respect differs from

most other Svecokarelian granitoids. Especially the high concentrations of barium (ranging up to 0.62 wt% BaO in K-feldspar) is curious.

The Na/K ratio is high and molar A/CNK (molar ratio of Al/(Ca+Na+K)) is low, resembling in this respect granitoids in Phanerozoic continental margins (cf. Nurmi 1988). The rocks in the Vaaraslahti intrusion are also analogous both mineralogically and chemically and can accordingly be classified as I-type granitoids. Their mineralogy certainly confirms better to the mineralogy of the I-type granites than to that of the S-type granites. Aluminium-rich minerals that are characteristic of the S-type granites are almost totally absent. The chemical analyses also confirm that the rocks are subaluminous. The A/CNK is low and varies from 1.0 to 1.1, as shown in Fig. 10. The high content of magnetite and high magnetic susceptibility is also character-

istic in the I-type granitoids (cf. Takashi et al. 1980, Ishihara 1981).

The clustering of analytical data on variation diagrams into two groups with continuous trends (Figs. 6 and 7) and the REE distribution diagrams (Fig. 9) suggest that the chemical and mineralogical differences between the quartz syenitic and granitic intrusion phases are obviously due to fractional crystallization. The depletion of Eu in the granite is characteristic and is most likely due to separation of early plagioclase-rich monzonitic and syenitic fractions. The scattering of the sum of REE's and Ce/Yb in the studied granite samples (Fig. 9) indicates various degrees of fractionation or locally more intense contamination.

Stable isotopes are widely used in studying the origin of granitic magmatic rocks. The initial $^{87}\text{Sr}/^{86}\text{Sr}$ of the rocks in the Vaaraslahti intrusion is low, i.e. 0.7048, and so are the

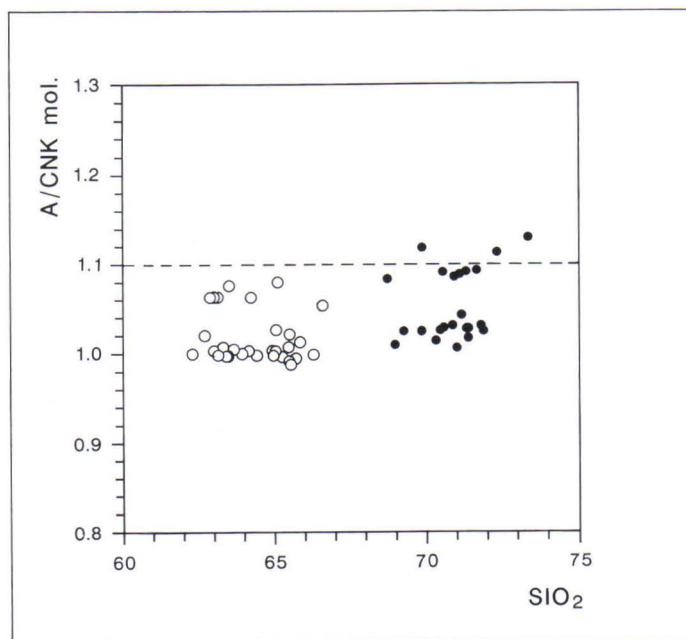


Fig. 10. Molar aluminium/alkali ratio plotted against SiO_2 in granites (dots) and quartz syenites (circles). Data from the Table no.4.

oxygen isotope values, with $\delta^{18}\text{O}$ being around 7.1 ‰ in both granitic and syenitic varieties (Haudenschild 1995). Both strontium and oxygen isotopic values fall within the range of typical I-type granitoids and suggest that the source of the melt was not a highly aluminous sedimentary assemblage. The Nd isotopic studies by Patchett and Kouvo (1986) gave an initial Nd isotopic value (ϵ_{Nd}) -0.6 for the Vaaraslahti pyroxene granite as well as for the

similar orthopyroxene-bearing granitoid from Voinsalmi, Rantasalmi (Patchett & Kouvo 1986). The result does not differ from the Nd isotopic composition of the other Svecokarelian syntectonic granitoids, which show ϵ_{Nd} values from -1 to +3 in the Svecofennian domain and from -9 to -6 in the Karelian domain indicating considerable involvement of Archaean crustal material during their generation (Huhma 1986).

ACKNOWLEDGEMENTS

I am grateful to Jukka Keskinen, who helped in the field work and in processing the chemical data. Pentti Hölttä kindly provided his geological expertise regarding the Pielavesi-Kiuruvesi area at my disposal and helped in the thermo-barometric interpretations. Dr. Juha Karhu determined the carbon isotope composition of a sample at the Isotope Geology Unit

of the Geological Survey of Finland. Dr. Mikko Nironen made valuable comments on the manuscript. I will also thank Mrs Leena Järvinen and Mrs Mirja Saarinen for their help during the mineralogical studies, and Mrs Ritva Forsman, who draw the final figures. The English was corrected by Dr. Peter Sorjonen-Ward.

REFERENCES

- Front, K. & Nurmi, P. A. 1987.** Characteristics and geological setting of synkinematic Svecokarelian granitoids in southern Finland. *Pecambrian Research* 35, 207–224.
- Gaál, G. & Rauhamäki, E. 1971.** Petrological and structural analysis of the Haukivesi area between Varkaus and Savonlinna, Finland. *Bulletin of the Geological Society of Finland* 43, 265–337.
- Haselton, H. T., Hovis, G. L., Hemingway, B. S. & Robie, R. A. 1983.** Calorimetric investigation of the excess entropy of mixing in analbite-sanidine solid solutions: lack of evidence for Na,K short-range order and implications for two-feldspar thermometry. *American Mineralogist* 68, 398–413.
- Haudenschild, U. 1995.** Rb-Sr and oxygen isotope geochemistry on a complex Proterozoic intrusive, Vaaraslahti, Finland. In: Hölttä, P. (ed.) Relationship of granitoids, structures and metamorphism at the eastern margin of the Central Finland Granitoid Complex. Geological Survey of Finland, Bulletin 382, 81–89. (this paper)
- Huhma, H. 1986.** Sm-Nd, U-Pb and Pb-Pb isotopic evidence for the origin of the Early Proterozoic Svecokarelian crust in Finland. Geological Survey of Finland, Bulletin 337. 338 p.
- Hölttä, P. 1988.** Metamorphic zones and evolution of granulite grade metamorphism in the early Proterozoic Pielavesi area, central Finland. Geological Survey of Finland, Bulletin 344. 50 p.
- Hölttä, P. 1995.** Contact metamorphism of the Vaaraslahti pyroxene granitoid intrusion in Pielavesi, Central Finland. In: Hölttä, P. (ed.) Relationship of granitoids, structures and metamorphism at the eastern margin of the Central Finland Granitoid Complex. Geological Survey of Finland, Bulletin 382, 27–79. (this paper)
- Ishihara, S. 1981.** The granitoid series and Mineralization. *Economic Geology*, 75th anniversary volume, 458–484.
- Korsman, K., Hölttä, P., Hautala, T. & Wasenius, P. 1984.** Metamorphism as an indicator of evolution and structure of the crust in eastern Finland. Geological Survey of Finland, Bulletin 328. 40 p.
- Korsman, K., Niemelä, R. & Wasenius, P. 1988.** Multistage evolution of the Proterozoic crust in

- the Savo schist belt, eastern Finland. In: Korsman, K. (ed.) Tectono-metamorphic evolution of the Raahe-Ladoga zone. Geological Survey of Finland, Bulletin 343, 89–96.
- Lahti, S. I. 1985.** Porphyritic pyroxene-bearing granitoids - a strongly weathered rock group in central Finland. *Fennia* 163 (2), 315–321.
- Lahti, S. I. & Mäkitie, H. 1990.** Jalasjärvi. Geological Map of Finland 1 : 100 000, Pre-Quaternary Rocks, Sheet 2221. Espoo: Geological Survey of Finland.
- LeMaitre, R. W. 1976.** Some problems of the projection of chemical data into mineralogical classification. *Contributions to Mineralogy and Petrology* 56, 181–189.
- Mäkitie, H. & Lahti, S.I. 1991.** Seinäjoen kartta-alueen kallioperä. Summary: Pre-Quaternary rocks of the Seinäjoki map-sheet area. Geological Map of Finland 1 : 100 000, Explanation to the Maps of Pre-Quaternary Rocks, Sheet 2222. Espoo: Geological Survey of Finland. 60 p.
- Marttila, E. 1976.** Evolution of the Precambrian volcanic complex in the Kiuruvesi area, Finland. Geological Survey of Finland, Bulletin 283. 109p.
- Marttila, E. 1977.** Kiuruvesi. Geological Map of Finland 1 : 100 000, Pre-Quaternary Rocks, Sheet 3323. Espoo: Geological Survey of Finland.
- Marttila, E. 1981.** Kiuruveden kartta-alueen kallioperä. Summary: Pre-Quaternary rocks of the Kiuruvesi map-sheet area. Geological Map of Finland 1:100 000, Explanation to the Maps of Pre-Quaternary Rocks, Sheet 3323. Espoo: Geological Survey of Finland. 48 p.
- Nurmi, P. & Haapala, I. 1986.** The Proterozoic granitoids of Finland: Granite types, metallogeny and relation to crustal evolution. *Bulletin of the Geological Society of Finland* 58 (1), 203–233.
- Patchett, J. & Kouvo, O. 1986.** Origin of continental crust of 1.9-1.7 Ga age: Nd isotopes and U-Pb zircon ages in the Svecokarelian terrain of South Finland. *Contributions to Mineralogy and Petrology* 92 (2), 1–12.
- Salli, I. 1977.** Pielavesi. Geological Map of Finland 1 : 100 000, Pre-Quaternary Rocks, Sheet 3314. Espoo: Geological Survey of Finland.
- Salli, I. 1983.** Pielaveden kartta-alueen kallioperä. Summary: Pre-Quaternary rocks of the Pielavesi map-sheet area. Geological Map of Finland 1 : 100 000, Explanation to the Maps of Pre-Quaternary Rocks, Sheet 3314. Espoo: Geological Survey of Finland. 29 p.
- Streckeisen, A. & Le Maitre R. W. 1979.** A chemical approximation to the modal QAPF classification of the igneous rocks. *Neues Jahrbuch für Mineralogie, Abhandlungen* 136, 169–206.
- Takashi, M., Aramaki, S. & Ishihara, S. 1980.** Magnetite-series/Ilmenite series vs. I-type/S-type granitoids. *Mining Geology, Special Issue* 8, 13–28.
- Vaasjoki, M. & Sakko, M. 1988.** The evolution of the Raahe-Ladoga zone in Finland: Isotopic constraints. In: Korsman, K. (ed.) Tectono-metamorphic evolution of the Raahe-Ladoga zone. Geological Survey of Finland, Bulletin 343, 7–32.
- Wahl, W. 1963.** The hypersthene granites and unakites of Central Finland. *Bulletin de la Commission géologique de Finlande* 212, 83–100.
- Wright, T. L. 1968.** X-ray and optical study of alkali feldspar: II. An X-ray method for determining the composition and structural state from measurements of 2θ values for three reflections. *American Mineralogist* 53, 88–104.

CONTACT METAMORPHISM OF THE VAARASLAHTI PYROXENE GRANITOID INTRUSION IN PIELAVESI, CENTRAL FINLAND

by

PENTTI HÖLTTÄ

Hölttä, P. 1995. Contact metamorphism of the Vaaraslahti pyroxene granitoid intrusion in Pielavesi, Central Finland. *Geological Survey of Finland, Bulletin* 382, 27–79. 14 figures, 3 tables and 4 appendices.

An orthopyroxene-bearing porphyritic I-type granitoid, dated by U-Pb zircon method at 1.884Ga, has intruded pelites at Vaaraslahti, central Finland. It has a thermal aureole in which metamorphic grade in the country rocks increases from the stability field of muscovite to granulite facies at the contact. Several closely spaced metamorphic zones have been mapped in metapelites in proximity to vicinity of the pluton. These are, approaching the contact, respectively, the muscovite, cordierite-K-feldspar, garnet-cordierite, garnet-cordierite-spinel and diatexite-stictolite zones. The temperature of metamorphism increases almost isobarically at ca. 5 kbars, from ca. 600°C in the muscovite zone to ca. 750°C at the contact. The minimum horizontal distance through which this change takes place is two kilometers. Decreased water activity was associated with the contact metamorphism. Dehydration melting produced garnetiferous melt segregations at the contact under granulite facies conditions, and along shear zones at the contact diatexites were produced. Igneous microtextures indicate the presence of melt in the melting zone. The thermal aureole developed during D₂ and D₃ deformations. Metamorphic reactions suggest cooling with minor uplift after the peak conditions; kyanite for example occurs as a retrograde mineral. Hydration, indicated e.g. by andalusite-biotite symplectites after cordierite, was connected with the cooling.

Key words (GeoRef, Thesaurus AGI): contact metamorphism, granulite, granites, charnockite, P-T-t paths, anatexis, Proterozoic, Vaaraslahti, Pielavesi, Finland

Pentti Hölttä, Geological Survey of Finland, FIN-02150 ESPOO, FINLAND

INTRODUCTION

Synkinematic granitoids, having zircon U-Pb ages ranging between 1930-1860 Ma, with a mode at ca. 1885 Ma, dominate the Proterozoic bedrock in Finland (Fig. 1). They tend to be calc-alkaline, are generally metaluminous and show I-type characteristics (Nurmi & Haapala 1986, Front & Nurmi 1987). The relationship between these granitoids and metamorphism is ambiguous, as the metamorphism of magmatic belts is also globally (see e.g. Barton & Hanson 1989 and P.H. Thompson 1989,

for references). It has been widely maintained that most thermal aureoles are developed at shallow levels in the earth's crust. However, with increasing depth, the specific structural and textural features of classical contact metamorphism can become obscured, and apparent regional metamorphism may actually have resulted from local cryptic magmatic heat sources several kilometres below the present exposure level (Miyashiro 1973, Dickerson & Holdaway 1989, Pattison & Tracy 1991).

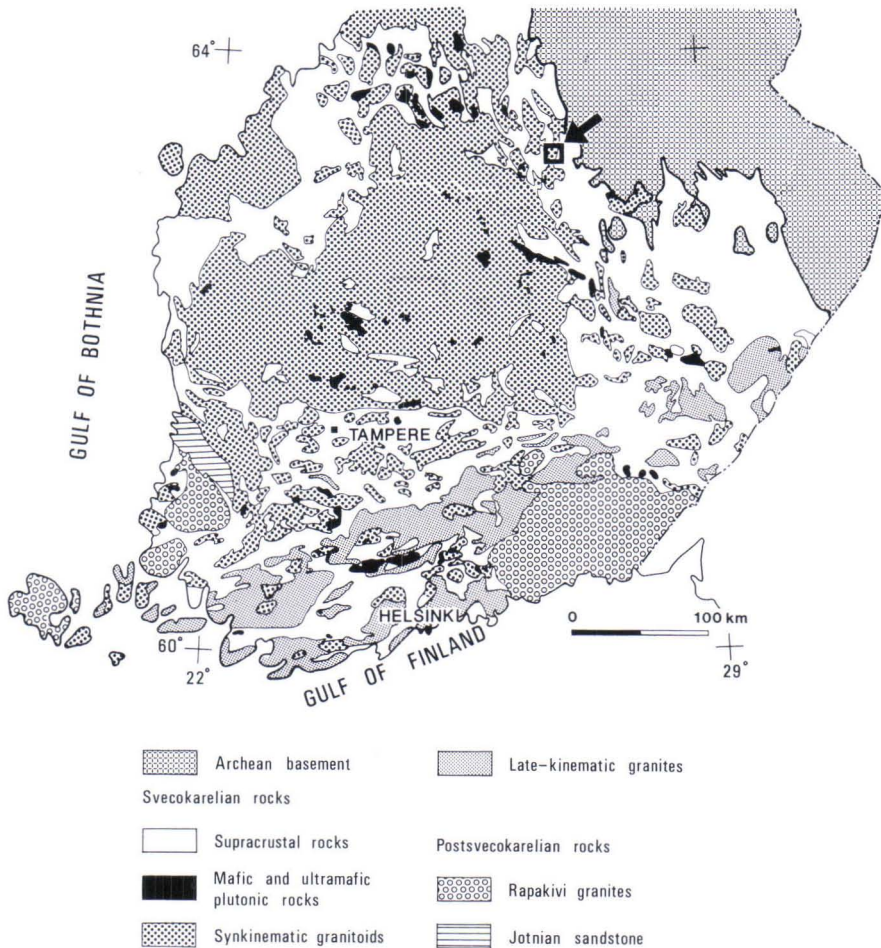


Fig. 1. A general geological map of southern Finland after Front & Nurmi (1987). The box indicated by the arrow shows the location of the study area.

In central Finland there are relatively low-pressure (5-6 kbars) granulite facies blocks, in which high-T metamorphism was clearly caused by 1.885 Ga pyroxene-bearing mafic and felsic intrusions (Korsman et al. 1984, Hölttä 1988, Vaasjoki & Sakko 1988). In and close to these blocks, there are porphyritic orthopyroxene granitoids which have especially well-developed thermal aureoles, including granulite facies rocks in the immediate vicinity of their contacts. The thermal

effect of orthopyroxene granitoids can be mapped up to several kilometres from the contact (Fig. 2). The purpose of this paper is to describe in detail the contact metamorphism of one such pyroxene granitoid pluton, and to discuss its relationship to deformation and regional metamorphism. The intrusion is located in the village of Vaaraslahti, Pielavesi district, central Finland (Fig. 1), and has been described by Lahti (1995).

GEOLOGICAL SETTING

The Pielavesi area is situated near the border of the Archean craton (Fig. 1). It is characterized by a block structure so that changes in metamorphic grade, as well as major lithological changes, are commonly marked by faults (Marttila 1976, Korsman et al. 1984, Hölttä 1988). There are two major strike- and oblique-slip fault systems. The older (regional D₃) mainly strikes NW, or as a conjugate system NE, and the younger strikes NNE. These deformation zones exhibit extensive shearing and mylonitization (Korsman et al. 1984, Pajunen 1986). The area was divided by Korsman et al. (1984) and Hölttä (1988) into metamorphic blocks (Fig. 2), whose metamorphic grade varies from amphibolite to granulite facies. The peak metamorphic temperatures in these blocks vary from ca. 550-600°C in the lowest grade blocks to 800-880°C in the Pielavesi granulite block. The pressures corresponding to these temperatures were ca. 5±1 kbars, without significant pressure changes between blocks, except for the andalusite grade rocks in the west, where the pressure was ca. 3-4 kbars (Hölttä 1988). Granitoids, both foliated tonalitic-granodioritic rocks and weakly or undeformed porphyritic granites are the dominant rock types near the craton margin (Salli 1969, 1977, Marttila 1977), while pelitic and semipelitic country rocks with volcanic intercalations are also common. Bimodal

volcanics are typical of the area between Säviä and Pyhäsalmi (Fig. 2), as well as cordierite-orthoamphibole/orthopyroxene rocks, at places associated with massive Cu-Zn ores (Huhtala 1979). Mafic volcanites in the area geochemically resemble tholeiitic basalts of primitive island arcs (Kousa et al. 1994).

The oldest dated rocks in the area are gneissose granitoids and volcanites, whose U-Pb zircon age is 1.92 - 1.93 Ga (Helovuori 1979, Vaasjoki & Sakko 1988, Kousa et al. 1994). The main phase of magmatism took place at 1.89-1.86 Ga, majority of intrusive rocks being intruded at ca. 1.885 Ga (Aho 1979, Marttila 1981, Salli 1983, Vaasjoki & Sakko 1988). The K-Ar and Rb-Sr ages of hornblendes and micas are considerably younger, ca. 1.65 - 1.79 Ga, being oldest in the granulite block (Haudenschild 1988, 1990). The age of the granulite facies metamorphism in the Pielavesi block is close to the age of the main phase of magmatism, shown by a U-Pb zircon age of 1889±13, Ma, obtained from a garnet-cordierite-orthopyroxene rock (Vaasjoki & Sakko 1988). Detrital zircon from the country rock adjacent to the contact with the Vaaraslahti orthopyroxene granitoid is reset, giving an age, 1895±1 Ma (Vaasjoki & Sakko 1988), which is close to, although somewhat older than the U-Pb age of the pluton, namely 1884±5 Ma (Salli 1983).

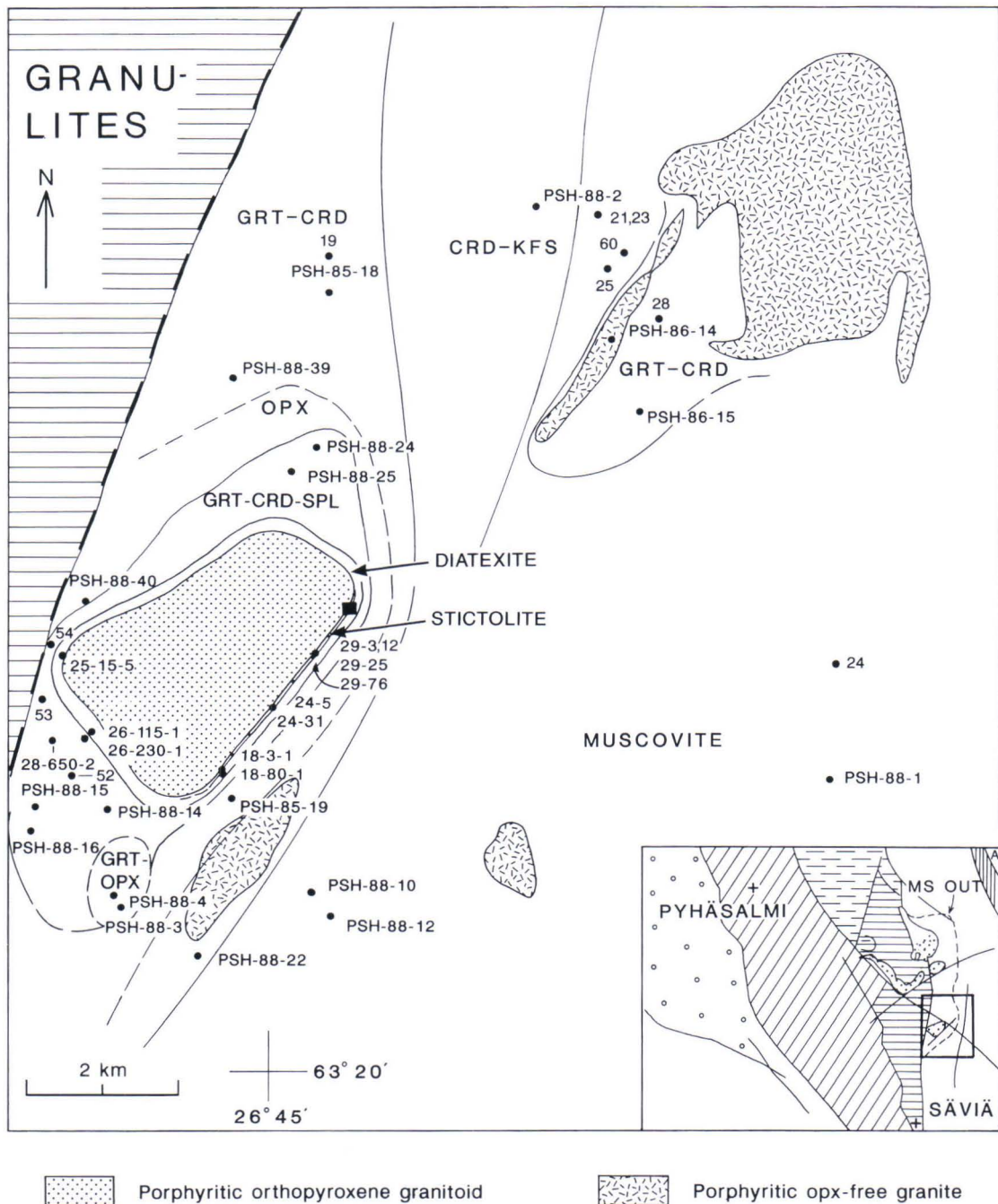


Fig. 2. Metamorphic zones of the study area. The inset map shows the metamorphic blocks of the Pielavesi area according to Hölttä (1988): A = Archean; vertical lines = staurolite grade; unshaded = medium amphibolite facies, muscovite mostly stable, dashed line = muscovite out; horizontal lines = granulite facies; dashed horizontal lines = transitional granulites; oblique lines = upper amphibolite facies; dotted = lower amphibolite facies, andalusite grade. Codes refer to the localities of samples presented in Appendices 1-3. Dashed lines refer to appearance of orthopyroxene and to breakdown of garnet into orthopyroxene and plagioclase in mafic rocks. The black square at the NE corner of the pyroxene granitoid refer to the area presented in Fig. 3c.

METAMORPHIC ZONES

The study area is located near the granulite block boundary (Fig. 2). A porphyritic pyroxene granitoid intruded into pelites, and is surrounded by a thermal aureole. Metamorphic zones around the porphyritic granitoid intrusions are recognized with increasing grade on the basis of pelite mineralogy: muscovite, cordierite-K-feldspar, garnet-cordierite, garnet-cordierite-spinel, and anatectic diatexite-stictolite zones (Fig. 2). The inner part of the diatexite zone at the SE contact exhibits nebulitic and flecky migmatites (stictolites), where garnets are surrounded by feldspathic mantles. Elsewhere in diatexites molten and unmolten portions cannot be distinguished from one another (nomenclature after Mehnert 1971). Within the flecky migmatites of the diatexite-stictolite zone, at the SE margin of the pyroxene granitoid, first there is a garnet-cordierite-orthopyroxene zone, which reaches few

meters from the contact.

At the SE contact of the pyroxene granitoid, and also close to the porphyritic pyroxene-free granitoids in the NE part of the area cordierite-K-feldspar zone was not found, but the metamorphic grade increases directly from muscovite to garnet-cordierite field. This may indicate the presence of a NE trending shear zone, which can be concluded also from the elongated granite bodies, which may have used the shear zone during their emplacement.

Rocks of mafic composition in the garnet-cordierite zone contain orthopyroxene. To the southwest of the orthopyroxene granitoid, and enveloped by the spinel zone, there is a small area where garnet is decomposed into orthopyroxene and plagioclase in mafic rocks. This area is interpreted as a small 'hot spot' where the grade locally attained granulite facies (Fig. 2).

DEFORMATION

The oldest recognized fold phase in the study area is F_2 , which deforms the penetrative S_1 schistosity parallel to lithological layering. The F_2 folds are isoclinal and are associated with a shear-type cleavage (Fig. 3a).

The D_3 deformation forms semi-open folds and is manifested in many places by strike- or oblique-slip faults and shear zones with NE-trending axial planes. The direction of the F_3 fold axis is variable, but in the northern side of the orthopyroxene granitoid intrusion it plunges mostly 30-45° to the SW and in the southern side 30-75° to the NE. The D_3 deformation has reoriented the S_2 schistosity, and a biotite schistosity and melt segregations at the contact were commonly developed in the axial plane of the F_3 folds (Fig. 3c). The early foliation is also commonly reoriented by D_3 faulting parallel with the contact (Fig. 3b, c). The pyroxene granitoid pluton is slightly elon-

gated in the direction of the D_3 axial plane (Fig. 2). The overall folial structure is generally concordant to the contacts of the pluton.

There were at least two later deformation phases after D_3 . In the 'hot spot' area, F_3 folds are superimposed by NW striking faults. Semi-open folds whose axial plane is in the same direction also occur. This deformation may be a conjugate of the late D_3 deformation, when folding was developed into faulting. The D_3 structures are also cut by N-S striking faults, which may be narrow seams on a millimeter scale or mylonites which are tens of meters thick as they are in the eastern part of the area. A late deformation phase whose axial plane is in an E-W direction forms crenulations and small faults. The mutual relationships between these two post- D_3 structures could not be observed in the study area.

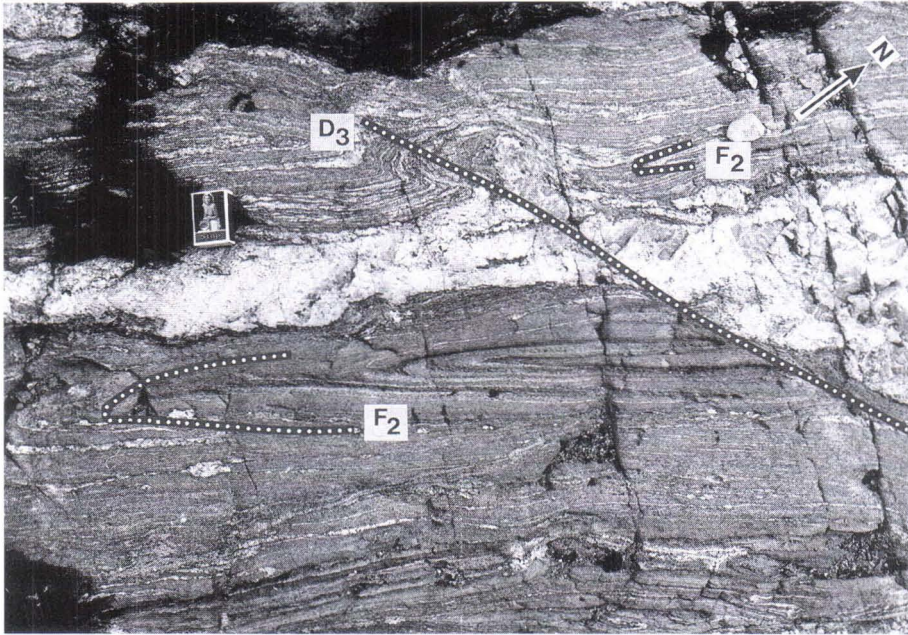


Fig. 3a. Deformation structures. F_2 fold cut by D_3 fault, garnet-cordierite zone, locality PSH-88-39 in Fig. 2.

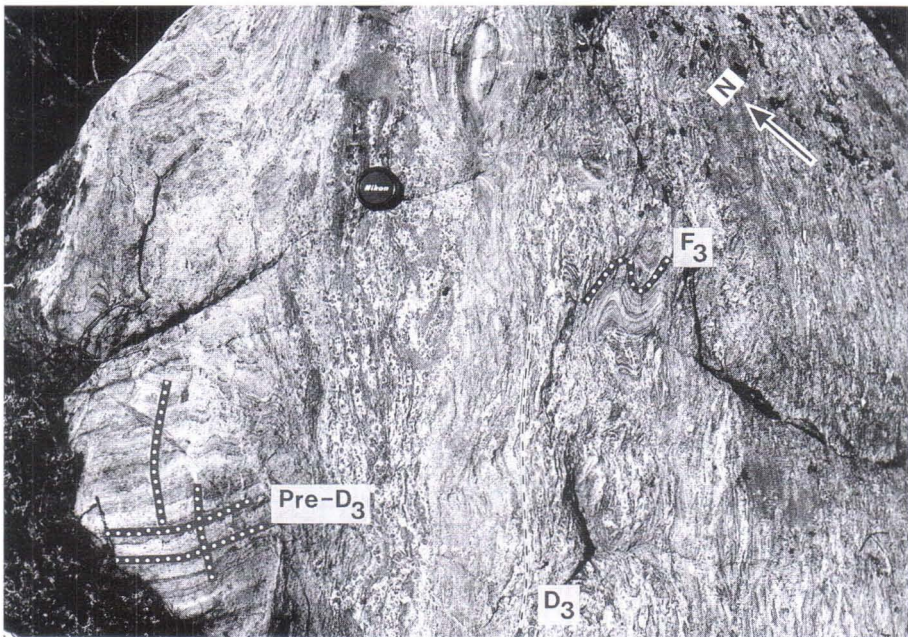


Fig. 3b. Deformation structures. Early foliation ($S_0+S_1+S_2$) reoriented by the D_3 , inner part of the diatexite-stictolite zone, loc. 29-25-1.

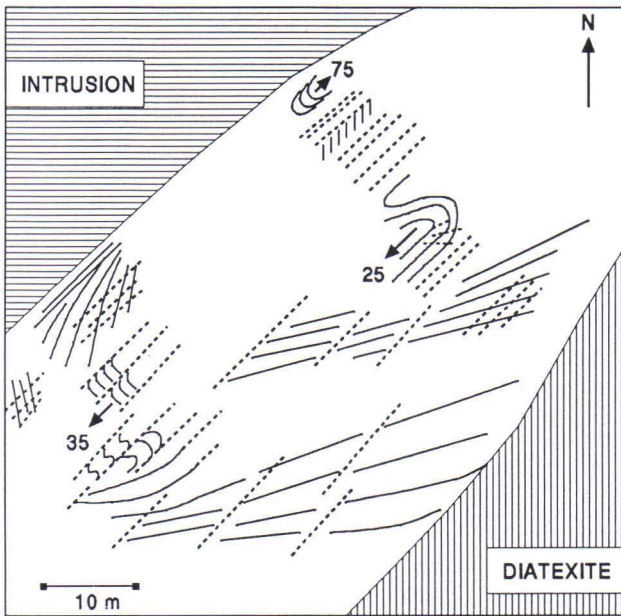


Fig. 3c. Deformation structures. The structural style at the SE contact of the pyroxene granitoid; solid lines = S_0 - S_2 , dashed lines = S_3 with melt segregations (c.f. Fig. 4c). The arrows with numbers show the direction and dip of the fold axis. The location of the area is shown in Fig. 2.

PETROGRAPHY

Assemblages in metapelites

The Vaaraslahti metapelites have a rather uniform chemical composition (Appendix 2; Fig. 10) with the mineral assemblages listed below being characteristic. The relative timing of the appearance of a particular mineral (prograde, retrograde) is listed in Table 1.

Muscovite zone: $bt-ms-pl-qtz-po-ilmsil \pm ky \pm st$;

Cordierite-K-feldspar zone: $bt-sil-and-pl-qtz-po-ilmsil \pm kfs \pm crd \pm st \pm ms$;

Garnet-cordierite zone: $grt-crd-bt-sil-and-ky-pl-qtz-po-ilmsil-gph \pm kfs \pm st$;

Garnet-cordierite-spinel zone: $grt-crd-bt-sil-and-ky-pl-qtz-po-ilmsil-gph \pm st \pm spl \pm kfs$;

Diatexite-stictolite zone, diatexite: $grt-crd-bt-and-pl-qtz-po-ilmsil-gph \pm sil \pm spl \pm st \pm kfs$. In the inner part of the diatexite at the SW contact there is also a less aluminous layer which has the assemblage $opx-bt-pl-qtz-po-ilmsil-gph \pm grt \pm kfs$. Spinel and primary sillimanite

Table 1. The type of occurrence of minerals in metapelites in the metamorphic zones of Vaaraslahti. - not present; + present, * present as a retrograde phase.

Zone	Ms	Crd-kfs	Grt-crd	Grt-crd-spl	Diat-Stic
grt	-	-	+	+	+
crd	-	+	+	+	+
spl	-	-	-	+	+
bt	+	+	+	+	+
ms	+	*	*	*	*
and	+	*	*	*	*
sil	+	+	+	+	*
ky	*	*	*	*	*
st	*	*	*	*	*
pl	+	+	+	+	+
kfs	-	+	+	+	+
qtz	+	+	+	+	+
po	+	+	+	+	+
ilm	+	+	+	+	+
gph	+	+	+	+	+
opx	-	-	-	-	+
melt	+	+	+	+	+

progressively disappear from the diatexite, occurring in its outer parts but not near the contact.

Diatexite zone, stictolite at the SE contact: the innermost few meters of nebulitic migmatite (garnet-cordierite-orthopyroxene zone) has the assemblage grt-opx-crd-bt-kfs-pl-qtz-po-ilm-gph. This zone is only a few meters thick, and it does not occur everywhere around

the pluton; so it is presumably controlled by whole rock composition. Some metapelite xenoliths in the orthopyroxene granitoid also have this mineral assemblage. Orthopyroxene is not present in the outer part of the nebulitic layer. In the flecky migmatite mesosomes have the assemblage crd-bt-kfs-pl±qtz and feldspathic segregations grt-kfs-pl-qtz±crd±bt.

Assemblages in basic and intermediate metavolcanic rocks

Muscovite zone: hbl-pl-qtz-ep-ttn.

Cordierite-K-feldspar zone: bt-pl-ilm-qtz±grt.

Garnet-cordierite zone: hbl-pl-qtz±cum±cpx±bt.

Garnet-cordierite-spinel zone: opx-pl-qtz±hbl±cum±cpx±bt±po±ilm.

Diatexite-stictolite zone: the high-grade assemblage in basic boudins is opx-pl-qtz±cpx; cummingtonite, hornblende and biotite are found as retrograde phases.

'Hot spot' in the garnet-cordierite-spinel zone: opx-cpx-hbl-bt-pl-qtz-po-ilm or opx-

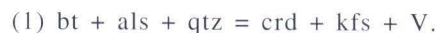
bt-pl-qtz-grt-po-ilm at less calcic compositions. Orthopyroxene, together with plagioclase, pseudomorphs or forms coronas on garnet in garnetiferous metatuffite boudins (Fig. 4r). The opx-pl corona on garnet in these boudins overgrows the S₂ schistosity, which indicates that a heating phase followed D₂. Metapelite in this area is migmatitic and comparable in grade with the diatexite-stictolite zone. It is possible that the 'hot spot' represents the wall rock of another intrusion, although the intrusion is not itself exposed.

Textures and reactions in metapelites

The metapelite minerals and their textures are described in detail in order to establish the metamorphic reactions which took place during the heating and cooling of the Vaaraslahti rocks. These reactions, together with the information given by thermometry and barometry, are then used to construct the pressure-temperature evolution.

Prograde biotite occurs as brown flakes, which are parallel to the S₂ axial plane, or, where S₃ is developed, is aligned within this foliation as well. Biotite also occurs as a retrograde phase due to the breakdown of cordierite or garnet, in which case it is randomly oriented, brown or greenish and forms intergrowths with Al-silicate (mostly andalusite) (Figs 4a and 4i). The grain size and abundance of biotite is smallest in the stictolite at the SE contact of the Vaaraslahti pluton (Table 2).

Cordierite is formed by reaction between biotite and sillimanite when they are in contact (Fig. 4b); this happens occasionally in the cordierite-K-feldspar zone but almost invariably in the garnet-cordierite and garnet-cordierite-spinel zones. Cordierite-K-feldspar intergrowths are common in the garnet-cordierite zone. These textures are indicative of the reaction



In the garnet-cordierite and garnet-cordierite-spinel zones, cordierites are larger than in the cordierite-K-feldspar zone, and some of them have only a few or no sillimanite inclusions. Primary biotite and sillimanite coexist in the cordierite-K-feldspar and garnet-cordierite zone but not longer in the inner parts of the

Table 2. Modal compositions of metapelites, calculated with point-counting method, 1000 points per thin section. Location of the samples is shown in Fig. 2. Diatexite-stictolite zone samples; m = mesosome, cl = cordierite-bearing leucosome (no garnet), gl = feldspathic mantle around large garnet, d = diatexite.

	Diatexite-stictolite zone						Garnet-cordierite-spinel zone				Western garnet-cordierite zone		
Sample	24-31		29-12		26-115		52	53	54	PSH-88-14	19	PSH-85-18	PSH-88-39
	m	cl	gl	m	gl	d							
Qtz	0.3	34.6	33.3	0.1	3.4	27.4	23.4	35.2	46.9	28.7	31.9	28.0	34.2
Pl	11.5	23.6	36.2	16.0	18.6	34.6	13.0	9.6	21.7	18.6	14.3	8.8	5.9
Kfs	8.0	22.0	12.5	22.2	73.2	4.0	5.4	4.3	0.2	4.9	0.7	3.8	3.6
Bt	27.7	5.3	7.7	17.7	3.0	24.9	29.4	26.6	28.9	21.3	36.8	37.0	36.8
Als	0.9	-	-	1.0	-	1.1	6.9	13.3	-	4.6	12.0	9.7	13.8
Crd	51.6	14.5	10.3	43.0	1.8	6.8	19.2	9.7	-	15.4	3.3	10.9	5.5
Grt	-	-	-	-	-	1.2	2.7	1.3	2.2	6.5	1.0	1.8	0.2
	Eastern garnet-cordierite zone						Muscovite zone						
Sample	PSH-86-14	28	PSH-86-15	60	25	24	21	23					
Qtz	23.6	38.3	52.7	32.1	30.7	36.0	34.5	25.9					
Pl	26.4	28.4	15.0	10.5	19.6	2.4	13.9	13.0					
Kfs	0.0	2.2	0.9	0.2	-	-	-	-					
Bt	38.9	29.3	25.1	40.8	35.2	21.4	32.2	40.7					
Ms	-	-	-	13.0	13.0	39.3	15.1	18.8					
Als	9.3	1.1	2.7	0.1	-	-	2.5	-					
Crd	0.6	0.1	0.6	-	-	-	-	-					
Grt	0.4	0.6	3.0	-	-	-	-	-					

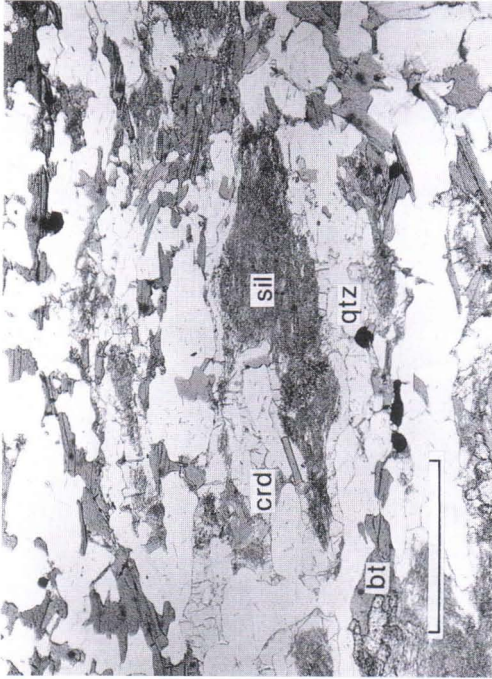


Fig. 4b)



Fig. 4d)

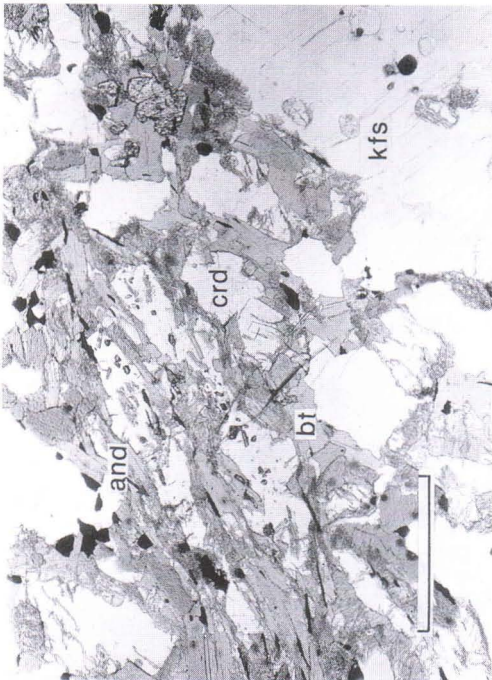


Fig. 4a)



Fig. 4c)

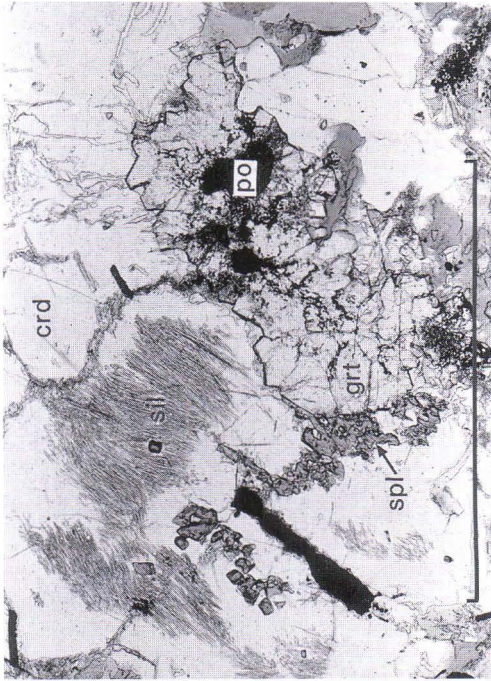


Fig. 4f)



Fig. 4h)

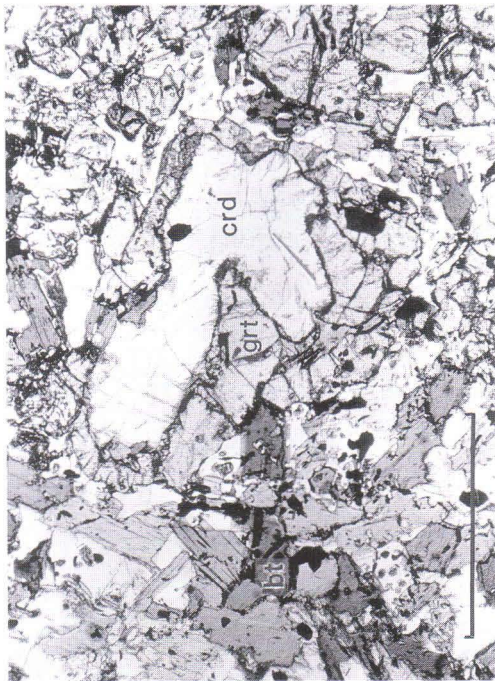


Fig. 4c)

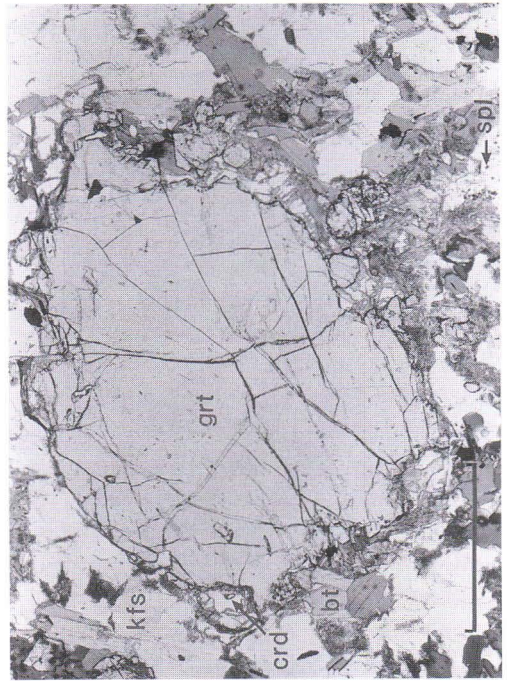


Fig. 4g)

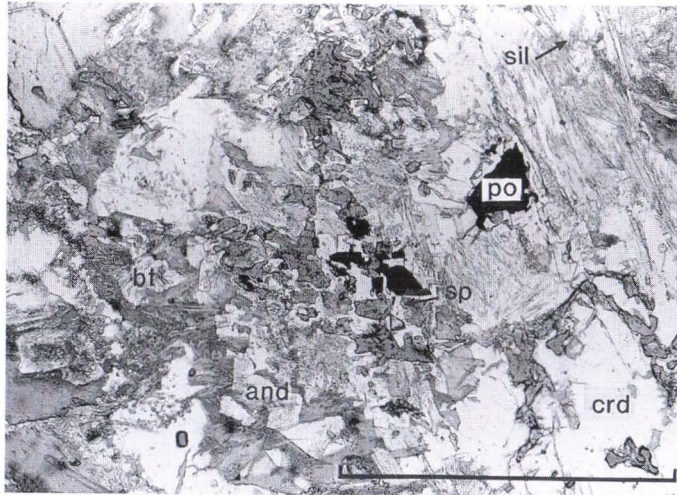


Fig. 4i)

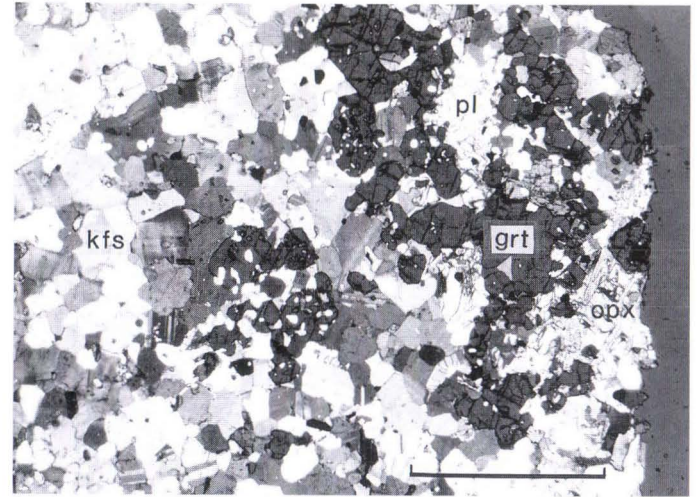


Fig. 4j)

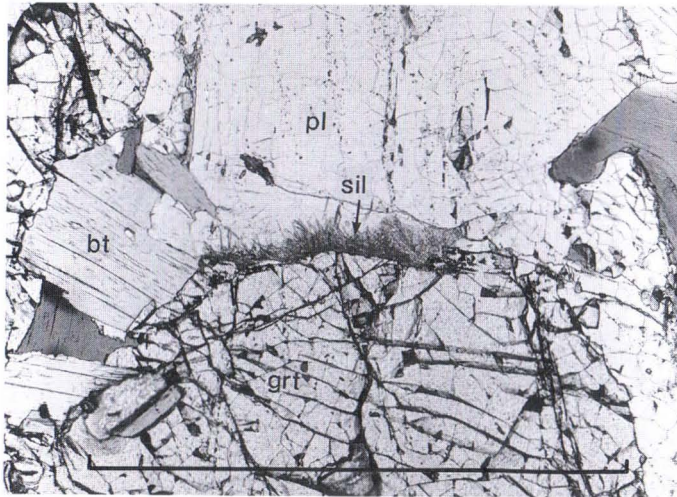


Fig. 4k)

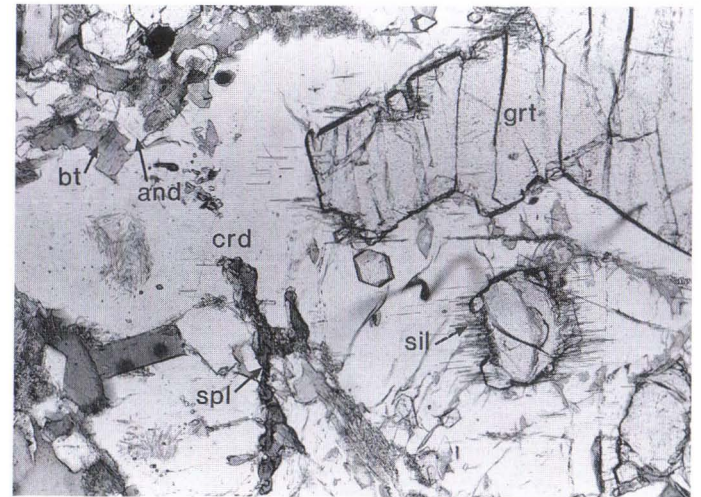


Fig. 4l)



Fig. 4n)

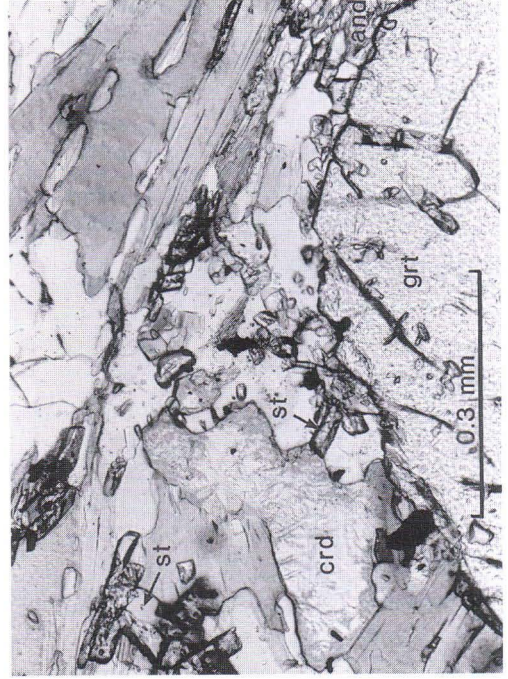


Fig. 4p)

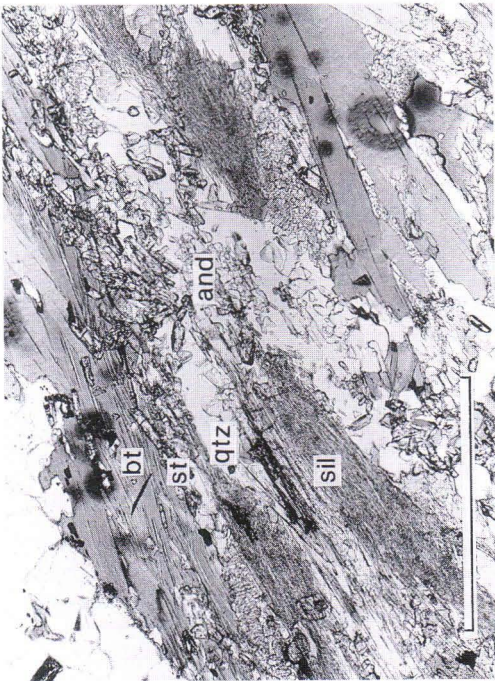


Fig. 4m)



Fig. 4o)

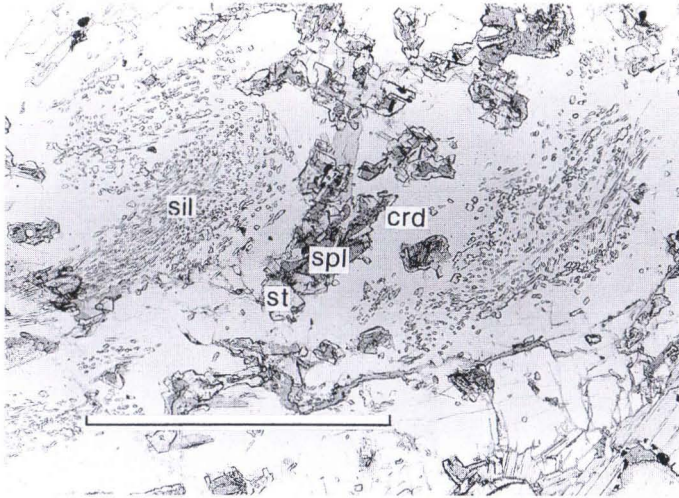


Fig. 4q)

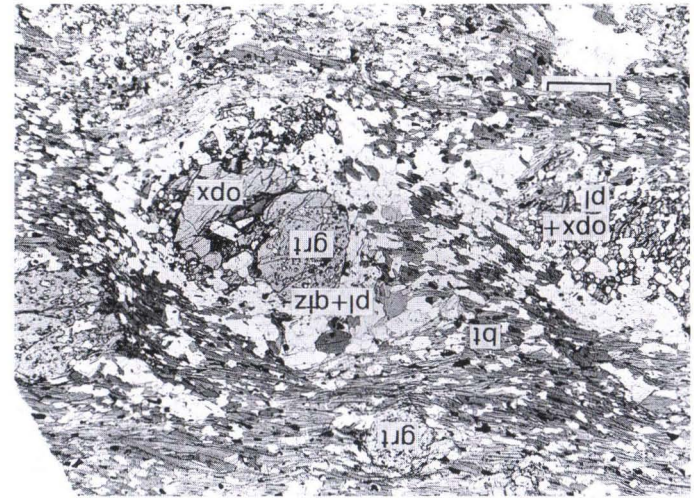


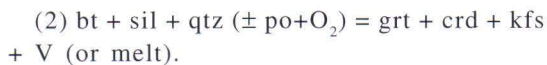
Fig. 4r)

Fig. 4a-r. Reaction textures. The scale bar in each photomicrograph is 1 mm. a) retrograde alteration of cordierite into biotite and andalusite/sillimanite in back-reaction (1); b) cordierite forming reaction (1) between biotite and sillimanite, garnet-cordierite zone; c) sector twinned cordierite with many biotite and quartz inclusions, flecky migmatite in diatexite-stictolite zone; d) garnet and cordierite produced in reaction (2) between biotite and sillimanite, garnet-cordierite zone; e) garnet corona on cordierite, garnet-cordierite-spinel zone; f) garnet overgrowing spinel and cordierite, garnet-cordierite-spinel zone; g) garnet altered from rims into cordierite and biotite, garnet-cordierite-spinel zone; h) skeletal spinel, together with pyrrhotite and sillimanite inclusions in cordierite, garnet-cordierite-spinel zone; i) spinel altering into andalusite and biotite, garnet-cordierite-spinel zone; j) garnet altered into orthopyroxene and plagioclase, felsic segregation at the SE contact; k) sillimanite needles between garnet and plagioclase; l) second generation sillimanite needles on garnet rims, sillimanite is interpreted to have been formed in reaction (3) (see text); retrograde andalusite on cordierite rims; m) fibrolitic sillimanite altering into andalusite, garnet-cordierite zone; n) the assemblage and-bt-qtz-ms-st, presumably formed in reaction (11) (see text), muscovite zone; o) staurolite crystals, formed in a reaction between cordierite and andalusite; p) staurolite produced by the decomposition of garnet and Al-silicate; q) spinel inclusions in cordierite, spinel is altering into staurolite in reaction (14); r) garnet altering into orthopyroxene and plagioclase, 'hot spot' area (Fig. 2).

spinel zone, where prograde biotite and sillimanite are separated by cordierite, such that early sillimanite occurs only as inclusions in cordierite.

Cordierite produced by reaction (1) is mostly elongated within the S_2 schistosity. In places where S_3 is well developed, cordierite occasionally has biotite and quartz inclusion trails; these are oblique or curved with respect to S_3 (Fig. 5a), suggesting that cordierite was also formed during the early D_3 . Cordierite is altered at the rims and along cleavages into pale yellow or bright brownish yellow amorphous pinite. Biotite and Al-silicate replace both cordierite and pinite. Biotite-Al-silicate intergrowths after cordierite show that reaction (1) proceeded from right to left during cooling (Fig. 4a). In the diatexite-stictolite zone cordierite is often rectangular in shape and mostly optically positive, with $2V$ ca. $88-89^\circ$, whilst in other zones it is generally negative. At the SE contact cordierites have sector twinning and many tiny biotite inclusions in the cores of the grains (Fig. 4c).

The appearance of coexisting garnet and cordierite in the garnet-cordierite zone is interpreted to mark the beginning of the univariant KFMASH reaction

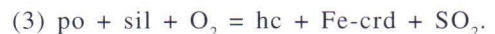


Both cordierite and garnet have sillimanite inclusions which tend to have a uniform optical orientation. Pyrrhotite, when present, also participated in reaction (2), because garnet forms coronas on iron sulphide occurring on cordierite rims (Fig. 4d).

Sillimanite, biotite, quartz and pyrrhotite inclusions are common in garnets, whereas plagioclase inclusions are rare. Some garnets have an inclusion-rich core and an inclusion-free rim, a texture which is common elsewhere in high-grade rocks in the Pielavesi area (Hölttä 1988), and which is interpreted to indicate a rapid initial growth rate (Tracy

1982). The breakdown of titaniferous biotite which is in contact with garnet has commonly produced a rim of secondary garnet-ilmenite intergrowth on old garnets. In the garnet-cordierite zone south of the pyroxene granulite, where S_3 is well developed, some garnets have pressure shadows indicating that they are pre-tectonic with respect to D_3 shear. These garnets are cut by D_3 microfaults.

Spinel occurs as inclusions (diameter 0.1-0.2 mm) in both cordierite and in garnet. It forms commonly a skeletal symplectitic texture with cordierite, which indicates their simultaneous crystallization (Fig. 4h). Spinel inclusions are found in those cordierites that also have sillimanite and pyrrhotite inclusions. Spinel may either overgrow sillimanite and have sillimanite inclusions, but often sillimanite and spinel are separated by cordierite. Spinel can also rim pyrrhotite (Fig. 4h). These textural features suggest that spinel was at least partly formed by a reaction involving iron sulphide and sillimanite, such as



Not all of the spinel observed can be explained by reaction (3) because spinel occurs also in rocks that contain only limited amounts of sulphides. Sillimanite always seems to have been one reactant, and sometimes inclusions of biotite, along with occasional garnet, are found in spinel-bearing cordierite. A possible reaction for producing spinel was the divariant KFMASH reaction

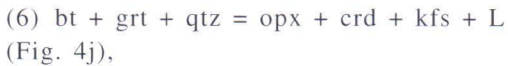


after cordierite formed in reactions (1) and (2) has isolated its sillimanite and biotite inclusions from quartz. Spinel never coexists with quartz; whenever quartz is present it is separated from spinel by cordierite. Spinel was altered into greenish biotite and andalusite in back-reaction (4) (Fig. 4i).

The grain diameter of garnet is normally

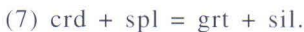
0.5-3 mm, but increases in the flecky migmatite at the SE contact up to 10-20 mm. These large garnets are helictic and they contain abundant quartz and some plagioclase and biotite inclusions. In those layers, where garnets are surrounded by feldspathic mantles, the mesosomes are almost quartz-free (Table 2). Sillimanite is also absent, so the possible melt producing reaction is (2) and the reaction has consumed effectively all the sillimanite and quartz present in the rock.

Orthopyroxene replaces and overgrows biotite. At the SE margin of the pluton orthopyroxene also coexists with K-feldspar and cordierite in the migmatite mesosomes, and orthopyroxene sometimes replaces garnet. It is likely that orthopyroxene was produced in reactions

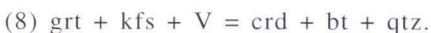


because there are garnet inclusions in those orthopyroxenes which are in contact with garnet.

In the garnet-cordierite and garnet-cordierite-spinel zones garnet has sometimes crystallized on cordierite rims, occasionally forming coronas on cordierite (Fig. 4e). This garnet may have spinel inclusions, or garnet can overgrow spinel inclusions in cordierite, as in Fig. 4f. This texture is interpreted to result from the reaction

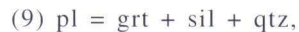


In the same thin section large garnets may have altered into cordierite and biotite from their rims (Fig. 4g). This type of alteration indicates the reaction



Two generations of sillimanite have been recognized. The first generation fibrolitic sillimanite occurs together with biotite and as

inclusions in cordierite, garnet and plagioclase, with c-axes mostly parallel with the S_2 plane (Fig. 4b). First generation sillimanite disappears in the inner part of the melting zone. The second generation sillimanite occurs as randomly oriented needles on the rims of K-feldspar and cordierite grains, produced in back-reaction (1), between garnet and plagioclase and between garnet and cordierite (Figs 4k-l). Sillimanite needles between garnet and plagioclase were probably produced in the reaction



because granular, recrystallized garnet is sometimes present on old garnet together with second generation sillimanite. Sillimanite needles between garnet and cordierite can be produced by reactions (2), (7) (Fig. 4l) or by



In the andalusite-bearing locality (PSH-88-10 in Fig. 2) in the muscovite zone, fibrolitic sillimanite has crystallized in plagioclase-quartz veins, which are K-feldspar-free. These are in the axial plane of the D_3 fault (NE) and formed during D_3 microfracturing. Sillimanite has replaced plagioclase and quartz in these veins. The process leading to the formation of sillimanite-bearing veins resembles that described by Vernon et al. (1987), who explain sillimanite-bearing veinlets in hornfelses in the contact of a quartz monzodiorite pluton in New South Wales, Australia, as a product of base cation leaching. Fibrolitic sillimanite locally replaces andalusite in the matrix outside the veins, indicating a prograde change.

Andalusite is found in biotite- Al_2SiO_5 symplectites after cordierite (Figs 4a, 4g, 4i). These symplectites are randomly oriented and show no relation to schistosity, indicating that they crystallized after the main phases of deformation (D_2 , D_3). Andalusite also replaces sillimanite (Fig. 4m), occurring as subhedral

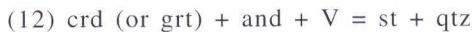
and euhedral grains on biotite rims, where it sometimes forms cross twins. Andalusite inclusions in biotite are rare. The grain size is normally 0.03 - 0.07 mm, but in the muscovite zone there are andalusites up to 0.5 mm in diameter. These andalusites are helicitic, containing quartz and biotite inclusions, and they may be prograde.

Kyanite occurs together with retrograde andalusite and they are difficult to distinguish from each other optically. Kyanite is smaller and it forms elongated prisms whilst andalusite is more quadrate. The amount of kyanite is small, but its existence in several samples from different metamorphic zones was verified by using the heavy liquid separation and X-ray diffraction (the Debye-Scherrer method). No obvious evidence for a phase transformation from andalusite to kyanite was observed, so that the kyanite may have formed by reaction (1) during cooling.

Staurolite is interpreted to be retrograde throughout the study area. In the andalusite-bearing rocks of the muscovite zone staurolite is formed in reaction

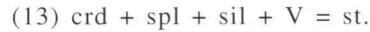


as shown by staurolite and muscovite overgrowing andalusite and biotite (Fig. 4n). In muscovite-absent rocks in the higher grade zones, staurolite was produced by the reaction



as shown by staurolite + quartz-filled cordierite pseudomorphs and small staurolite prisms crystal-

lized on garnet rims (Figs 4o, 4p). Staurolite occurs in all zones except in the inner parts of the melting zone. Spinel inclusions in cordierite have sometimes altered into staurolite in the presence of sillimanite (Fig. 4q). This texture indicates the reaction

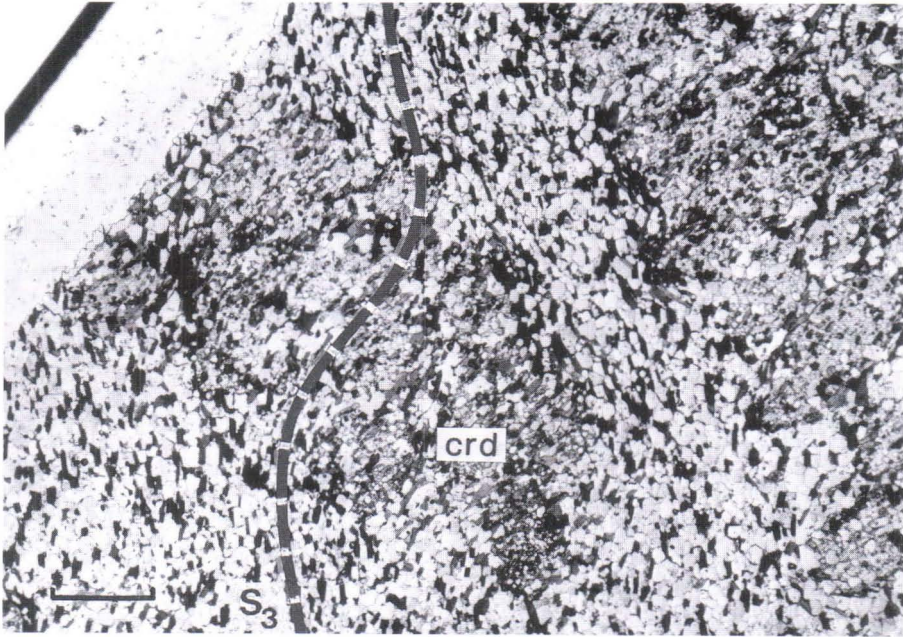


Ilmenite has mostly crystallized on biotite rims, but also occurs as inclusion in garnet. The amount of ilmenite increases as biotite decomposes. In the melting zone at the SE contact biotites have coronas that consist of small ilmenite grains.

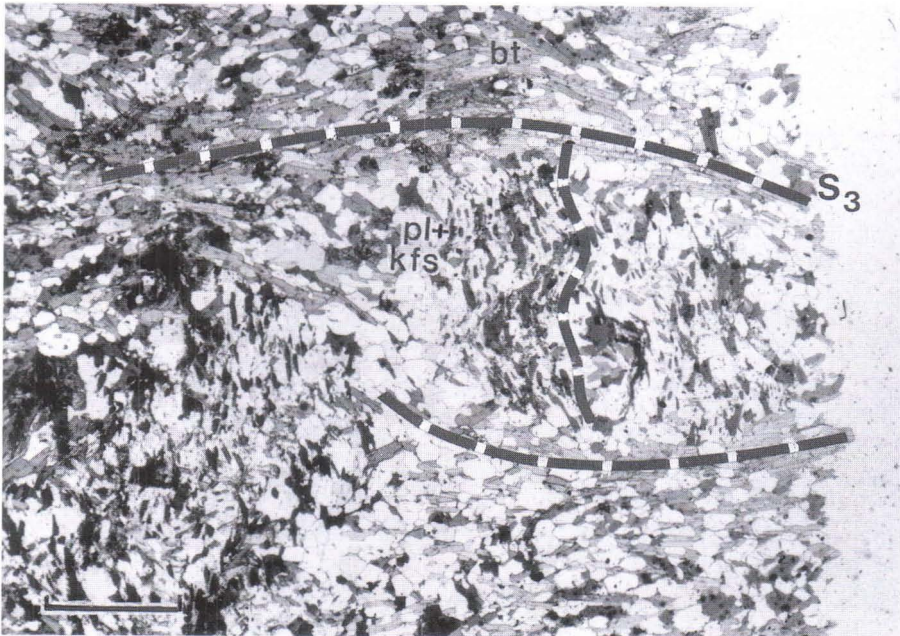
Large K-feldspar porphyroblasts (5-10 mm) with biotite, muscovite and quartz inclusion trails occur in the cordierite-K-feldspar zone. Where the S_3 schistosity is strong, these inclusion trails may be almost perpendicular to S_3 , as are inclusion trails in cordierite (Fig. 5b). Some inclusion trails are crenulated, again indicating growth during early S_3 . In the higher grade zones the matrix K-feldspar often forms symplectitic intergrowths with plagioclase and cordierite. Potassium feldspar was mostly produced during reactions (1) and (2), because it contains biotite and sillimanite inclusions. In the diatexites some K-feldspars attain grain size of 10-15 mm. Potassium feldspar is replaced in some places by muscovite in the reaction



shown by muscovite-quartz symplectites after K-feldspar.



a)



b)

Fig. 5. a) curved inclusion trails in cordierite, indicating growth during early D_3 , garnet-cordierite zone, locality PSH-88-22; b) crenulated biotite inclusion trails in feldspar, cordierite-K-feldspar zone, loc. PSH-88-2.

MINERAL CHEMISTRY

Analytical procedure

Microprobe analyses were carried out by Mr. Lassi Pakkanen at the Geological Survey of Finland using a JEOL-JCXA 733 and CAMECA-CAMEBAX microprobe. The beam width was 10 μm for micas and feldspars and 1 μm

for other minerals. The sample current was 25 nA for micas, garnets and pyroxenes and 15 nA for feldspars and cordierites. The acceleration voltage was 15 kV. Natural standards and the ZAF correction program were used.

Metapelites

Representative analyses of minerals are given in Appendix 1, and the mineral compositions are plotted on the AFM diagrams in Fig. 6. The AFM diagrams also give whole-rock compositions, which do not show wide scatter.

Biotites with lowest Mg-numbers ($\text{Mg}/(\text{Mg}+\text{Fe})$) of 0.47-0.52, are found in the diatexite-stictolite zone, except for some in the orthopyroxene zone at the contact where Mg-numbers are slightly higher, around 0.53-0.54. In other zones the Mg-number ranges from 0.48 to 0.56, and tends to be higher in biotites formed by alteration of cordierite or for those in contact with garnet, compared to those in the matrix. The TiO_2 -content of primary biotites is highest, at approximately 4-5 wt% in the diatexite-stictolite zone, 3-4 wt% in the spinel zone and 2-3 wt% in the other zones. The poorest in Ti are biotites formed by breakdown of cordierite, with TiO_2 values of 0.0-1.8 wt%. In the flecky migmatites biotites are commonly surrounded by an ilmenite corona. With decreasing temperature, Ti solubility in biotite decreases (Shearer & Robinson 1988). During cooling biotite lattices were not able to retain titanium; it was therefore exsolved and ilmenite crystallized on the biotite rims.

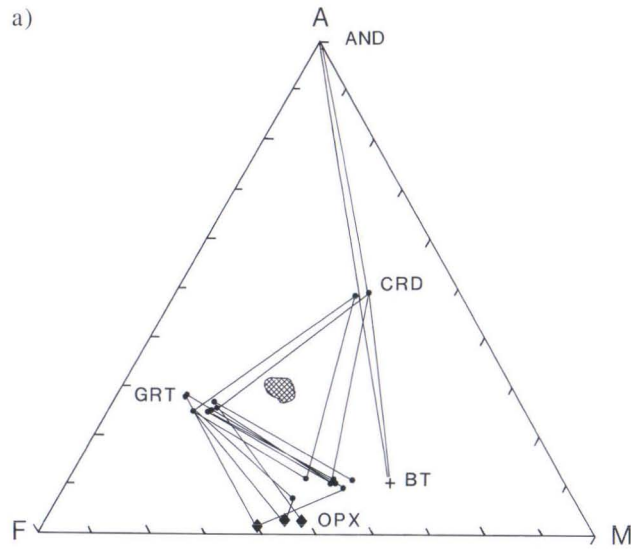
Only a few muscovite analyses were made; these were from the cordierite-K-feldspar and the muscovite zones. Phengite contents are highest in a muscovite coexisting with garnet in a feldspathic rock from the muscovite zone. Muscovite from the cordierite-K-feldspar zone,

where muscovite is supposed to be retrograde, has a significant paragonite component.

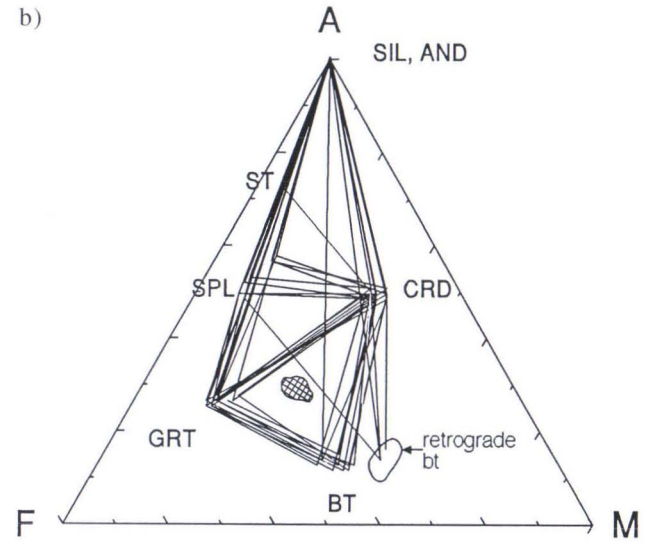
Cordierites in the diatexite-stictolite zone have the lowest Mg-number, from 0.62-0.67. In other zones the Mg-number is slightly higher, between 0.63-0.73. Calcium and alkali contents are low. In the cordierite analyses the sum of oxides is higher in the diatexite-stictolite zone (97-98) than in other zones (95-96), reflecting low water contents in the highest grade area.

Garnet compositions are strongly dependent on the distance from the orthopyroxene granitoid contact. The X_{Mg} ($\text{Mg}/(\text{Fe}+\text{Mn}+\text{Mg}+\text{Ca})$) increases from ca. 0.1 in the muscovite zone to 0.25 in stictolites. The X_{Mn} decreases as a function of the increasing grade, when the amount of garnet also increases (Fig. 7). The X_{Ca} of pelite garnets is low, around 0.03. The pelitic garnets analyzed normally lack the Ca and Mn zoning but there are garnets which have Ca-rich cores. Small garnets also show only weak Mg zoning, but some of the largest garnets exhibit Mg zoning where the X_{Mg} first increases slightly and then decreases from the core to the rim (Fig. 8a). There are also garnets that seem to have altered to cordierite, but these show increasing X_{Mg} toward the rims (Fig. 8b), as could be expected, if Mg was progressively transferred from decomposing cordierite into garnet. This kind of garnet zoning profile in such an assemblage apparently indicates the growth of garnet and cordierite according to reaction (2). Of the garnets

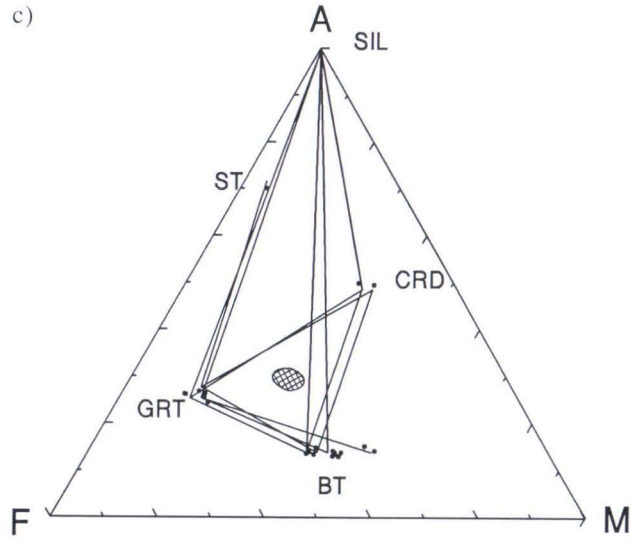
Fig. 6. a)



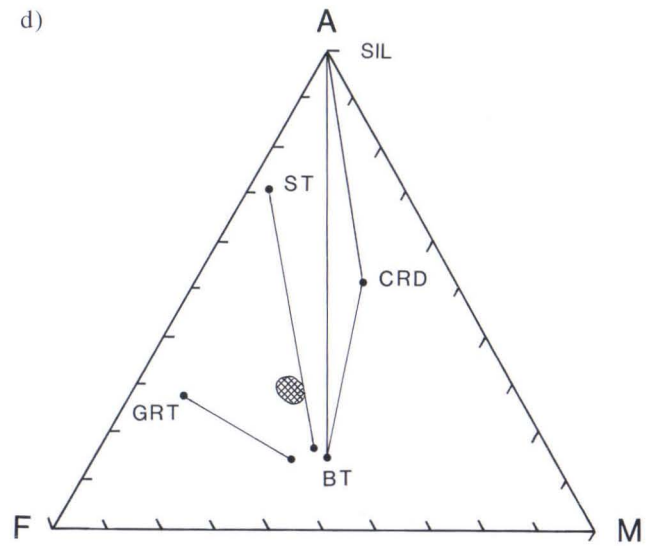
b)



c)



d)



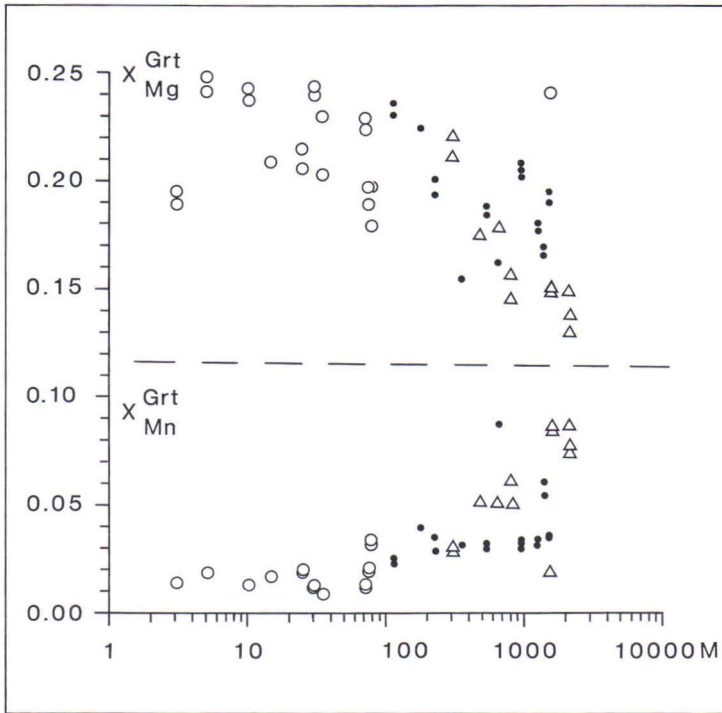


Fig. 7. The change in the X_{Mg} ($Mg/Fe+Mn+Mg+Ca$) and X_{Mn} of garnet with distance from the orthopyroxene granitoid contact. Open dots = diatexite-stictolite zone and 'hot spot', black dots = garnet-cordierite-spinel zone, triangles = garnet-cordierite zone.

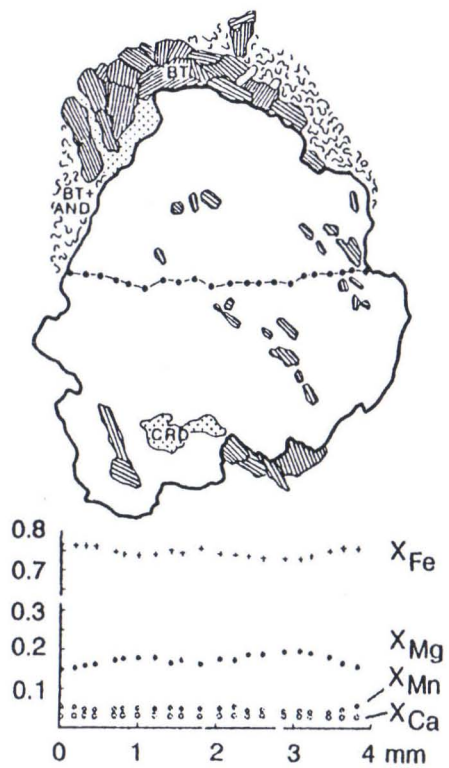
analyzed from stictolite, those that have an inclusion-free rim show increasing X_{Mg} from the core to the rim (Fig. 8c). Wholly poikiloblastic grains are not zoned (Fig 8d).

Spinel is hercynitic and gahnitic (Fig. 9). The hercynitic spinels have Mg-numbers between 0.18 and 0.20, with X_{Zn} ($Zn/Zn+Mg+Fe$) being 0.03 - 0.10. The zincian spinels have higher Mg-numbers, 0.22 - 0.25 and X_{Zn} from 0.17 - 0.27. The highest zinc contents are normally in spinels which break down via reactions (4) and (7) during cooling into gar-

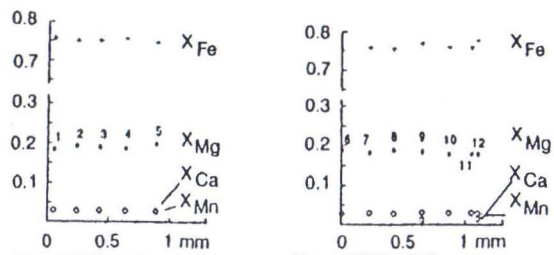
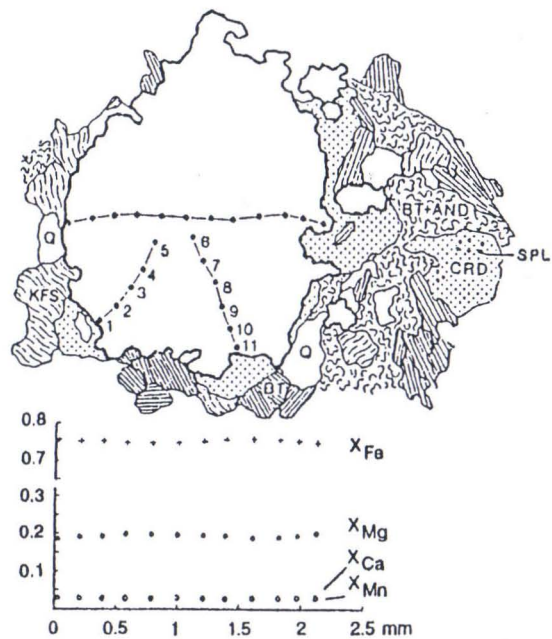
net or Al-silicate and biotite. The X_{Zn} in these spinels increases from the core to the rim. Retrograde breakdown of spinel has enriched Zn in the remaining mineral.

The anorthite content of matrix plagioclases is An_{27-34} , and is independent of metamorphic grade. The composition is approximately the same in the plagioclase inclusions in low calcium garnets. However, in the spinel zone one garnet was analyzed whose plagioclase inclusions had higher anorthite content, ca. An_{40} , than the matrix minerals (ca. An_{35}). The gros-

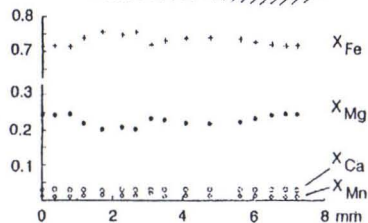
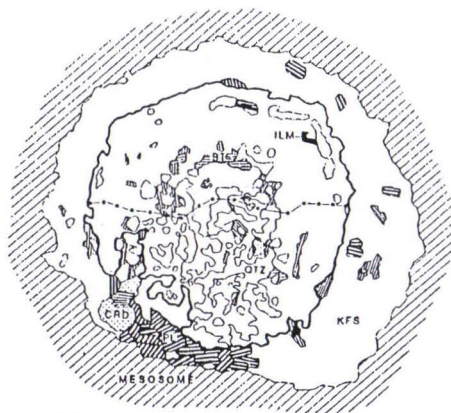
Fig. 6. Mineral compositions presented in the AFM diagrams (K-feldspar projection, A = $Al_2O_3-K_2O$, F = FeO, M = MgO). Coexisting minerals are connected with tie lines. Crosses indicate biotites which are alteration products of cordierites; squares refer to orthopyroxenes. The shaded areas show the range of the whole-rock compositions. a) diatexite-stictolite zone and 'hot spot'; b) garnet-cordierite-spinel zone. High A-values in some spinels may be due to tiny sillimanite inclusions; c) garnet-cordierite zone; d) cordierite-K-feldspar zone.



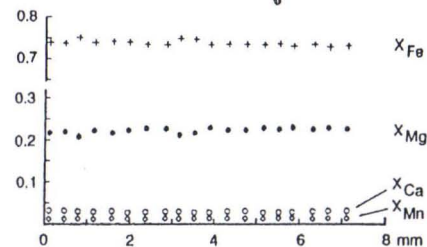
a)



b)



c)



d)

Fig. 8. Zoning profiles of metapelite garnets: a) specimen PSH-88-39 from the garnet-cordierite zone; a weak increase of the X_{Mg} from core to rims suggests growth during heating. A decrease of Mg in the edges of the grain, together with a slight increase of the X_{Mn} is due to decomposition of garnet into a magnesian phase (biotite), in which case Mn enriches in the remaining mineral; b) specimen 27-450-2 from the garnet-cordierite-spinel zone. The garnet is the same as in Fig. 6g. It seems that garnet was altered at the rims into cordierite, but there is a weak increase in the X_{Mg} to the edge. This kind of zoning could be expected if a magnesian phase (cordierite) was altered into garnet. An interpretation is that the right edge of garnet was produced in reaction (8), because there are spinel inclusions in the adjacent cordierite; c) garnet from the melting zone, surrounded by feldspathic mantle, locality 29 (Fig. 2), garnet has an inclusion-free edge where the X_{Mg} increases. There is a drop in the Mg content in the area where the garnet is altered into biotite; d) entirely poikilitic garnet, without zoning, from the melting zone, specimen 24-18.

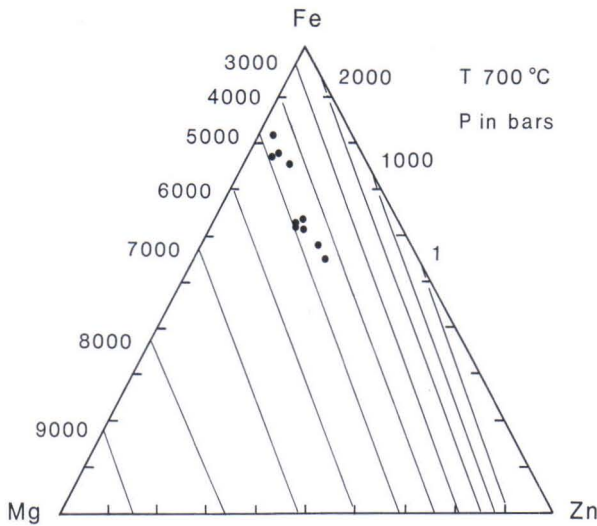


Fig. 9. Compositions of spinels plotted on the Mg-Fe-Zn diagram (cordierite-spinel-quartz barometer of Seifert & Schumacher 1986). The most zincian spinels are those which have altered during retrogression into garnet, staurolite or biotite and Al-silicate.

sular content of this garnet core was also higher than normal ($X_{Ca} = 0.05$). In one case in the garnet-cordierite zone in the eastern part of the study area plagioclase inclusions in garnet had a lower calcium content ($X_{Ca} = 0.26$) than the matrix plagioclases (0.32).

Staurolites are the most magnesian in the garnet-cordierite and garnet-cordierite-spinel zones, where they are produced by reaction (13), the Mg-number being 0.16 - 0.17. In the muscovite zone, where staurolite is produced in re-

action (12), the Mg-number is lower, ca. 0.14. The X_{Zn} ($Zn/Zn+Mg+Fe$) varies from 0.03 to 0.06.

Orthopyroxenes are Al-poor, the X_{Al} (Al/2) being between 0.02 - 0.05. The Mg-number is 0.40 - 0.50.

Ilmenites have the X_{Fe} ($Fe/Fe+Mg+Mn$) between 0.95 and 0.99, an exception being an ilmenite inclusion in a manganese-rich garnet (X_{Mn} 0.35) in the muscovite zone, which has X_{Fe} of 0.85 and X_{Mn} 0.15.

Mafic rocks

Garnets in mafic rocks differ in compositional zoning from those of pelites in that they normally have also Ca and Mn zoning. The X_{Ca} of plagioclase is high, 0.8 - 0.9. In the 'hot spot' area south of the orthopyroxene granitoid (Fig. 2) large garnet from a mafic boudin in metapelite was studied in detail. It displays concentric zoning such that X_{Ca} and X_{Mn} decrease and X_{Mg} increase from the core to the rim (Fig. 10). The garnet has plagioclase inclusions whose X_{Ca} does not differ much from

plagioclases in the matrix, with the exception of a few grains in which lower X_{Ca} is probably caused by a retrograde breakdown to carbonate (Fig. 10b). The garnet has also cumingtonite inclusions with Mg-numbers of 0.44 - 0.46 in the core of the grain, increasing to 0.48 when the X_{Mg} of the host garnet starts to increase (Fig. 10a). Garnet broke down from rims into plagioclase_{An 84-91} and orthopyroxene_{Mg 39-40} (Figs. 10a,b).

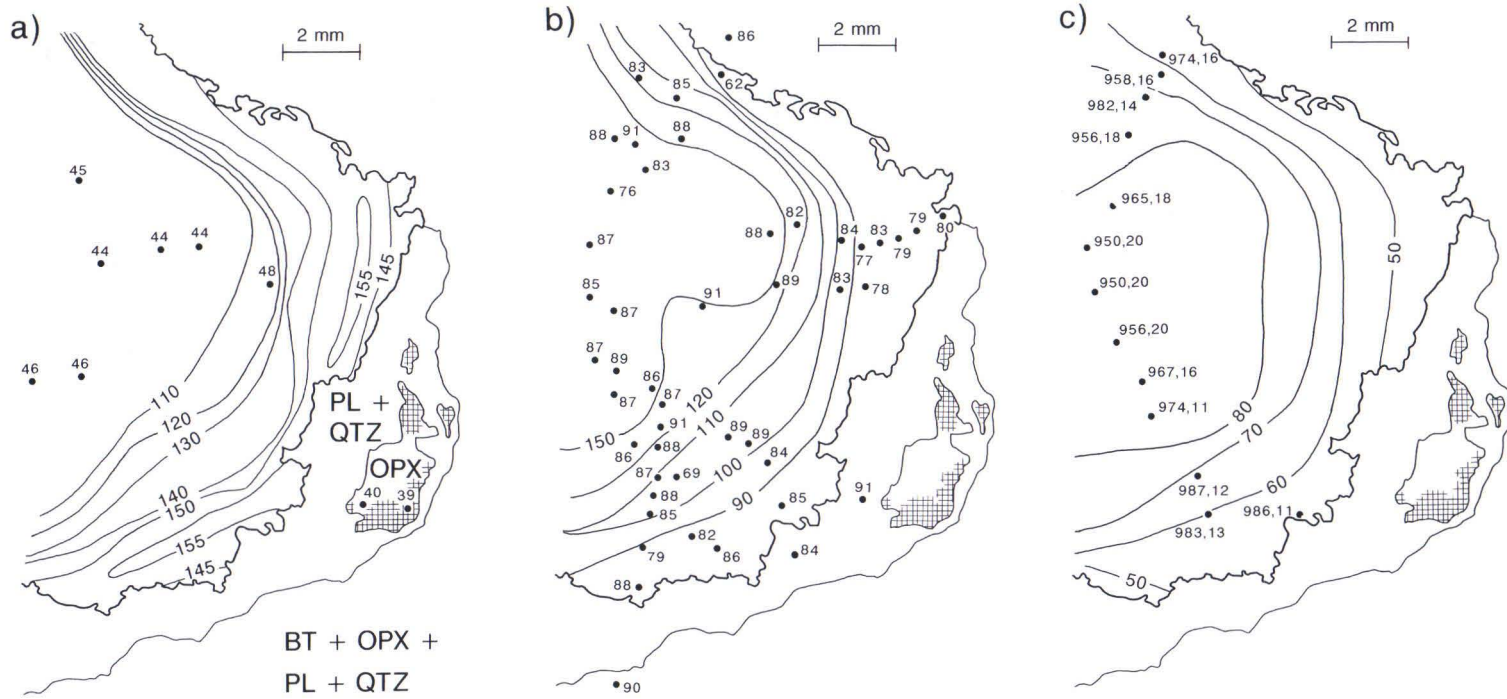


Fig. 10. Zoning profiles of a garnet from metabasite boudin in the 'hot spot' (assemblage in the rock is grt-opx-bt-pl-qtz-ilm), specimen PSH-88-4, based on 340 analysis points; a) contours for garnet $X_{Mg} \times 1000$, small numbers close to the dots are for the Mg-number $\times 100$ of cummingtonite inclusions; b) contours for garnet $X_{Ca} \times 1000$, small numbers for $X_{Ca} \times 100$ of plagioclase inclusions; c) contours for garnet $X_{Mn} \times 1000$, small numbers for $X_{Fe} \times 1000$ and $X_{Mn} \times 1000$ of ilmenite inclusions ($X_i = i/Fe + Mn + Mg$).

ANATEXIS

Migmatites can be formed by different mechanisms, including subsolidus differentiation, metasomatic processes, injection of granitoid magmas and partial melting. Of these, partial melting is believed to be the most important process for forming neosomes (Johannes 1988). The anatexitic behaviour of most rocks can be related to the experimentally determined melting reactions of quartz-feldspar mixtures. Melting processes are controlled mainly by temperature, proportions of quartz, alkali-feldspar and plagioclase and the availability of free water in the rock. If there is no free water, rocks undergo dehydration melting where micas break down into H_2O -undersaturated silicate liquid and anhydrous solids (Thompson 1982, 1988, Grant, 1985). Dehydration melting is capable of producing significant amounts of melt at high temperatures only (Holtz & Johannes 1994).

In the Vaaraslahti rocks, various mechanisms have been involved in the formation of leucosomes and anatexitic melts. This has been determined on the basis of the leucosome mineralogy and textures.

In the cordierite-K-feldspar, garnet-cordierite and garnet-cordierite-spinel zones, leucosomes are mostly narrow granitic pods and veinlets which constitute ca. 10 - 15 % of the rock and which precede the D_3 faulting (Fig. 3a). In the diatexite-stictolite zone rocks exhibit evidence of partial melting, which at the SE margin of the intrusion produced garnetiferous felsic segregations (Figs 3b and 11c) and, along shear zones near the granite contact, diatexites, which have randomly oriented metapelite and metabasite fragments and garnet xenocrysts but no distinguishable leucosomes (Figs. 11b and 11d). This rock type is called diatexite, which is defined by Jones & Brown (1990) as a migmatite produced by moderate to high degrees of partial melting which exceeds the rheologically critical melt percentage and results in the disruption of

migmatitic and pre-migmatitic structures.

In the area southeast of the orthopyroxene granitoid, beginning from the muscovite zone, metagreywackes contain granitic pods which are mostly associated with the D_3 faulting. In the axial plane of the D_3 faults, medium-grained granitic veins are common, and cut and brecciate the layers (Fig. 11e). These veins are muscovite- and biotite-bearing in the muscovite zone, the modal amount of hydrous phases being up to ca. 5 %. In the higher grade zones granitic veins may contain garnet but only rare biotite. This indicates either of the higher amount of available water in shear zones, which promoted melting already in relatively low temperatures, or simply that shear zones were channelways for granitic melts. With increasing temperature H_2O -undersaturated liquids with anhydrous solids were the main melting products, except the biotite-rich diatexite near the contact.

The lithological composition of the diatexite-stictolite zone nearest the contact differs between the SE and SW margins of the intrusion.

Next to the contact on the SE margin a garnetiferous nebulitic migmatite is present for up to 5 - 35 meters from the contact (Fig. 11a). Garnets are ca. 1 - 5 mm in diameter, and commonly occur in the felsic part of the rock. There are also garnetiferous porphyritic granite pods in the migmatite. Beyond the nebulitic zone there is a flecky migmatite, 15 - 50 m thick, containing abundant leucocratic segregations, with garnets up to 10 - 20 mm in size (Figs 3b and 11b). These segregations locally develop into veinlets that may disrupt the layering (Fig. 11c). Most of the garnetiferous segregations and veins formed during the development of the D_3 faulting and schistosity (Fig. 3b, c), although it is possible that D_3 has reoriented some earlier segregations. Garnet also overgrows the $S_0+S_1+S_2$ schistosity in banded mesosomes.

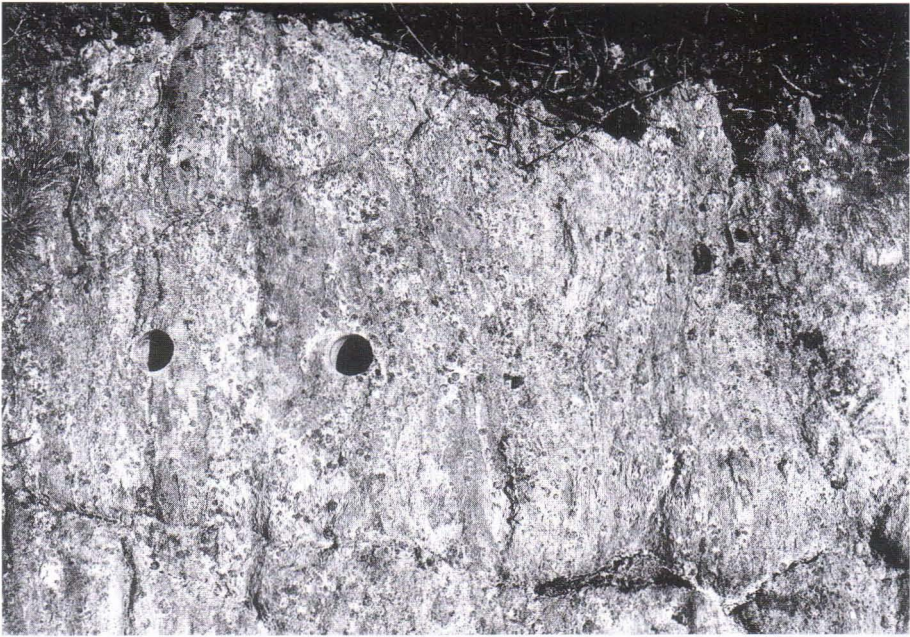


Fig. 11a)

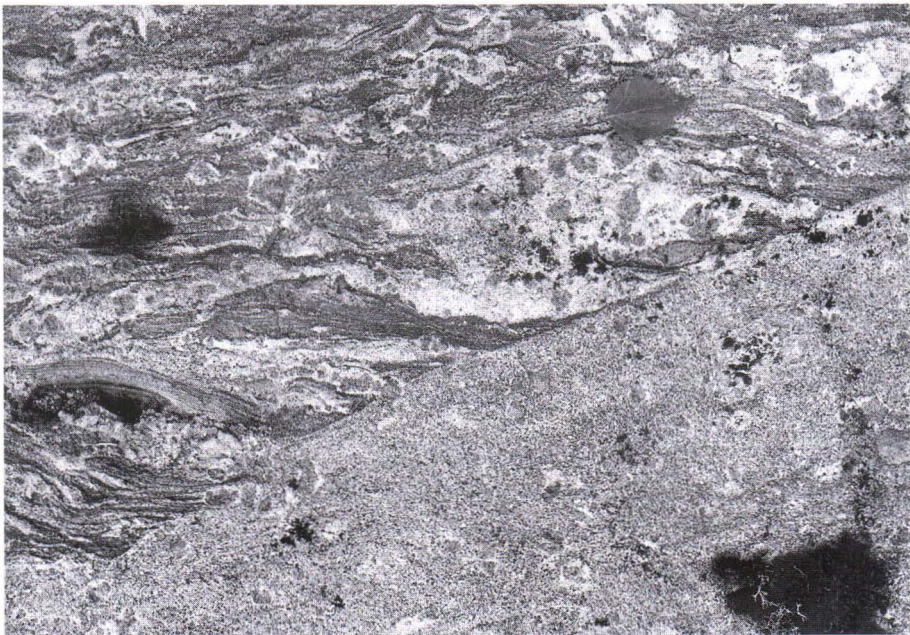


Fig. 11b)



Fig. 11c)



Fig. 11d)

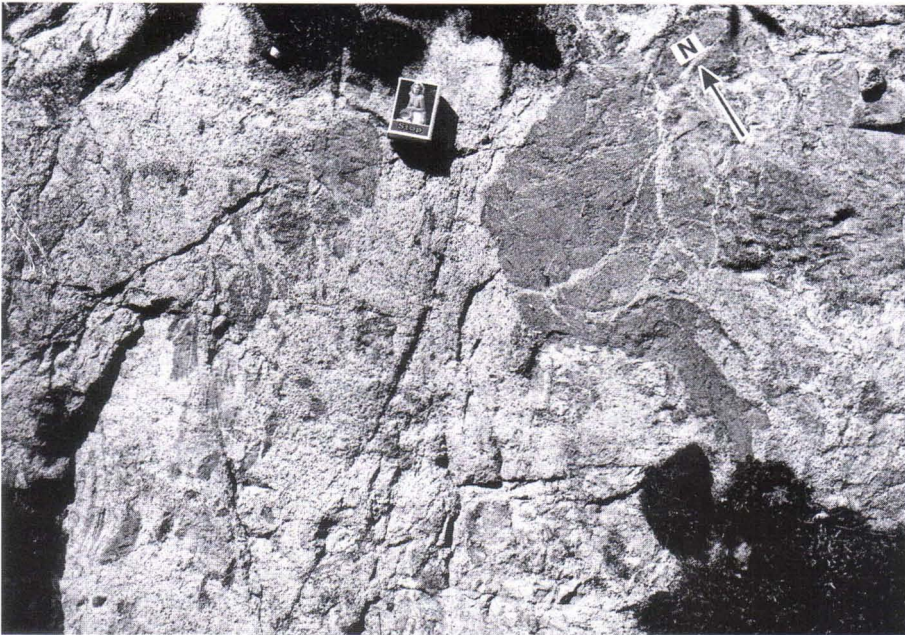


Fig. 11e)

Fig.11. Migmatite structures: a) nebulitic migmatite at the SE contact, loc. 29; b) diatexite cutting flecky migmatite in the melting zone, loc. 24-5; c) garnetiferous segregations developed into veins, loc. 29; d) diatexite c. 140 metres from the orthopyroxene granitoid contact, loc. 29; e) brecciating granite from the muscovite zone, loc. PSH-88-10.

Diatexite, which cuts the flecky migmatite, contains many large garnet xenocrysts which often have retained felsic mantles (Fig. 11b). Further from the contact the grain size of garnet in diatexite is smaller and felsic haloes do not occur. On the southwestern margin, there

is no flecky migmatitic layer next to the contact, only diatexite, which is, however, coarser grained than on the SE margin. Feldspar crystals up to 1 cm in diameter are common and the foliation is weak or absent.

Melting textures in the diatexite-stictolite zone

Garnets surrounded by quartzo-feldspathic mantles have been described from several high-grade regions, where they are mostly interpreted as a product of dehydration melting (Tracy & Robinson 1983, Waters & Whales 1984, Stüwe & Powell 1989, Powell & Downes 1990).

The occurrence of abundant crystal faces in feldspars and cordierites in leucosomes is considered as evidence of former melt, because

these minerals do not generally grow crystal faces in metamorphic rocks. Preservation of igneous microstructures requires a lack of penetrative deformation during or after the melting (Vernon & Collins 1988, Vernon & al. 1990).

At Vaaraslahti, the preferred orientation is weak or absent in feldspathic mantles surrounding garnets. In K-feldspar-rich portions alkali feldspar crystals can have crystal faces

against quartz (Fig. 12a). Idiomorphic cordierites, sometimes with sector twinning (Figs. 12b and 4c), are also common. In the presence of plagioclase, K-feldspar is often interstitial between euhedral plagioclase grains (Fig. 12c). The amount of interstitial quartz (Fig. 12e) is small in the feldspathic mantles but in contrast there are many quartz inclusions in the poikilitic garnet grains (Figs 8c-d). K-feldspar and cordierite sometimes have a core with biotite and quartz inclusions (Figs 4c, 12e). If the mesosome contains abundant K-feldspar the segregation is also rich in K-feldspar, often being syenitic (Table 2). These features may be due to the slower nucleation rate of quartz compared to other minerals and to the nucleation of feldspars and cordierites on incompletely melted, pre-existing grains. Almost complete dissolution of quartz in the melt, indicated by the absence of quartz in mesosomes, leaves very few unmelted nuclei on which to crystallize (Vernon & Collins 1988). Because quartz is dissolved in the melt in larger amounts than other minerals, and if there is some melt loss, it is likely that silica is removed from the segregations more easily than other constituents and is retained only within inclusions in the growing garnet grains.

McLellan (1983) and Ashworth & McLellan (1985) have developed a method for studying anatexis on a textural basis. A random distribution of minerals is likely to develop if minerals are crystallized from melt or from hydrothermal fluid. Metamorphic segregation is characterized by aggregate distribution, because solid state nucleation is controlled by pre-existing crystals. A dispersed distribution, with few contacts between grains of the same mineral phase, characterizes high grade metamorphic rocks affected by annealing, which tends to destroy the high-energy contacts between grains of the same minerals. Possible differences in the textural maturity of mesosomes and leucosomes can provide evidence for post-annealing migmatization (McLellan

1983).

McLellan (1983) used the line-transect method of Kretz (1969) and the χ^2 independence test (e.g. Vasama & Vartia 1973) to study the randomness of distribution. In the feldspathic mantles around garnets in the Vaaraslahti aureole, the quantitative textural analysis shows an aggregate distribution with high χ^2 values (Table 3). Plagioclase often occurs in almost monomineralic aggregates, where the size of plagioclase grains is considerably smaller than that of the coexisting alkali feldspars (Fig. 12d). Because textures indicate the presence of melt, the aggregate distribution can be explained by the growth of minerals on pre-existing unmelted nuclei. At low fluid: rock ratios, which are likely during dehydration melting, growth can be epitaxial on pre-existing minerals (McLellan 1983). The observed: expected ratio of contacts between grains of the same minerals is high in leucosomes but also in some mesosomes and in diatexites, which indicates the lack of annealing after melting.

Although the diatexite contains many xenocrysts from the migmatite, the rock texture is hypidiomorphic. Rectangular and sector-twinning cordierites are common, and feldspars have crystal faces against quartz (Fig. 12f). Plagioclase rims are often myrmekitic. The amount of potassium feldspar is less in diatexite than in the flecky migmatite. Triple junctions of cordierite-quartz-feldspar and garnet-quartz-feldspar are common. These textural features indicate that garnet and cordierite were in equilibrium with the melt. Diatexite cuts the segregation-bearing migmatite (Fig. 11b), and is therefore younger, but the age difference is not necessarily great, because both migmatite types developed during the D_3 . The amount of melt, and the amount of water in the melt, produced along the shear zone at the contact were probably larger than in the segregation-bearing rock, resulting in the generation of biotite-bearing diatexite.

Fig. 12a)

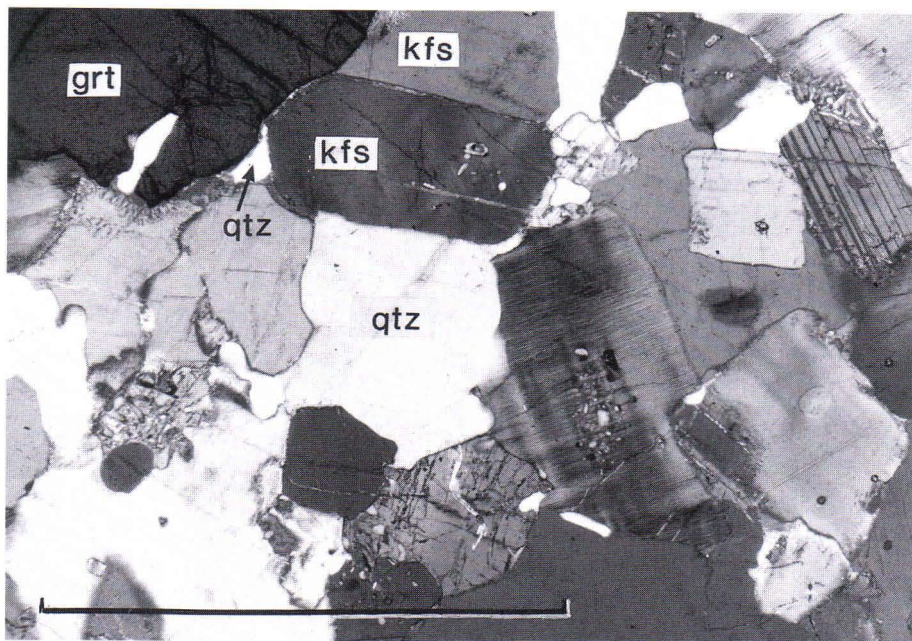


Fig. 12b)

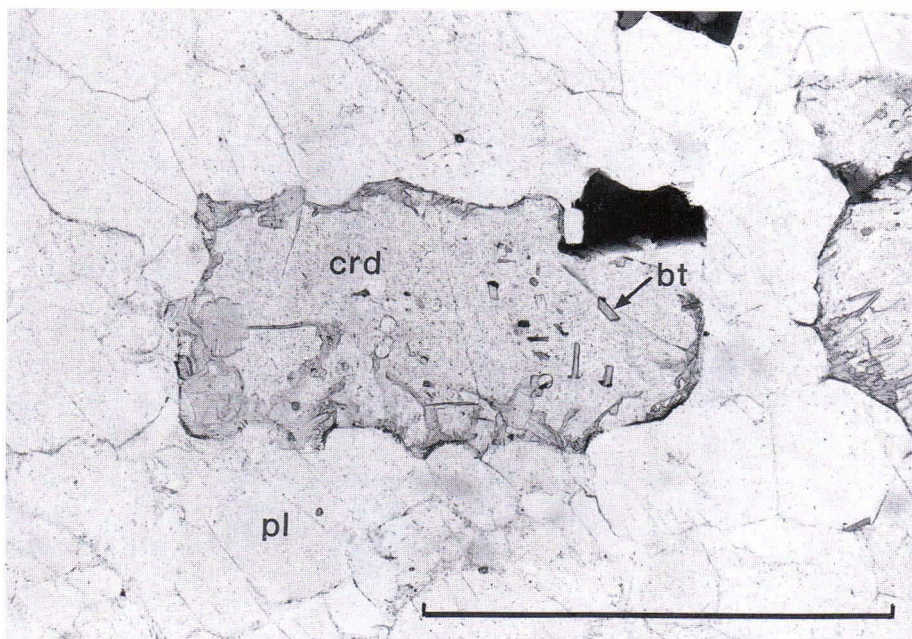


Fig. 12c)

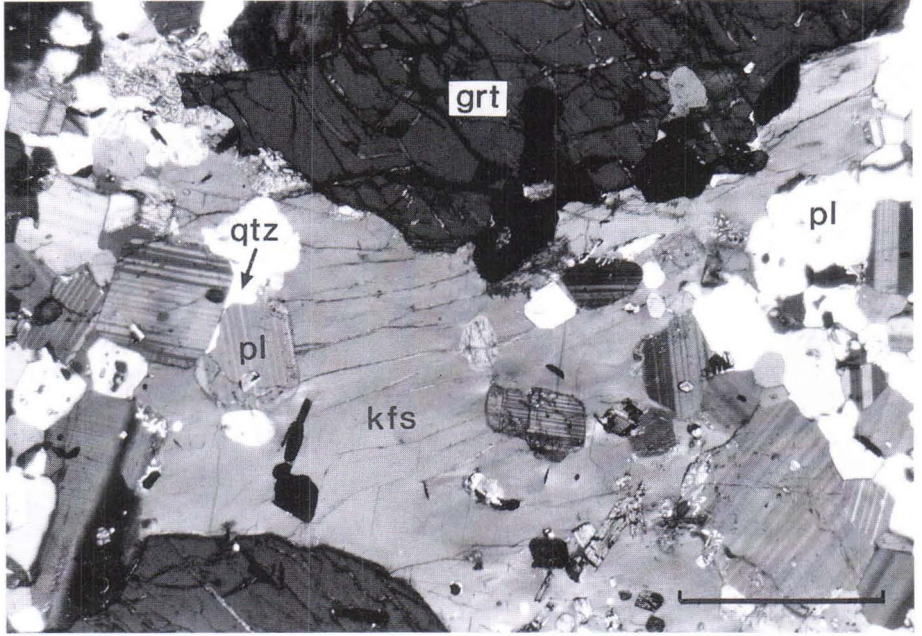


Fig. 12d)

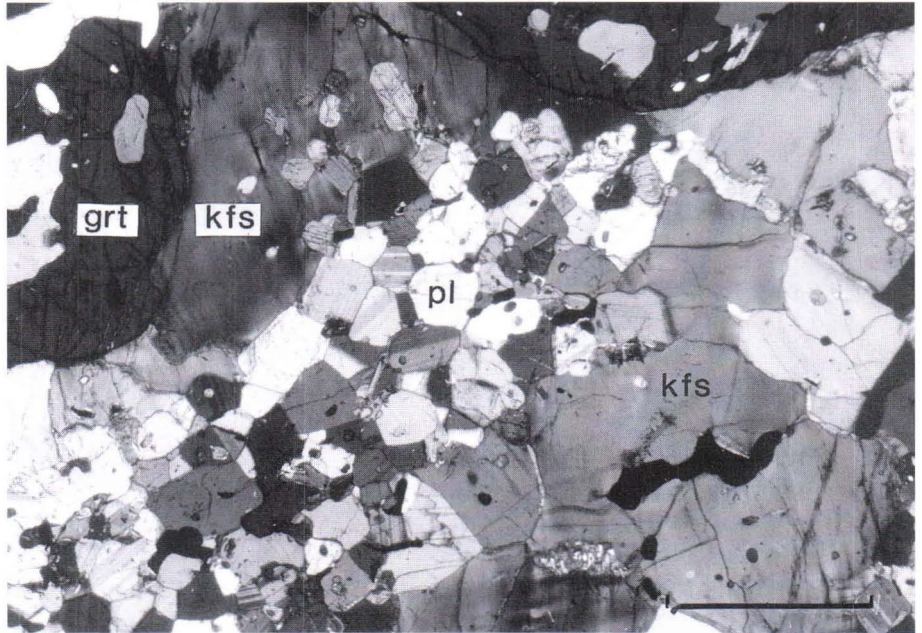


Fig. 12e)

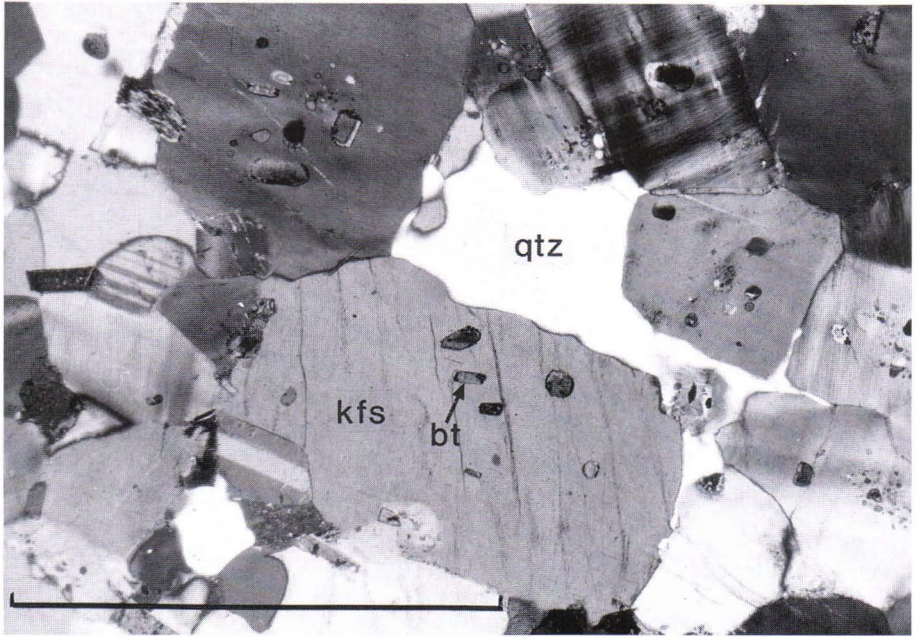


Fig. 12f)

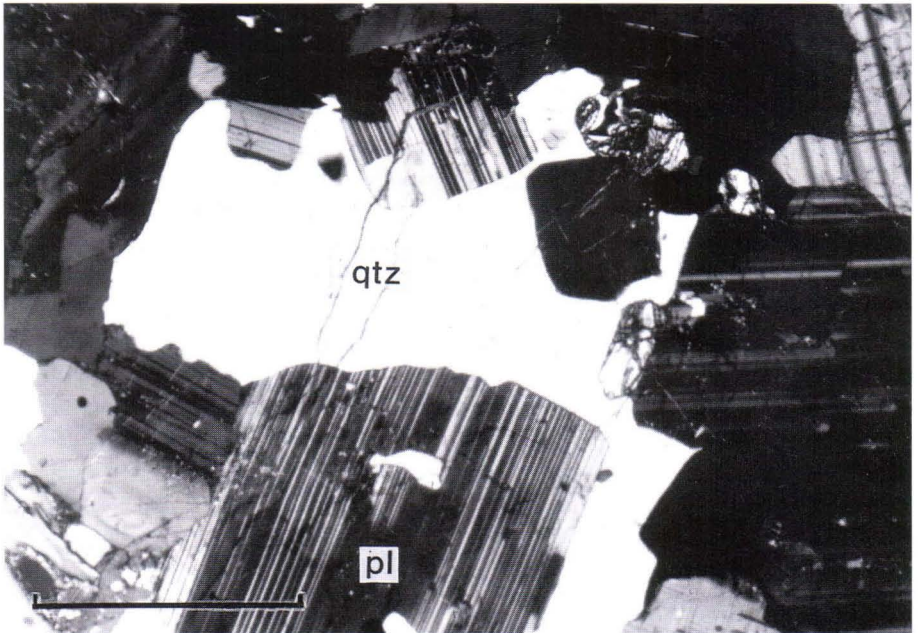


Fig. 12. Microstructures in felsic segregations and diatexite in the diatexite-stictolite zone; a) crystal faces of K-feldspar against quartz; b) rectangular cordierite; c) interstitial K-feldspar between idiomorphic plagioclase crystals and garnet; notice the weak concentric zoning in a plagioclase on the left side of the photomicrograph; d) an aggregate of plagioclase grains, surrounded by K-feldspars; e) small biotite inclusions in K-feldspars and interstitial quartz between feldspar crystals; f) crystal faces of plagioclase against quartz, diatexite on the SW contact of the orthopyroxene granitoid.

Table 3. Textural analyses of diatexite-stictolite zone rocks. Q = quartz, P = plagioclase, K = K-feldspar, B = biotite, C = cordierite, M = cordierite, garnet. L/L = average observed:expected ratio for contacts between the same minerals; L/U = average observed:expected ratio for the contacts between different minerals. $\nu = 9$: $\chi^2_{0.05} = 16.92$, $\chi^2_{0.01} = 21.67$, $\chi^2_{0.001} = 27.88$; $\nu = 16$: $\chi^2_{0.05} = 26.30$, $\chi^2_{0.01} = 32.00$, $\chi^2_{0.001} = 39.25$.

Sample	Phases	n	ν	χ^2	χ^2/ν	Observed:expected																Specimen type		
						Q/Q	P/Q	K/Q	B/Q	C/Q	P/P	K/P	B/P	C/P	K/K	B/K	C/K	B/B	C/B	C/C	L/L		L/U	
19-1-PSH-86	Q,P,K, B,C	245	16	202.7	12.67	1.24	2.48	2.15	1.51	2.31	1.89	1.00	2.10	1.75	2.10	3.54	1.13	0.00	4.28	1.37	1.32	2.30	feldspathic mantle on garnet	
19-1-PSH-86	Q,P,K, B,C	566	16	513.0	32.06	0.00	1.50	0.00	2.31	2.10	2.72	3.49	2.10	1.79	0.00	1.80	2.10	0.62	2.95	1.29	0.92	1.97	mesosome	
29-45-1	Q,P,K, B,C	588	16	504.67	31.54	0.00	0.00	0.00	1.98	4.19	2.17	2.38	2.20	1.54	6.37	1.70	1.41	0.90	3.19	1.24	2.14	2.13	mesosome	
						Q/Q	P/Q	K/Q	M/Q	P/P	K/P	M/P	K/K	M/K	M/M	L/L	L/U							
19-1-PSH-86	Q,P,K, M	419	9	282.07	31.34	1.47	2.00	2.07	2.73	2.34	1.03	2.08	3.86	1.42	1.32	2.25	1.92						cordierite-bearing leucosome	
						Q/Q	P/Q	K/Q	B/Q	M/Q	P/P	K/P	B/P	M/P	K/K	B/K	M/K	B/B	M/B	M/M	L/L	L/U		
24-39	Q,P,K, B,M	652	16	402.07	25.13	0.98	2.36	1.56	2.35	2.83	1.60	2.58	2.30	1.93	1.93	1.98	2.52	1.35	1.55	0.82	1.34	2.14	diatexite	
26-130-2	Q,P,K, B,M	293	16	282.10	17.63	0.72	2.67	1.90	2.50	2.37	1.66	0.73	2.41	2.16	11.4	0.56	0.56	0.19	2.52	1.18	3.02	1.96	diatexite	

GEO THERMOMETRY AND GEOBAROMETRY

Temperatures and pressures were calculated using the program GEOPATH by Gerya & Perchuk (1992), which uses internally consistent thermodynamic data. Thermometers used were garnet-biotite, garnet-cordierite, garnet-spinel, cordierite-spinel, garnet-orthopyroxene and biotite-orthopyroxene. Barometers were cordierite-sillimanite-garnet-quartz (CAGS) and cordierite-spinel-quartz. In addition, pressures were calculated with the garnet-plagioclase-sillimanite-quartz (GASP) barometer of Koziol & Newton (1988), the garnet-biotite-muscovite-plagioclase barometer (GPBM) by Hodges & Crowley (1985) and the garnet-orthopyroxene-plagioclase-quartz (GAFS) barometer by Essene (1989). Pressures and temperatures during the growth of the large garnet in Fig. 10a were estimated using the garnet-ilmenite thermometer of Pownceby et al. (1987), and the thermodynamic TWEEQU software (Berman 1988, 1990, 1991). The results are presented in Appendix 3 and in Fig. 13.

In the garnet-biotite thermometry, the compositions of garnet cores and biotites not in contact with garnet were used to estimate the peak temperatures. The averages of garnet-biotite and garnet-cordierite (in brackets) temperatures are 547°C in the muscovite zone, 624°C in the cordierite-K-feldspar zone, 640°C (631°C) in the garnet-cordierite zone, 650°C (623°C) for the garnet-cordierite-spinel zone and 696°C (715°C) for the diatexite-stictolite zone.

The garnet-biotite and garnet-cordierite temperatures should be treated with caution because of the strong rehydration and possible cation exchange during cooling. The cordierite hydration reaction (1) that produced biotite and Al-silicate (sil, and, kya) was very prominent, and during that reaction cordierite and biotite compositions become more magnesian (Thompson 1976a). Disequilibrium is indicated by a large difference between grt-crd and grt-bt temperatures in some speci-

mens, e.g. sample PSH-88-24.1a (Appendix 3), where the garnet-cordierite temperature is almost 100°C lower than the garnet-biotite temperature. Garnet-spinel temperatures are unrealistically high, which may be caused by the retrograde net-transfer reaction (4) and exchange between cordierite and spinel during cooling, which is also indicated by low crd-spl temperatures.

The garnet-orthopyroxene thermometer gave temperatures between 680° and 750°C for the melting zone and 'hot spot' when the compositions of garnet and orthopyroxene after garnet were used. In cases where there are small garnets on orthopyroxenes the calculated temperatures are considerably lower, ca. 570°C (sample 25-15-2 in Appendix 3). The biotite-orthopyroxene temperature for the same specimen is 826°C, which is evidence for late garnet growth.

The calcium zoning in garnets in metapelites is normally weak (Fig. 8) and the core compositions of minerals in contact with each other were used in the grt-pl-sil-qtz (GASP) barometry. Where garnet had plagioclase inclusions, also the composition of the inclusion and an analysis point in garnet next to the inclusion were used in the calculation. Estimated temperatures were used in GASP calculations instead of solving the barometer equation simultaneously with the garnet-biotite thermometer, because of the possible retrograde effects on thermometry. The GASP pressures are close to the crd-sil-grt-qtz (CAGS) pressures. The averages of the GASP (CAGS in brackets) pressures are 4.3 (4.0) kbars in the garnet-cordierite and garnet-cordierite-spinel zones and 5.3 (5.1) kbars in the melting zone. The KD:s of the GASP reaction are approximately the same in all zones.

When plagioclase inclusions in garnet are used, the GASP pressures in the garnet-cordierite zone are ca. 1 kbar higher than pressures calculated using matrix plagioclases (Appen-

dix 3), if the same temperature is used in the calculation. This also holds true for garnets that have calcium-rich cores. If the calcium distribution between garnet and plagioclase in these rocks is mainly controlled by the reaction $\text{an} = \text{grs} + \text{sil} + \text{qtz}$, a lower temperature or higher pressure during the early garnet growth is a possible explanation for this kind of calcium distribution between garnet and plagioclase inclusions.

The spinel barometer of Seifert & Schumacher (1986) gives consistent results with the GASP barometer, at 4.4 - 4.9 kbars (Fig. 9). The zincian spinels, for which the high gahnite component was interpreted as the result of retrogression, give the same pressure as other spinels. This indicates compositional changes under isobaric conditions.

The garnet-orthopyroxene-plagioclase-quartz barometer (GAFS, Fe-reaction because the phases are iron-rich) gives pressures of 4.4-4.7 kbars ($\log K = 2.2-2.4$), when the compositions of garnet and orthopyroxene after garnet are used in the calculations. When using the compositions of small garnet grains on orthopyroxene, temperatures are around 570°C, but the $\log K$ of the GAFS reaction remains close to 2.2, giving a pressure of 3.0 kbars. This indicates an uplift of ca. 6-7 kilometres during cooling by 150-200°C. These garnets are, however, small and their compositions may have been changed by late diffusion, so that they may record somewhat lower pressure than that during the net transfer reaction (7), through which they formed.

The compositions of inclusions in garnet have been used to construct the PT path during garnet growth (e.g. St. Onge 1987), provided that the compositions of possible pre-peak inclusions did not change during the metamorphic maximum or cooling. In the 'hot

spot' area there are large (>10 mm in diameter) garnets in basic boudins in migmatite that contain abundant plagioclase, ilmenite, biotite, quartz and apatite inclusions, as well as sporadic cummingtonite, K-feldspar and carbonate. The matrix assemblage is bt-opx-pl-qtz-ilm-cm and garnet rims have plagioclase-orthopyroxene coronas on rims. The zoning of one such garnet and the compositions of its plagioclase, cummingtonite and ilmenite inclusions are presented in Fig. 10. The garnet-ilmenite temperatures for the garnet core, using the inclusion data, are ca. 615 - 625°C (Appendix 3). Towards the rims the garnet-ilmenite temperatures first decrease and then increase again. Although some calculated temperatures are unrealistically low, this trend is similar to that observed in a large garnet in the nearby Pielavesi granulite block (Hölttä 1988). The temperatures and pressures for the growth of garnet core and rim, using both the amphibole and plagioclase inclusion data and compositions of orthopyroxene and plagioclase on the garnet rim, were also calculated with TWEEQU software (Berman 1988, 1990, 1991), using Berman's own and Holland & Powell's (1990) data sets. The results are presented in Fig. 13, and show a higher pressure of ca. 1-1.5 kbars for the growth of the garnet core. The interpretation of cummingtonite inclusions as prograde relics is supported by the fact that cummingtonite is abundant in lower grade mafic rocks. In the matrix surrounding garnets in the analysed specimen cummingtonite is present as a rather rare alteration product of orthopyroxene, which occurs never as inclusions in garnet. The effect of the possible later Fe-Mg exchange between garnet and amphibole is reflected mainly in the calculated temperature but does not influence pressure appreciably in those reactions employed by TWEEQU.

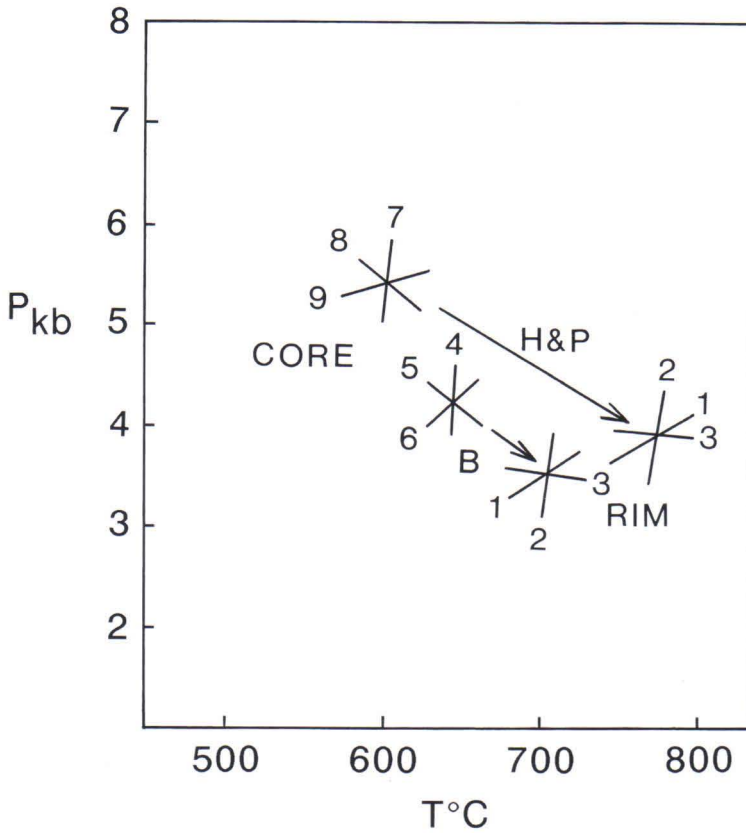


Fig. 13. Pressures and temperatures, calculated with the TWEEQU, for cores and rims for garnet PSH-88-4.3. H&P: calculated using the Holland & Powell (1990) data set; B: calculated using Berman's own data set. Reactions are:
 1. $3qtz + grs + 2alm = 3an + 3fs$
 2. $3en + 2alm = 3fs + 2prp$
 3. $grs + 2prp + 3qtz = 3en + 3an$
 4. $3tr + 5alm = 5prp + 3Fetr$
 5. $27qtz + 10prp + 11grs + 6W = 21an + 6tr$
 6. $27qtz + 10alm + 11grs + 6W = 21an + 6Fetr$
 7. $7alm + 3cum = 7prp + 3gru$
 8. $27qtz + 14prp + 7grs + 6W = 21an + 6cum$
 9. $27qtz + 14alm + 7grs + 6W = 21an + 6gru$

DISCUSSION

Pressure-temperature- a_{H_2O} grids and the P-T path

Reactions described above were placed on the PT diagrams in Fig. 14 by using the program THERMOCALC (Holland & Powell 1990) and representative compositions of minerals. The granite melting curve is from Thompson (1982) and the biotite dehydration melting curve from Le Breton & Thompson (1988).

From Fig. 14 it can be concluded that the initial water activity must have been rather high close to the D_3 shear zones in the muscovite zone, where melting had begun before muscovite and biotite decomposition (if e.g. the granite in Fig. 11e represents in situ melt-

ing and not coming from deeper sources through the shear zones). The lowered water activity is a possible explanation for many of the reactions observed at the garnet-cordierite and garnet-cordierite-spinel zones. The spinel-producing biotite breakdown reaction (6) is more dependent on the water activity than reaction (1), so, by lowering the a_{H_2O} , the temperature difference between these two reactions becomes smaller at fixed pressure and compositions. This is in accordance with the fact that geothermometers show a difference in temperature of only about 30°C between the cordierite-

K-feldspar zone and the garnet-cordierite-spinel zone. A reason for slowly increasing temperature could also be the univariant reaction (2) $bt + als + qtz = grt + crd + kfs + melt$, which buffered the temperature increase. In the diatexite-stictolite zone no primary sillimanite remains and the temperature was thus able to increase.

Therefore, an explanation for the appearance of spinel in reaction (4) may be lowered water activity towards the pyroxene granitoid. This is attributed to initial partial melting in pelitic rocks or the granitoid itself, because H_2O is strongly partitioned into silicate melts (c.f. Powers & Bohlen 1985). The formation of garnet and sillimanite from spinel and cordierite (reaction 8) might be result of either cooling or the continuing decrease in water activity (Fig. 14b). The water activities in fluid, calculated with the GEOPATH, are mostly less than 0.4 in the garnet-cordierite-spinel and garnet-cordierite zones, except for the specimen farthest from the contact, but higher than 0.4 in the diatexite-stictolite zone, where spinel is rare. Another explanation for the appearance of spinel is the whole rock zinc content, which shifts spinel-forming reactions to lower temperatures (Montel et al. 1986, Hand et al. 1994).

The release of water from the solidifying granitoid body has enhanced melting, and may also have been responsible for the disappearance of spinel in the inner part of the diatexite zone. However, a more plausible cause may be intensive biotite melting, which would have first consumed all sillimanite in the rock, after which melting reaction would have continued, consuming in the process another aluminous phase, which in this case was spinel.

The decrease in grossular content and increase in pyrope content towards the edges in the large garnet PSH-88-4.3 (Fig. 10) suggests that the rim crystallized at a lower pressure than the core. Because these kind of zoning profiles are not present in garnets in pelites (although there are a few garnets with

relatively Ca-rich cores), and because garnet is already present in mafic rocks in the muscovite zone, the garnet interiors can be interpreted as representing an earlier stage of metamorphism than the biotite breakdown reaction (2), attributed to the contact metamorphism and which produced most garnets in pelites. Evidently there were two metamorphic events, the first taking place in the muscovite field and at a slightly higher pressure than the second, which was caused by pyroxene granitoids after some decompression and which was in turn followed by cooling with minor uplift.

Barometers show a difference of ca. 1 kbar in crystallization pressure between the diatexite-stictolite zone and the garnet-cordierite zone in Vaaraslahti. This can be explained by uplift during the emplacement of the orthopyroxene granitoids, the heat flow from the cooling pluton to the surrounding pelites taking place during exhumation, and the contact metamorphic effect reaching the points farthest from the contact relatively late (Norton & Knight 1977, Peacock 1989). However, this assumption is based only upon thermobarometry, which may have been affected by retrograde phenomena, especially in the case of relatively small garnets in the garnet-cordierite zone farthest from the contact. The contact metamorphic heating was more probably near-isobaric, because the rocks near the contact do not show especially intensive decompression reactions: e.g. the reaction (10) $grt+sil+qtz=crd$ would have altered garnet formed in (2) into cordierite, if there had been substantial exhumation during the thermal maximum. This would also have taken place during isobaric heating, if the dP/dT slope of the reaction (10) is positive, as presented in Fig. 14a. Both negative (Thompson 1976b, Holdaway & Lee 1977) and positive (Hutcheon et al. 1974, Martignole & Sisi 1981, Aranovich & Podlesskii 1983) slopes have been suggested for reaction (10) on the basis of theoretical and experimental studies. According to Newton & Wood (1979) the slope

is gently negative in low pressures and positive in higher pressures. If the contact meta-

morphic heating was isobaric, a negative slope is favoured for these compositions.

Tectono-metamorphic evolution

Pyroxene granitoids represent much hotter magma compared with other synkinematic granitoids, because other granitoids only seldom have granulite facies contacts. However, within the study area the grade also increases near the contacts of pyroxene-free porphyritic granitoids (Fig. 2). Questions which arise include: a) was the contact metamorphism associated with pyroxene granitoids a discrete event that post-dated regional metamorphism; b) was mantle-derived magmatism the cause of low-P - high-T regional metamorphism near the Archean craton.

The high-grade metamorphism in the Pielavesi granulite block and nearby areas was concurrent with regional D_2 deformation (Pajunen 1986, 1988). Rocks in the granulite block are mostly intermediate and basic pyroxene-bearing intrusives which exhibit the S_2 schistosity. Most of the 1.885 Ga granitoids in the craton margin have the S_2 schistosity, although there are differences in its intensity, and on this basis they are classified as D_1 - D_2 rocks (Ward 1988, Luukas 1991). The Vaaraslahti pluton does not show either the S_2 or the S_3 foliation, but its contact metamorphic aureole started to develop during the D_2 and the early D_3 , as indicated by the syn- S_2 cordierites and early D_3 feldspars, cordierites and garnets, observed in the cordierite-K-feldspar and garnet-cordierite zones (Fig 5). For this reason it is probable that there was no considerable time gap between D_2 and D_3 ; the growth of cordierites, alkali feldspars and garnets can be related both to D_2 and D_3 . Furthermore, the development of D_2 and D_3 was a short-lived event because the U-Pb zircon ages of the D_2 intrusions and pyroxene granitoids are the same. The weak deformation in the pyroxene granitoid shows that it was not sufficiently

crystallized during the D_3 to deform; late solidification is also indicated by the relatively young Rb-Sr age of the pluton (Haudenschild 1995).

The crystallization pressure, shown by the barometry, in the Pielavesi granulite block is c. 1 kbar higher than in the Vaaraslahti contact aureole and in the contact zones of other porphyritic orthopyroxene granitoids intruding the Pielavesi block (Hölttä 1988). If this relatively small pressure difference is real, it means uplift of the Pielavesi block before the emplacement of orthopyroxene granitoids. The zoning and inclusion data in garnet PSH-88-4.3 (Fig. 10) also suggest that during the early stage of metamorphism rocks were at pressures 1-1.5 kbars higher than during the highest grade event, evidently due to heat from the pyroxene. In this sense the contact metamorphism due to the orthopyroxene granitoids is slightly younger than granulite metamorphism in the Pielavesi block, although the zircon U-Pb ages are within error limits the same for pyroxene-bearing igneous rocks and related granulite facies metamorphics both in the Pielavesi block and in the Vaaraslahti aureole.

Being near-isobaric, the contact metamorphic heating of the pyroxene granitoids was a rapid event in regard to the rate of uplift. The preservation of growth zoning profiles in garnets of the granulite facies rocks (Fig. 8c) indicates rapid initial cooling for the Vaaraslahti rocks, because in high-temperature rocks diffusion would have otherwise homogenized minerals (Tracy 1982). The lack of annealing in the melting zone also suggests rapid cooling. Nevertheless, the cooling rate must have been retarded at some stage, because the K-Ar ages on biotite in the garnet-cordierite and higher grade zones are all 1.74-

1.79 Ga, and in lower grade zones even younger. (Haudenschild 1988).

It has been suggested that low-P metamorphic belts can develop through numerous local metamorphic events associated with intrusions (Barton & Hanson 1989, Stüwe et al. 1993). The abundance of exposed synkinematic, 1.88 - 1.89 Ga I-type granitoids and other igneous rocks in central Finland suggests that the main cause of regional low-

pressure metamorphism was high heat flow connected with magmatism. The regional metamorphism may have been developed through successive local heating events at slightly different levels in the crust, the pyroxene-bearing intrusions releasing more heat into their surroundings than other infracrustals. The inclusion data in garnet PSH-88-4.3 (Fig 10a) also suggests that there might have been two heating stages.

ACKNOWLEDGEMENTS

The author gratefully acknowledges the comments of Leonid Aranovich, Bas Hensen, Kalevi Korsman, Mikko Nironen, Matti Pajunen, Pekka Tuisku and Atso Vormaa. Especial thanks to Geoffrey Clarke and to an anonymous review-

er for their very constructive critiques. Liisa Sirén and Elsa Järvimäki drafted the figures and Lassi Pakkanen did the microprobe analyses. The English was corrected by Anthony G. Meadows and Peter Ward.

REFERENCES

- Aho, L. 1979.** Petrogenetic and geochronological studies of metavolcanic rocks and associated granitoids in the Pihtipudas area, central Finland. Geological Survey of Finland, Bulletin 300. 22 p.
- Aranovich, L.Ya. & Podlesskii, K.K. 1983.** The cordierite-garnet-sillimanite-quartz equilibrium: experiments and applications. In: Saxena, S.K. (ed.) Kinetics and Equilibrium in Mineral Reactions. Advances in Physical Chemistry 3, 173-198.
- Ashworth, J.R. & McLellan, E.L. 1985.** Textures. In: Ashworth, J.R. (ed.) Migmatites. Glasgow: Blackie, 180-203.
- Barton, M.D. & Hanson, R.B. 1989.** Magmatism and the development of low-pressure metamorphic belts: Implications from the western United States and thermal modeling. Geological Society of America, Bulletin 101, 1051-1065.
- Berman, R.G. 1988.** Internally-consistent thermodynamic data for stoichiometric minerals in the system Na₂O-K₂O-CaO-MgO-FeO-Fe₂O₃-Al₂O₃-SiO₂-TiO₂-H₂O-CO₂. Journal of Petrology 29, 445-522.
- Berman, R.G. 1990.** Mixing properties of Ca-Mg-Fe-Mn garnets. American Mineralogist 75, 328-344.
- Berman, R.G. 1991.** Thermobarometry using multiequilibrium calculations: a new technique with petrologic applications. Canadian Mineralogist 29, 833-855.
- Dickerson, R.P. & Holdaway, M.J. 1989.** Acadian metamorphism associated with the Lexington batholith, Bingham, Maine. American Journal of Science 289, 945-974.
- Essene, E.J. 1989.** The current status of thermobarometry in metamorphic rocks. In: Daly, J.S., Cliff, R.A. & Yardley, B.W.D. (eds) Evolution of metamorphic belts. Geological Society Special Publication 43, 1-44.
- Front, K. & Nurmi, P.A. 1987.** Characteristics and geological setting of synkinematic Svecokarelian granitoids in southern Finland. Precambrian Research 35, 207-224.
- Gerya, T.V. & Perchuk, L.L. 1992.** GEOPATH - a thermodynamic database for geothermobarometry and related calculations with the IBM PC AT/XT computer. 29th International Geological Congress, Kyoto, V.2, p.1026.
- Grant, J.A. 1985.** Phase equilibria in low-pressure partial melting of pelitic rocks. American Journal of Science 285, 409-435.
- Hand, M., Scrimgeour, I., Powell, R., Stüwe, K.**

- & Wilson, C.J.L. 1994. Metapelitic granulites from Jetty Peninsula, east Antarctica: formation during a single event or by polymetamorphism? *Journal of Metamorphic Geology* 12, 557–573.
- Haudenschild, U. 1988. K-Ar age determination on biotite and muscovite in the Pihtipudas-Iisalmi and Joroinen areas, eastern Finland. In: Korsman, K. (ed.) *Tectono-metamorphic evolution of the Raahe-Ladoga zone*. Geological Survey of Finland, Bulletin 343, 33–50.
- Haudenschild, U. 1990. Cooling history of the eastern Svecofennides: whole-rock and mica Rb-Sr and hornblende K-Ar ages in the areas of Pihtipudas-Iisalmi and Joroinen-Sulkava. *Bulletin of the Geological Society of Finland* 62(1), 39–59.
- Haudenschild, U. 1995. Rb-Sr whole rock and K-Ar mineral datings on the Vaaraslahti pyroxene granitoid intrusion and its country rock, central Finland. In: Hölttä, P. (ed.) *Relationship of granitoids, structures and metamorphism at the eastern margin of the Central Finland Granitoid Complex*. Geological Survey of Finland, Bulletin 382, 81–89. (this paper)
- Helovuori, O. 1979. Geology of the Pyhäsalmi ore deposit, Finland. *Economic geology* 74, 1084–1101.
- Hodges, K.V. & Crowley, P.D. 1985. Error estimation and empirical geothermobarometry for pelitic systems. *American Mineralogist* 70, 702–709.
- Holdaway, M.J. & Lee, S.M. 1977. Fe-Mg cordierite stability in high grade pelitic rocks based on experimental, theoretical and natural observations. *Contributions to Mineralogy and Petrology* 63, 175–198.
- Holland, T.J.B. & Powell, R. 1990. An enlarged and updated internally consistent thermodynamic dataset with uncertainties and corrections: the system $K_2O-Na_2O-CaO-MgO-MnO-FeO-Fe_2O_3-Al_2O_3-TiO_2-SiO_2-C-H_2O_2$. *Journal of Metamorphic Geology* 8, 89–124.
- Holtz, F. & Johannes, W. 1994. Maximum and minimum water contents of granitic melts: implications for chemical and physical properties of ascending magmas. *Lithos* 32, 149–159.
- Hölttä, P. 1988. Metamorphic zones and the evolution of granulite grade metamorphism in the early Proterozoic Pielavesi area, central Finland. *Geological Survey of Finland, Bulletin* 344, 50 p.
- Huhtala, T. 1979. The geology and zinc-copper deposits of the Pyhäsalmi-Pielavesi district, Finland. *Economic Geology* 74, 1069–1083.
- Hutcheon, I., Froese, E. & Gordon, T.M. 1974. The assemblage quartz-sillimanite-garnet-cordierite as an indicator of metamorphic conditions in the Daly Bay Complex, N.W.T. *Contributions to Mineralogy and Petrology* 44, 29–34.
- Johannes, W., 1988. What controls partial melting in migmatites? *Journal of Metamorphic Geology* 6, 451–465.
- Jones, K.A. & Brown, M. 1990. High-temperature 'clockwise' P-T paths and melting in the development of regional migmatites: an example from southern Brittany, France. *Journal of Metamorphic Geology* 8, 551–578.
- Korsman, K., Hölttä, P., Hautala, T. & Wasenius, P. 1984. Metamorphism as an indicator of evolution and structure of the crust in Eastern Finland. *Geological Survey of Finland, Bulletin* 328, 40 p.
- Kousa, J., Marttila, E. & Vaasjoki, M. 1994. Petrology, geochemistry and timing of early Proterozoic metavolcanic rocks in the Pyhäjärvi region, central Finland. *Geological Survey of Finland, Special Paper* 19, 7–28.
- Koziol, A.M. & Newton, R.C. 1988. Redetermination of the garnet breakdown reaction and improvement of the plagioclase-garnet- Al_2SiO_5 -quartz geobarometer. *American Mineralogist* 73, 216–223.
- Kretz, R. 1969. On the spatial distribution of crystals in rocks. *Lithos* 2, 39–66.
- Kretz, R. 1983. Symbols for rock-forming minerals. *American Mineralogist* 68, 277–279.
- Lahti, S. 1995. Mineralogy and geochemistry of the Vaaraslahti pyroxene granitoid intrusion. In: Hölttä, P. (ed.) *Relationship of granitoids, structures and metamorphism at the eastern margin of the Central Finland Granitoid Complex*. Geological Survey of Finland, Bulletin 382, 5–25. (this paper)
- Le Breton, N. & Thompson, A.B. 1988. Fluid-absent (dehydration) melting of biotite in metapelites in the early stages of crustal anatexis. *Contributions to Mineralogy and Petrology* 99, 226–237.
- Luukas, J. 1991. *Salahmin-Pyhännän alueen stratigrafia ja rakennegeologia*. (Stratigraphy and structural geology of the Salahmi-Pyhäntä area, in Finnish). *Res Terrae, Ser. B, No. 16*. Publications of the Department of Geology, University of Oulu.
- Martignole, J. & Sisi, J.C. 1981. Cordierite-garnet- H_2O equilibrium: A geological thermometer, barometer and water fugacity indicator. *Contributions to Mineralogy and Petrology* 77, 38–46.
- Marttila, E. 1976. Evolution of the Precambrian volcanic complex in the Kiuruvesi area, Finland. *Geological Survey of Finland, Bulletin* 283, 109 p.
- Marttila, E. 1977. Kiuruvesi. *Geological Map of Finland 1 : 100 000, Pre-Quaternary Rocks, Sheet 3323*. Espoo: Geological Survey of Finland.
- Marttila, E. 1981. Kiuruveden kartta-alueen kallioperä. Summary: Pre-Quaternary rocks of the

- Kiuruvesi map sheet area. Geological Map of Finland 1 : 100 000, Explanation to the Maps of Pre-Quaternary Rocks, Sheet 3323. Espoo: Geological Survey of Finland. 48 p.
- McLellan, E.L. 1983.** Contrasting textures in metamorphic and anatectic migmatites: an example from the Scottish Caledonides. *Journal of Metamorphic Geology* 1, 241–262.
- Mehnert, K.R. 1971.** Migmatites and the origin of granitic rocks. Amsterdam: Elsevier. 405 p.
- Miyashiro, A. 1973.** Metamorphism and metamorphic belts. London: George Allen & Unwin. 491 p.
- Moehler, D.P., Essene, E.J. & Anovitz, L.M. 1988.** Calculation and application of clinopyroxene-garnet-plagioclase-quartz geobarometers. *Contributions to Mineralogy and Petrology* 100, 92–106.
- Montel, J.-M., Weber, C. & Pichavant, M. 1986.** Biotite-sillimanite-spinel assemblages in high-grade metamorphic rocks: occurrences, chemographic analysis and thermobarometric interest. *Bulletin de Minéralogie* 109, 555–573.
- Newton, R.C. & Wood, B.J. 1979.** Thermodynamics of water in cordierite and some petrologic consequences of cordierite as a hydrous phase. *Contributions to Mineralogy and Petrology* 68, 391–405.
- Newton, R.C. & Haselton, H.T.I. 1981.** Thermodynamics of the garnet-plagioclase- Al_2SiO_5 -quartz geobarometer. In: Newton, R.C., Navrotsky, A. & Wood, B.J. (eds.) *Thermodynamics of Minerals and Melts*. New York: Springer-Verlag, 129–145.
- Norton, D. & Knight, R. 1977.** Transport phenomena in hydrothermal systems: cooling plutons. *American Journal of Science* 277, 937–981.
- Nurmi, P.A. & Haapala, I. 1986.** The Proterozoic granitoids in Finland: granite types, metallogeny and relation to crustal evolution. *Bulletin of the Geological Society of Finland* 58(1), 203–233.
- Pajunen, M. 1986.** Deformation analysis of cataclastic structures and faults in the Tervo area, central Finland. In: Korsman, K. (ed.) *Development of deformation, metamorphism and metamorphic blocks in eastern and southern Finland*. Geological Survey of Finland, Bulletin 339, 16–31.
- Pajunen, M., 1988.** Tectono-metamorphic evolution of the Hallaperä pyrrhotite-pyrite ore deposit, central Finland. In: Korsman, K. (ed.) *Tectono-metamorphic evolution of the Raabe-Ladoga zone*. Geological Survey of Finland, Bulletin 343, 51–76.
- Pattison, D.R.M. & Tracy, R.J. 1991.** Phase equilibria and thermobarometry of metapelites. *Reviews in Mineralogy* 26, 105–206.
- Peacock, S.M. 1989.** Thermal modeling of metamorphic pressure-temperature-time paths: a forward approach. In: Spear, F.S. & Peacock, S.M. (eds.) *Metamorphic pressure-temperature-time paths*. American Geophysical Union, Short Course in Geology, Vol. 7., 57–102.
- Powell, R. & Downes, J. 1990.** Garnet porphyroblast-bearing leucosomes in metapelites: mechanisms, phase diagrams, and an example from Broken Hill, Australia. In: Ashworth, J.R. & Brown, M. (eds.) *High-temperature metamorphism and crustal anatexis*. London: Unwin Hyman, 105–123.
- Powers, E.P. & Bohlen, S.R. 1985.** The role of synmetamorphic igneous rocks in the metamorphism and partial melting of metasediments, Northwest Adirondacks. *Contributions to Mineralogy and Petrology* 90, 401–409.
- Pownceby, M.I., Wall, V.J. & O'Neill, H.St.C. 1987.** Fe-Mn partitioning between garnet and ilmenite: experimental calibration and applications. *Contributions to Mineralogy and Petrology* 97, 116–126.
- Salli, I. 1969.** Pihtipudas. Geological Map of Finland 1 : 100 000, Pre-Quaternary Rocks, Sheet 3312. Espoo: Geological Survey of Finland.
- Salli, I. 1977.** Pielavesi. Geological Map of Finland 1 : 100 000, Pre-Quaternary Rocks, Sheet 3314. Espoo: Geological Survey of Finland.
- Salli, I. 1983.** Pielaveden kartta-alueen kallioperä. Summary: Pre-Quaternary rocks of the Pielavesi map-sheet area. Geological Map of Finland 1 : 100 000, Explanation to the Maps of Pre-Quaternary Rocks, Sheet 3314. Espoo: Geological Survey of Finland. 29 p.
- Seifert, F. & Schumacher, J.C. 1986.** Cordierite-spinel-quartz assemblages: a potential geobarometer. *Bulletin of the Geological Society of Finland* 58(1), 95–108.
- Shearer, C.K. & Robinson, P. 1988.** Petrogenesis of metaluminous and peraluminous tonalites within the Merrimack synclinorium: Hardwick tonalite, central Massachusetts. *American Journal of Science* 288-A, 148–195.
- St-Onge, M.R. 1987.** Zoned poikiloblastic garnets: P-T paths and syn-metamorphic uplift through 30 km of structural depth, Wopmay Orogen, Canada. *Journal of Petrology* 28, 1–22.
- Stüwe, K. & Powell, R. 1989.** Metamorphic segregations associated with garnet and orthopyroxene porphyroblast growth: two examples from the Larsemann Hills, east Antarctica. *Contributions to Mineralogy and Petrology* 103, 523–530.
- Stüwe, K., Sandiford, M. & Powell, R. 1993.** Episodic metamorphism and deformation in low-pressure, high-temperature terranes. *Geology* 21, 829–832.

- Thompson, A.B. 1976a.** Mineral reactions in pelitic rocks: I. Prediction of P-T-X Fe-Mg phase relations. *American Journal of Science* 276, 401–424.
- Thompson, A.B. 1976b.** Mineral reactions in pelitic rocks: II. Calculations of some P-T-X (Fe-Mg) phase relations. *American Journal of Science* 276, 425–445.
- Thompson, A.B. 1982.** Dehydration melting of pelitic rocks and the generation of H₂O-undersaturated granitic liquids. *American Journal of Science* 282, 1567–1595.
- Thompson, A.B. 1988.** Dehydration melting of crustal rocks. *Rendiconti della societa italiana di mineralogia e petrologia* 43, 41–60.
- Thompson, P.H. 1989.** Moderate overthickening of thinned sialic crust and the origin of granitic magmatism and regional metamorphism in low-P-high-T terranes. *Geology* 17, 520–523.
- Tracy, R.J. 1982.** Compositional zoning and inclusions in metamorphic minerals. *Reviews in Mineralogy* 10, 355–397.
- Tracy, R.J. & Robinson, P. 1983.** Acadian migmatite types in central Massachusetts. In: Atherton, M.P. & Gribble, C.D. (eds.) *Migmatites, melting and metamorphism*. Shiva: Nantwich, 163–173.
- Vaasjoki, M. & Sakko, M. 1988.** Evolution of the Raahe-Ladoga zone in Finland: Isotopic constraints. In: Korsman, K. (ed.) *Tectono-metamorphic evolution of the Raahe-Ladoga zone*. Geological Survey of Finland, Bulletin 343, 7–32.
- Vernon, R.H., Flood, R.H. & D'Arcy, W.F. 1987.** Sillimanite and andalusite produced by base-cation leaching and contact metamorphism of felsic igneous rocks. *Journal of Metamorphic Geology* 5, 439–450.
- Vernon, R.H. & Collins, W.J. 1988.** Igneous microstructures in migmatites. *Geology* 16, 1126–1129.
- Vernon, R.H., Clarke, G.L. & Collins, W.J. 1990.** Local, mid-crustal granulite facies metamorphism and melting: an example in the Mount Stafford area, central Australia. In: Ashworth, J.R. & Brown, M. (eds.) *High-temperature metamorphism and crustal anatexis*. London: Unwin Hyman, 272–319.
- Vasama, P.-M. & Vartia, Y. 1973.** Johdatus tilastotieteeseen, osa II. Helsinki: Kyriiri Oy.
- Ward, P. 1988.** Mesoscopic scale structural analysis. In: Gaál, G. (ed.) *Exploration target selection by integration of geodata using statistical and image processing techniques: an example from Central Finland, Part I (text)*. Geological Survey of Finland, Report of Investigation 80, 50–53.
- Waters, D.J. & Whales, C.J. 1984.** Dehydration melting and the granulite transition in metapelites from southern Namaqualand, S. Africa. *Contributions to Mineralogy and Petrology* 88, 269–275.
- Wood, B.J. & Banno, S. 1973.** Garnet-orthopyroxene and orthopyroxene-clinopyroxene relationships in simple and complex systems. *Contributions to Mineralogy and Petrology* 42, 109–124.

Appendix 1. Representative microprobe analyses of minerals. If not mentioned, analyses represent core compositions. Sample locations are shown in Fig. 2. r = rim composition, i = inclusion in garnet. n.d. = not determined.

	1	2	3	4	5	6	7	8	9	10	11	12	13
SiO ₂	32.52	34.34	34.50	35.09	36.23	35.41	35.57	34.82	35.58	38.34	37.39	36.50	35.99
TiO ₂	4.22	4.96	4.03	1.76	2.85	2.53	1.62	2.44	2.57	0.02	0.03	0.10	0.04
Al ₂ O ₃	17.17	16.26	16.51	18.68	17.52	18.75	18.68	17.06	16.85	21.90	21.30	21.39	21.35
FeO	20.16	17.88	19.17	18.91	16.69	18.43	20.73	20.78	24.89	31.86	32.14	33.67	36.69
MnO	0.04	0.04	0.04	0.15	0.04	0.12	0.03	0.05	0.42	0.83	2.41	0.90	0.66
MgO	10.44	11.28	10.90	9.64	11.45	10.04	8.74	9.47	7.06	6.12	4.08	6.64	5.08
CaO	0.03	0.02	0.01	0.03	0.04	0.02	0.03	0.04	0.16	1.07	3.20	1.01	1.09
Na ₂ O	0.06	0.05	0.10	0.09	0.13	0.08	0.19	0.17	0.05	0.02	0.01	n.d.	0.04
K ₂ O	9.55	9.38	9.47	9.74	9.75	9.87	9.07	8.96	8.86	0.01	0.01	0.01	0.01
ZnO	n.d.	0.00	0.02	n.d.	n.d.	0.06	n.d.	n.d.	n.d.	0.00	0.02	n.d.	0.01
Total	94.19	94.21	94.75	94.09	94.70	95.31	94.65	93.79	96.44	100.18	100.59	100.21	100.96
Formula	22 (O)	22 (O)	22 (O)	22 (O)	22 (O)	22 (O)	22 (O)	22 (O)	22 (O)	12 (O)	12 (O)	12 (O)	12 (O)
Si	5.0966	5.2926	5.3180	5.4177	5.4858	5.3841	5.4687	5.4317	5.4981	3.0029	2.9725	2.9033	2.8827
Ti	0.4974	0.5749	0.4672	0.2044	0.3245	0.2893	0.1867	0.2861	0.2989	0.0011	0.0018	0.0060	0.0024
Al	3.1714	2.9536	2.9994	3.3991	3.1265	3.3600	3.3839	3.1364	3.0685	2.0219	1.9959	2.0052	2.0155
Fe	2.6422	2.3046	2.4712	2.4416	2.1134	2.3435	2.6655	2.7110	3.2158	2.0868	2.1368	2.2397	2.4577
Mn	0.0053	0.0052	0.0052	0.0196	0.0051	0.0155	0.0043	0.0071	0.0551	0.0553	0.1621	0.0606	0.0448
Mg	2.4387	2.5913	2.5043	2.2184	2.5841	2.2754	2.0023	2.2008	1.6266	0.7150	0.4838	0.7872	0.6065
Ca	0.0050	0.0033	0.0017	0.0050	0.0065	0.0033	0.0041	0.0067	0.0260	0.0900	0.2726	0.0857	0.0935
Na	0.0182	0.0149	0.0299	0.0269	0.0382	0.0236	0.0560	0.0502	0.0141	0.0027	0.0014	n.d.	0.0062
K	1.9092	1.8442	1.8621	1.9183	1.8832	1.9144	1.7785	1.7820	1.7456	0.0015	0.0008	0.0008	0.0008
Zn	n.d.	0.0006	0.0023	n.d.	n.d.	0.0067	n.d.	n.d.	n.d.	0.0000	0.0012	n.d.	0.0006

- 1 = Biotite, 18-3-1
- 2 = Biotite, 24-5
- 3 = Biotite, 29-25-1
- 4 = Biotite, PSH-85-18.1
- 5 = Biotite, PSH-88-25
- 6 = Biotite, PSH-88-40
- 7 = Biotite, PSH-88-2.3
- 8 = Biotite, PSH-88-12.2
- 9 = Biotite, PSH-88-1
- 10 = Garnet, 29-3-1
- 11 = Garnet, PSH-88-4.3
- 12 = Garnet, 24-5
- 13 = Garnet, 18-3-1

Appendix 1. Cont.

	14	15	16	17	18	19	20	21	22	23	24	25	26
SiO ₂	36.22	37.72	38.45	37.88	38.28	37.79	0.09	0.05	0.04	46.47	47.37	48.30	49.51
TiO ₂	0.04	0.00	0.04	0.04	0.02	0.01	57.06	51.22	48.36	n.d.	0.01	0.01	n.d.
Al ₂ O ₃	21.62	21.14	20.42	21.55	21.54	20.91	0.03	0.04	0.02	32.48	32.94	32.79	31.84
FeO	37.56	35.03	33.05	33.38	32.44	21.17	43.51	45.27	41.83	7.73	9.13	8.18	7.51
MnO	0.72	2.77	1.33	2.33	2.44	14.72	0.29	0.48	7.52	0.04	0.04	0.23	0.14
MgO	4.69	3.75	5.15	4.50	2.99	1.05	0.10	0.44	0.00	9.05	8.64	8.43	8.85
CaO	1.00	0.99	1.11	1.71	2.87	4.31	0.17	0.07	0.08	n.d.	0.03	0.01	n.d.
Na ₂ O	0.06	0.03	0.03	n.d.	0.01	0.02	n.d.	0.00	0.00	0.05	0.09	0.11	0.08
K ₂ O	0.10	0.01	0.02	n.d.	0.01	0.00	0.04	0.00	0.00	0.01	0.02	0.01	0.02
ZnO	n.d.	n.d.	n.d.	n.d.	n.d.	n.d.	n.d.	n.d.	n.d.	n.d.	n.d.	n.d.	0.05
Total	102.01	101.44	99.60	101.39	100.60	99.99	101.29	97.58	97.85	95.83	98.27	98.07	98.00
Formula	12 (O)	12 (O)	12 (O)	12 (O)	12 (O)	12 (O)	3 (O)	3 (O)	3 (O)	18 (O)	18 (O)	18 (O)	18 (O)
Si	2.8798	2.9948	3.0601	2.9837	3.0326	3.0437	0.0022	0.0013	0.0010	4.9087	4.9098	4.9877	5.0917
Ti	0.0024	0.0002	0.0024	0.0024	0.0010	0.0009	1.0462	0.9944	0.9544	n.d.	0.0007	0.0008	n.d.
Al	2.0259	1.9781	1.9153	2.0006	2.0116	1.9848	0.0009	0.0012	0.0007	4.0436	4.0238	3.9907	3.8592
Fe	2.4975	2.3259	2.1997	2.1988	2.1490	1.4262	0.8871	0.9772	0.9180	0.6829	0.7914	0.7064	0.6459
Mn	0.0485	0.1863	0.0897	0.1555	0.1636	1.0043	0.0061	0.0106	0.1672	0.0036	0.0035	0.0201	0.0122
Mg	0.5558	0.4438	0.6109	0.5283	0.3526	0.1264	0.0036	0.0170	0.0000	1.4249	1.3348	1.2975	1.3566
Ca	0.0852	0.0842	0.0946	0.1443	0.2438	0.3716	0.0044	0.0020	0.0022	n.d.	0.0033	0.0011	n.d.
Na	0.0092	0.0046	0.0046	n.d.	0.0023	0.0027	n.d.	0.0000	0.0000	0.0102	0.0181	0.0220	0.0160
K	0.0101	0.0010	0.0020	n.d.	0.0009	0.0000	0.0012	0.0000	0.0000	0.0013	0.0026	0.0013	0.0026
Zn	n.d.	n.d.	n.d.	n.d.	n.d.	n.d.	n.d.	n.d.	n.d.	n.d.	n.d.	n.d.	0.0038

- 14 = Garnet, 18-3-1-r
- 15 = Garnet, PSH-85-18.1
- 16 = Garnet, PSH-88-25
- 17 = Garnet, PSH-88-40
- 18 = Garnet, PSH-88-2.3
- 19 = Garnet, PSH-88-1
- 20 = Ilmenite, 18-3-1
- 21 = Ilmenite, PSH-88-2.3
- 22 = Ilmenite, PSH-88-1
- 23 = Cordierite, 24-5
- 24 = Cordierite, 18-3-1
- 25 = Cordierite, PSH-85-18.1
- 26 = Cordierite, PSH-88-25

Appendix 1. Cont.

	27	28	29	30	31	32	33	34	35	36	37	38	39
SiO ₂	45.31	47.42	49.37	48.78	59.46	58.95	58.62	44.50	60.74	60.53	59.74	57.95	59.19
TiO ₂	0.61	0.01	0.16	0.10	0.01	0.01	0.03	n.d.	0.01	n.d.	0.02	0.06	0.00
Al ₂ O ₃	34.64	33.62	3.66	1.01	24.66	24.69	23.88	32.86	24.30	24.19	25.35	2.87	25.33
FeO	0.87	3.75	31.00	36.17	0.06	0.02	0.05	0.02	0.02	0.02	0.01	0.20	0.05
MnO	n.d.	0.05	0.26	0.90	0.01	0.01	0.02	n.d.	0.06	n.d.	0.00	0.01	0.00
MgO	0.57	0.65	15.30	13.24	0.00	0.00	0.01	n.d.	n.d.	0.02	0.00	n.d.	0.00
CaO	0.01	0.06	0.13	0.40	6.43	6.35	5.71	16.80	5.98	6.73	7.27	8.91	6.78
Na ₂ O	0.83	0.22	0.01	0.00	7.55	7.66	8.30	1.53	7.91	7.53	7.23	6.49	7.90
K ₂ O	8.96	10.14	0.00	0.00	0.22	0.26	0.28	0.01	0.22	0.16	0.19	0.16	0.10
ZnO	0.02	n.d.	0.00	n.d.	0.00	0.03	0.02	n.d.	0.01	n.d.	n.d.	0.02	n.d.
Total	91.82	95.92	99.90	100.59	98.40	97.98	96.92	95.72	99.25	99.18	99.81	100.67	99.35
Formula	24 (O)	24 (O)	6 (O)	6 (O)	8 (O)	8 (O)	8 (O)	8 (O)	8 (O)	8 (O)	8 (O)	8 (O)	8 (O)
Si	6.1954	6.3143	1.9151	1.9425	2.6880	2.6794	2.6962	2.1369	2.7185	2.7131	2.6661	2.5810	2.6571
Ti	0.0627	0.0014	0.0048	0.0030	0.0005	0.0002	0.0010	n.d.	0.0003	n.d.	0.0007	0.0020	0.0000
Al	5.5822	5.2770	0.1671	0.0473	1.3139	1.3226	1.2945	1.8597	1.2818	1.2779	1.3334	1.4104	1.3404
Fe	0.0995	0.4177	1.0054	1.2047	0.0023	0.0008	0.0019	0.0008	0.0007	0.0007	0.0004	0.0074	0.0018
Mn	n.d.	0.0054	0.0087	0.0304	0.0003	0.0003	0.0008	n.d.	0.0023	n.d.	0.0000	0.0004	0.0000
Mg	0.1162	0.1298	0.8848	0.7859	0.0000	0.0002	0.0007	n.d.	n.d.	0.0013	0.0001	n.d.	0.0002
Ca	0.0015	0.0083	0.0054	0.0171	0.3115	0.3092	0.2814	0.8644	0.2868	0.3232	0.3476	0.4252	0.3263
Na	0.2200	0.0563	0.0011	0.0000	0.6615	0.6750	0.7402	0.1424	0.6864	0.6544	0.6256	0.5604	0.6875
K	1.5628	1.7219	0.0000	0.0000	0.0127	0.0154	0.0164	0.0006	0.0126	0.0091	0.0108	0.0091	0.0056
Zn	0.0020	n.d.	0.0000	n.d.	0.0000	0.0010	0.0007	n.d.	0.0003	n.d.	n.d.	0.0007	n.d.

- 27 = Muscovite, PSH-88-10.1
- 28 = Muscovite, PSH-88-1
- 29 = Orthopyroxene, 29-3-1
- 30 = Orthopyroxene, PSH-88-4.3
- 31 = Plagioclase, 29-3-1
- 32 = Plagioclase, 18-3-1
- 33 = Plagioclase, 24-5
- 34 = Plagioclase, PSH-88-4.3
- 35 = Plagioclase, PSH-85-18.1
- 36 = Plagioclase, PSH-88-25
- 37 = Plagioclase, PSH-88-40
- 38 = Plagioclase, PSH-88-40-i
- 39 = Plagioclase, PSH-88-2.3

Appendix I. Cont.

	40	41	42	43	44	45	46	47	48	49	50
SiO ₂	45.35	64.23	45.09	0.03	0.03	0.03	28.77	26.72	65.51	64.25	52.50
TiO ₂	0.01	0.00	0.00	0.06	0.01	0.00	0.02	0.35	0.02	0.02	0.05
Al ₂ O ₃	33.61	18.27	33.67	58.07	56.36	56.34	53.74	51.47	19.03	19.10	0.48
FeO	0.17	0.06	0.12	23.79	33.30	34.96	13.51	12.81	0.00	0.04	29.40
MnO	0.02	0.00	0.00	0.15	0.09	0.10	0.08	0.62	0.00	0.00	0.69
MgO	0.00	0.00	0.00	4.40	3.94	3.70	1.46	1.13	0.00	0.00	12.90
CaO	16.92	0.03	16.80	0.01	0.02	0.00	0.02	n.d.	0.10	0.15	0.83
Na ₂ O	1.65	0.66	1.41	0.23	0.13	0.06	0.04	0.01	1.22	2.14	0.05
K ₂ O	0.02	15.52	0.02	0.01	0.02	0.00	0.01	0.01	13.98	13.42	0.01
ZnO	n.d.	n.d.	n.d.	7.54	2.71	1.41	1.25	0.59	n.d.	n.d.	n.d.
Total	97.76	98.75	97.11	94.29	96.61	96.61	98.90	93.71	99.86	99.12	96.62
Formula	8 (O)	8 (O)	8 (O)	4 (O)	4 (O)	4 (O)	24 (O)	24(O)	8(O)	8(O)	23(O)
Si	2.1330	2.9984	2.1321	0.0009	0.0009	0.0009	3.7877	3.7127	2.996	2.968	7.990
Ti	0.0004	0.0000	0.0000	0.0013	0.0002	0.0000	0.0020	0.0366	0.001	0.001	0.006
Al	1.8632	1.0050	1.8760	2.0249	1.9564	1.9573	8.3384	8.4288	1.026	1.040	0.085
Fe	0.0066	0.0023	0.0047	0.5886	0.8202	0.8618	1.4874	1.4885	0.000	0.001	3.741
Mn	0.0008	0.0000	0.0000	0.0038	0.0022	0.0025	0.0089	0.0730	0.000	0.000	0.089
Mg	0.0000	0.0000	0.0000	0.1940	0.1730	0.1626	0.2865	0.2340	0.000	0.000	2.906
Ca	0.8528	0.0013	0.8513	0.0003	0.0006	0.0001	0.0028	n.d.	0.005	0.007	0.138
Na	0.1509	0.0596	0.1289	0.0132	0.0074	0.0034	0.0102	0.0027	0.108	0.192	0.005
K	0.0013	0.9239	0.0012	0.0004	0.0008	0.0001	0.0017	0.0018	0.816	0.791	0.003
Zn	n.d.	n.d.	n.d.	0.1647	0.0589	0.0307	0.1215	0.0605	n.d.	n.d.	n.d.

- 40 = Plagioclase, PSH-88-12.2
 41 = Plagioclase, PSH-88-1
 42 = Plagioclase, PSH-88-12.2
 43 = Spinel, PSH-88-16.1
 44 = Spinel, PSH-88-25
 45 = Spinel, PSH-88-25
 46 = Staurolite, PSH-88-40
 47 = Staurolite, PSH-88-10.1
 48 = K-feldspar, 29-25-1
 49 = K-feldspar, 18-3-1
 50 = Cummingtonite, PSH-88-4.3

Appendix 2. Selected whole-rock analyses of metapelites in Vaaraslahti. The analyses were made with the XRF method at the Rautaruukki Oy, except the last two samples which were analysed at the Geological Survey.

Sample	18-3-1	18-80-1	26-115-1	26-230-1	28-650-2	25-15-5	PSH-85-19	PSH-88-10	PSH-88-14
SiO ₂	62.33	57.57	58.46	62.17	60.13	60.00	67.47	56.53	61.23
TiO ₂	0.80	0.98	0.88	0.92	0.89	1.17	0.65	0.77	0.83
Al ₂ O ₃	18.18	17.35	18.99	16.02	17.66	16.08	15.11	19.16	17.54
FeO	7.49	10.69	8.58	8.80	9.03	8.45	5.47	8.50	7.60
MnO	0.08	0.10	0.11	0.09	0.10	0.10	0.07	0.07	0.10
MgO	3.09	4.87	3.86	4.11	4.09	3.13	2.27	3.68	3.71
CaO	1.75	1.06	1.87	1.53	1.24	3.80	1.47	1.43	2.14
Na ₂ O	2.16	1.33	2.46	1.81	1.55	2.87	2.15	1.52	2.48
K ₂ O	2.80	4.00	3.17	2.99	3.68	2.72	4.18	4.03	2.32
P ₂ O ₅	0.14	0.06	0.07	0.05	0.07	0.15	0.10	0.10	0.06
Cr	300	350	450	340	300	180	210	n.d.	n.d.
Ni	90	180	100	120	100	60	50	n.d.	n.d.
V	150	240	200	210	180	180	130	n.d.	n.d.
Cu	30	190	130	100	50	60	30	n.d.	n.d.
Zn	110	170	140	140	150	150	100	n.d.	n.d.
S	130	7990	3090	2440	3020	3350	1270	n.d.	n.d.
Ba	660	800	750	510	680	1100	1230	n.d.	n.d.
Sr	150	100	160	110	110	190	150	n.d.	n.d.
Zr	180	170	220	190	180	510	230	n.d.	n.d.
Total	98.99	99.02	98.98	98.91	98.92	99.04	99.28	95.79	98.01

Appendix 3.

a) Garnet-biotite, garnet-cordierite, garnet-spinel and cordierite-spinel temperatures (°C) and grt-crd-sil-qtz and crd-spl-qtz pressures (kbars), calculated with the program GEOPATH by Gerya & Perchuk (1992); grt-pl-sil-qtz pressures after Koziol & Newton (1988).

Temperatures:

$T_1 = \text{grt-crd}$; $T_2 = \text{grt-bt}$; $T_3 = \text{grt-spl}$; $T_4 = \text{crd-spl}$;

Pressures:

$P_1 = \text{grt-crd-sil-qtz}$; $P_2 = \text{crd-spl-qtz}$; $P_{KN} = \text{grt-pl-sil-qtz}$;

The H_2O activity was calculated with GEOPATH by using the reaction $\text{bt} + \text{sil} + \text{qtz} = \text{grt} + \text{kfs} + H_2O$. The X_K represents an average of 2-7 analysis points. When the a_{H_2O} was not calculated, the pressures P_1 and P_2 were calculated at the H_2O activity in fluid = 0.4.

If not specially mentioned, core compositions of minerals were used in calculations. + = spinel inclusion in garnet; * = garnet core + plagioclase inclusion, ** = near-rim composition of garnet + matrix plagioclase, *** = late granular garnet on early garnet + plagioclase adjacent to it. Pressures were calculated at 600°C for the muscovite zone, 650°C for the grt-crd and grt-crd-spl zones and 730°C for the melting zone, except the Gerya & Perchuk pressures which were calculated in the pressures given by their thermometers. Locations, where the analyzed specimens are taken from, are given in Fig. 2 and Appendix 4.

Specimen	X_{Fe}^{Grt}	X_{Mn}^{Grt}	X_{Mg}^{Grt}	X_{Ca}^{Grt}	X_{Ca}^{Pl}	X_{Fe}^{Crd}	X_{Fe}^{Spl}	X_{Zn}^{Spl}	X_{Mg}^{Bt}	X_{Fe}^{Bt}	X_{Ti}^{Bt}	X_{Al}^{Bt}	X_K^{kfs}	T_1	T_2	T_3	T_4	P_1	P_{KN}	P_2	a_{H_2O}
Muscovite zone																					
PSH-88-1	0.487	0.343	0.043	0.127					0.285	0.563	0.052	0.099			507						
PSH-88-12	0.713	0.080	0.108	0.099					0.381	0.470	0.050	0.098			586						
Cordierite-K-feldspar zone																					
PSH-88-2.3	0.739	0.056	0.121	0.084					0.351	0.467	0.033	0.149			624						
Garnet-cordierite zone																					
PSH-85-18.1	0.765	0.061	0.146	0.028	0.291	0.353			0.390	0.430	0.036	0.144	0.830	580	614			3.3	3.8		0.42
PSH-88-22.3	0.759	0.073	0.138	0.031	0.316	0.392			0.408	0.429	0.050	0.113		610	592			3.3	3.8		
PSH-88-39	0.732	0.042	0.195	0.031	0.312				0.402	0.408	0.039	0.151	0.883		674					4.1	0.31
PSH-88-40a	0.750	0.061	0.156	0.033	0.353													3.7**			
PSH-88-40b	0.726	0.051	0.175	0.048	0.405	0.297			0.403	0.415	0.051	0.132		702	653			4.6	4.9*		
PSH-86-14.1a	0.732	0.024	0.211	0.033	0.261													5.3*			
PSH-86-14.1b	0.732	0.023	0.213	0.032	0.318				0.453	0.388	0.047	0.112			663					4.2**	
PSH-86-14.1c	0.771	0.040	0.148	0.041	0.318															5.1***	
PSH-86-15.1a	0.742	0.033	0.201	0.024	0.244				0.439	0.385	0.052	0.123	0.878		646					4.2	0.28

Appendix 3. Cont.

Specimen	X _{Fe} ^{Grt}	X _{Mn} ^{Grt}	X _{Mg} ^{Grt}	X _{Ca} ^{Grt}	X _{Ca} ^{Pl}	X _{Fe} ^{Crd}	X _{Fe} ^{Spl}	X _{Zn} ^{Spl}	X _{Mg} ^{Bi}	X _{Fe} ^{Bi}	X _{Ti} ^{Bi}	X _{Al} ^{Bi}	X _K ^{kfs}	T ₁	T ₂	T ₃	T ₄	P ₁	P _{KN}	P ₂	a _{H2O}		
Garnet-cordierite-spinel zone																							
PSH-85-19.1	0.759	0.031	0.178	0.032	0.305	0.368					0.396	0.432	0.073	0.099		664	665				4.3	4.3	
PSH-88-14	0.752	0.031	0.187	0.030	0.306	0.351					0.476	0.386	0.065	0.073		661	615				4.3	4.1	
PSH-88-15.1	0.756	0.034	0.181	0.030	0.296	0.327					0.453	0.410	0.077	0.061	0.864	627	618				3.8	4.1	0.33
PSH-88-16.1a	0.687	0.041	0.242	0.029	0.301	0.272	0.632	0.165			0.455	0.383	0.071	0.092		658	697	843	524		5.1	4.3	3.3
PSH-88-24.1a	0.736	0.060	0.169	0.035	0.284	0.286					0.406	0.423	0.053	0.119		552	640				3.5	4.9	
PSH-88-25c	0.734	0.030	0.204	0.032	0.328	0.323	0.775	0.058			0.458	0.375	0.058	0.109		658	671	911	525		4.5	4.0	
26-230-1a	0.737	0.028	0.201	0.034		0.287					0.452	0.373	0.062	0.113	0.824	604	635				3.9		0.27
26-230-1b	0.745	0.032	0.191	0.032		0.287	0.580	0.237								590		698	523		3.8		3.5*
Diatexite-stictolite zone																							
18-3-1	0.760	0.014	0.195	0.031		0.372					0.452	0.417	0.085	0.046	0.830	703	674				4.9		0.44
24-5	0.706	0.019	0.248	0.027	0.271	0.324					0.453	0.403	0.100	0.043		736	717				5.6	5.6	
29-25-1	0.740	0.019	0.215	0.026	0.268	0.360					0.435	0.429	0.081	0.056	0.820	726	730				5.2	5.3	0.45
24-31a	0.722	0.012	0.240	0.026	0.278																5.2*		
24-31b	0.719	0.011	0.244	0.027	0.296	0.337					0.406	0.415	0.086	0.092		748	746				5.7	5.1	
29-76-1	0.763	0.018	0.189	0.030		0.362					0.405	0.426	0.080	0.089	0.858	678	669				4.3		0.30
18-80-1	0.745	0.034	0.198	0.024	0.296	0.382					0.429	0.416	0.071	0.084		723	666				5.0	4.5	
26-115-1a	0.707	0.024	0.236	0.033	0.311	0.339					0.451	0.379	0.080	0.090		741	690				5.6	5.8	
26-115-1c	0.736	0.026	0.208	0.030		0.323	0.768	0.054								665	651	866	562		4.6		4.0

Appendix 3. Cont.

b) Garnet-orthopyroxene (T_5), biotite-orthopyroxene (T_6), garnet-biotite (T_2) temperatures, calculated with the GEOPATH; garnet-ilmenite temperatures (T_{gi}) after Pownceby & al. (1987); P_{grips} = grt-rt-ilm-pl-qtz maximum pressures according to Essene (1989) in the grt-ilm temperature. P_{gafs} = grt-pl-opx-qtz pressure according to Essene (1989) (Fe-reaction). The activity models of Moecher et al. (1988) for garnet, of Newton & Haselton (1981) for plagioclase and of Wood & Banno (1973) for pyroxenes were used for the GRIPS and the GAFS barometers of Essene (op. cit.). For the other barometers the activity models were those used by the authors in their original papers. In the sample PSH-88-4.3 the results are calculated by using the inclusions across garnet, except plagioclases 1 and 2, which are outside garnet.

Specimen	X_{Fe}^{Grt}	X_{Mn}^{Grt}	X_{Mg}^{Grt}	X_{Ca}^{Grt}	X_{Ca}^{Pl}	X_{Fe}^{Ilm}	X_{Fe}^{Opx}	X_{Al}^{Opx}	logK GRIPS	T_{gi}	T_2	T_5	T_6	P_{grips}	P_{gafs}
25-15-2	0.720	0.075	0.149	0.056	0.385		0.557	0.045			646	571	826		3.0
PSH-88-3	0.702	0.019	0.240	0.040	0.419		0.523	0.047			667	733	682		4.4
29-3-1	0.707	0.019	0.243	0.031	0.316		0.532	0.084				751			4.7
PSH-88-4.3															
1	0.710	0.046	0.153	0.092	0.845	0.983	0.605		3.506	591			683	<5.3	4.5
rim	0.699	0.053	0.158	0.089	0.860	0.986			3.579	576				<5.1	
	0.702	0.062	0.139	0.062	0.822	0.983			3.478	577				<5.3	
	0.687	0.074	0.119	0.120	0.699	0.987			3.245	483				<4.7	
	0.651	0.082	0.104	0.163	0.863	0.961			3.010	498				<5.1	
	0.645	0.082	0.106	0.167	0.869	0.974			3.037	440				<4.3	
	0.660	0.084	0.101	0.154	0.869	0.967			3.092	526				<5.5	
core	0.663	0.081	0.108	0.149	0.871	0.956			3.083	626				<6.6	
	0.645	0.082	0.108	0.165	0.854	0.950			2.968	613				<6.5	
	0.651	0.082	0.106	0.161	0.868	0.950			3.002	619				<6.6	
	0.658	0.086	0.103	0.152	0.766	0.965			3.027	557				<6.1	
	0.657	0.080	0.103	0.160	0.881	0.956			3.022	579				<6.4	
	0.664	0.074	0.106	0.156	0.826	0.982			3.041	519				<5.4	
rim	0.666	0.066	0.114	0.153	0.826	0.958			2.961	618				<6.9	
2	0.696	0.057	0.135	0.112	0.856	0.974			3.311	684				<6.8	

c) GPBM pressures for a muscovite zone specimen. P_{HC} = grt-pl-bt-ms pressures after Hodges & Crowley (1985). The temperature in brackets was used to calculate the pressure.

Specimen	X_{Fe}^{Grt}	X_{Mn}^{Grt}	X_{Mg}^{Grt}	X_{Ca}^{Grt}	X_{Ca}^{Pl}	X_{Fe}^{Bt}	X_{Mg}^{Bt}	$X_{Al}^{Vl}^{Ms}$	X_{Na}^{Ms}	X_{K}^{Ms}	T	P_{HC}
PSH-88-1	0.484	0.350	0.040	0.126	0.667	0.560	0.263	0.867	0.032	0.963	(570)	2.8

Appendix 4. Map coordinates of the analysed specimens.

Specimen	Map sheet	Northing	Easting
18-3-1	3314 08	7029910	3486780
18-80-1	3314 08	7029850	3486830
24-5	3314 09	7030820	3487450
24-31	3314 09	7030800	3487470
25-15-5	3314 09	7031240	3484750
26-115-1	3314 09	7030540	3485000
26-230-1	3314 09	7030470	3484920
28-650-2	3314 09	7030320	3484440
29-3	3314 09	7031420	3488050
29-25	3314 09	7031400	3488070
29-76	3314 09	7031380	3488100
PSH-85-15	3314 09	7033340	3486300
PSH-85-18	3314 09	7036360	3488320
PSH-85-19	3314 08	7029590	3486940
PSH-86-14	3314 12	7035580	3491900
PSH-86-15	3314 12	7034600	3492320
PSH-88-1	3314 11	7029390	3494730
PSH-88-2	3314 12	7037420	3491000
PSH-88-3	3314 08	7028190	3485390
PSH-88-4	3314 08	7028280	3485250
PSH-88-10	3314 08	7028340	3487920
PSH-88-12	3314 08	7028000	3488160
PSH-88-14	3314 08	7029480	3485270
PSH-88-15	3314 08	7029600	3484320
PSH-88-16	3314 08	7029230	3484250
PSH-88-22	3314 08	7027480	3486400
PSH-88-24	3314 09	7034280	3488120
PSH-88-25	3314 09	7033960	3487750
PSH-88-39	3314 09	7035240	3487030
PSH-88-40	3314 09	7032260	3485060
19	3314 09	7036550	3488460
21,23	3314 12	7037400	3491040
24	3314 11	7031080	3495020
25	3314 12	7036340	3491890
28	3314 12	7035760	3492220
52	3314 08	7030160	3484700
53	3314 08	7030840	3484460
54	3314 09	7031300	3484500
60	3314 12	7036580	3492020

THE VAARASLAHTI PYROXENE GRANITOID INTRUSION AND ITS CONTACT AUREOLE: ISOTOPE GEOLOGY

by

UELI HAUDENSCHILD

Haudenschild, U. 1995. The Vaaraslahti pyroxene granitoid intrusion and its contact aureole: isotope geology. *Geological Survey of Finland, Bulletin 382, 81–89*. 4 figures and 2 tables.

Rb-Sr whole-rock isochrons for a pyroxene granitoid complex and its contact-metamorphically overprinted host-rock yielded ages of 1807 ± 10 Ma and 1889 ± 8 Ma respectively. The whole-rock age of the host-rock within the contact aureole corresponds to the zircon U-Pb age (1884 ± 5 Ma) of the intrusion while the plutonic body itself shows prolonged strontium equilibration without any interaction with the host-rock. K-Ar ages on hornblende (1847 ± 10 Ma) and biotite (1781 ± 14 Ma, 1783 ± 11 Ma) date cooling to about 550°C and 300°C , respectively. According to these data strontium exchange ceased at temperatures as low as $400\text{--}450^\circ\text{C}$. The explanation for this behaviour may be found in the mineralogy of the plutonic rock, in which the main strontium bearing phases are feldspars (closure temperature), texture (fluid circulation) and its position within the Proterozoic crust (long-lasting moderate temperature).

Keywords (GeoRef, Thesaurus AGI): absolute age, Rb/Sr, K/Ar, aureoles, cooling, granites, charnockite, contact metamorphism, Proterozoic, Vaaraslahti, Pielavesi, Finland

Ueli Haudenschild, Abteilung für Isotopengeologie, Erlachstr. 9a, CH-3012 Bern, Switzerland. Present address: Sonneggsteig 6, CH-3008 Bern.

INTRODUCTION AND GEOLOGICAL SETTING

This paper presents Rb-Sr and K-Ar data on mineral and whole-rock samples from the Vaaraslahti pyroxene granitoid and its contact aureole, central Finland.

Detailed investigations of this area have been made by Hölttä (1988), Korsman (1986, 1988), Korsman et al. (1984), Salli (1977, 1983) during the past decade. A description of the Vaaraslahti intrusive is given by Lahti (1995), while the metamorphic evolution of its contact aureole was examined by Hölttä (1995). The location of the area is presented in Fig. 1.

Lithologically the Vaaraslahti area consists mainly of a metapelitic-metavolcanic sequence of amphibolite to granulite facies rocks. A number of foliated synkinematic 1885 Ma gneissose tonalites intrude into the metasedimentary succession. In contrast, coarse-grained pyroxene granitoid intrusions described in the

Vaaraslahti and Kiuruvesi areas (Marttila 1976) do not show any preferred orientation, although they are broadly coeval with the tonalites. The Vaaraslahti pyroxene granitoid intrusion developed a contact aureole within which the grade of metamorphism increases from amphibolite to granulite facies conditions.

In this work Rb-Sr whole-rock isochrons were determined on the pyroxene granitoid and its host rock to obtain information on the timing of the high grade metamorphic event affecting the host-rocks and a possible post-plutonic overprint upon the intrusive. K-Ar mineral ages were measured to date the cooling of the Vaaraslahti area through the blocking temperatures of hornblende and biotite, the term "blocking temperature" being defined as the temperature present at the time corresponding to the age measured (Hauden-

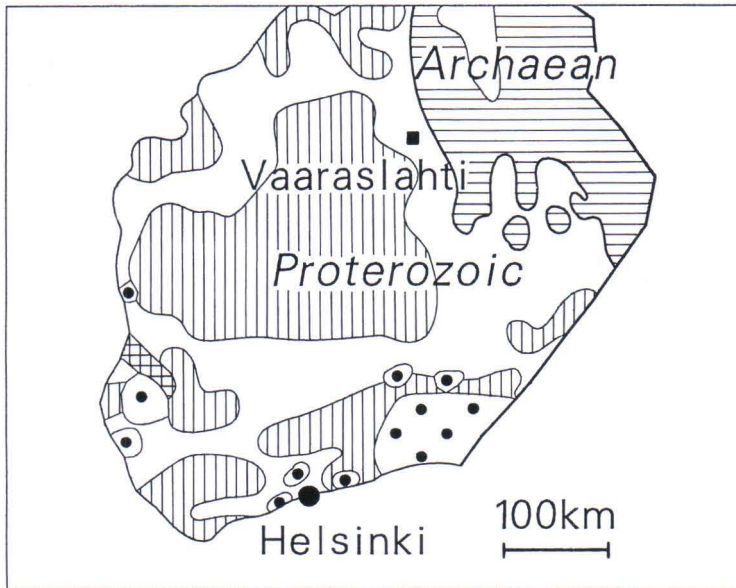


Fig. 1. The location of the study area (box). The main units of the bedrock are: horizontal lines = Archean gneisses; unshaded = Paleoproterozoic schists and gneisses; vertical lines = Paleoproterozoic (1.9-1.8 Ga) granitoids; dotted = rapakivi granites (1.6 Ga).

schild 1990). Blocking temperatures of 300°C and 550°C were used for interpreting the bio-

tite (Jäger 1979) and hornblende (Haudenschild 1990) data, respectively.

PREVIOUS DATINGS

The Pielavesi area has been isotopically investigated over a period of nearly three decades. Pioneer work on the Vaaraslahti intrusive was done by Wetherill et al. (1962), using the Rb-Sr and the K-Ar methods for biotite. A U-Pb zircon age of 1884±5 Ma was published for the Vaaraslahti granite by Salli (1983). Similar ages were measured on several synkinematic intrusive rocks from the same area (Marttila 1976, Salli 1983). A concordant monazite from the Vaaraslahti granite yields an age of 1874 Ma (Salli 1983). U-Pb studies of the host rock at different distances from the contact reveal that the zircons immediately

adjacent to the contact (1895±1 Ma) were reset to the intrusion age while at a distance of 80 meters zircon has only partly lost its radiogenic memory (Vaasjoki & Sakko 1988). The U-Pb age on monazite from the contact is 1879±3 Ma, but 1887±4 Ma 80 meters away. K-Ar studies of mica and hornblende around the intrusion have been used to develop a detailed model of the late uplift history of the area, giving ages around 1750 Ma for the cooling through the blocking temperature of the K-Ar system in biotite (Haudenschild 1988, 1990).

SAMPLE MATERIAL AND ANALYTICAL PROCEDURE

Rb-Sr whole-rock isochrons were measured for the intrusive and its host rock, to obtain information on the time and dimension of the contact metamorphic overprint. K-Ar ages of biotite from a granitic and a monzonitic sample were measured to allow direct comparison between the ages of different radiometric systems of both the hypersthene granite intrusion and its host rock.

Eleven samples were collected across the Vaaraslahti intrusive. Six samples were taken from the monzonitic, and five from the granitic part of the intrusion. Five samples of the metapelitic host-rock were taken from the garnet-cordierite-spinel zone along roadcuts within the first 500 to 1000 meters from the southwest contact. The weight of all the samples exceeds 30 kg. Whole-rock samples of about 500 g, obtained by splitting the sample after crushing were ground for 18 to 24 hours to analytical powder in ethanol absolute. Min-

erals were separated using magnetic and heavy-liquid separation techniques and finally hand-picked to a purity of >99%.

All samples were dissolved in a perchloric-hydrofluoric acid mixture. Rb-Sr samples were spiked with highly enriched ⁸⁴Sr and ⁸⁷Rb spike. Rb and Sr were separated on ion-exchange columns. A microwave dissolution technique was applied to the hornblende sample, adding 3 g HF Suprapur 40% and 1 g HNO₃ Suprapur 65% to 10 mg of sample material. The solution was spiked with a ⁴⁰K tracer.

The potassium concentration of the micas was measured by flame photometry, with a standard error corresponding to ±1%. Argon measurements were carried out on a VG MM1200 mass-spectrometer. Analyses were done according to the ID method (Kirsten 1966, Dalrymple & Lanphere 1969). Samples were packed in aluminium foil and melted in a molybdenum crucible, using a high-frequency genera-

tor, in a high-vacuum glass-extraction line (Flisch 1986). The extracted gas was spiked with a 99,99975 ³⁸Ar spike (Schumacher 1975), purified and transferred to the mass-spectrometer by a direct connection. Biotite B-4B and LP-6 (Flisch 1982) were used as standard minerals.

Rubidium and potassium from the hornblende sample were measured on a solid-source

single collector mass-spectrometer made by "Ion Equipments" with a 35 cm radius and a triple-filament ion source.

Strontium analyses were done on a VG Sector mass-spectrometer with a 26 cm radius, five collectors and a single-filament ion source. The ages were calculated using IUGS constants (Steiger & Jäger 1977).

RESULTS

Rubidium-strontium dating

Five metapelite samples from the garnet-cordierite-spinel zone plot on an isochron showing an age of 1889±8 Ma (Table 1, Fig. 2). The initial ⁸⁷Sr/⁸⁶Sr ratio is 0.7056. The

whole-rock age corresponds well with the 1895±1 Ma U-Pb age of the zircons extracted from the metapelite near the contact (Vaasjoki & Sakko 1988) as well as with the 1884±5 Ma

Table 1. Rb-Sr analytical data.

Sample No.	Rb _{total} ppm	Sr _{total} ppm	⁸⁷ Rb/ ⁸⁶ Sr	⁸⁷ Sr/ ⁸⁶ Sr	Rel. Std. Div.
Granite					
KAW 2705	160.61	119.07	3.940400	0.807175	0.000035
KAW 2706	164.43	121.06	3.964630	0.808466	0.000070
KAW 2707	150.42	132.97	3.299070	0.789575	0.000092
KAW 2708	155.52	126.31	3.593750	0.798037	0.000060
KAW 3328	156.75	115.07	3.980125	0.808508	0.000014
Monzonite					
KAW 2709	106.19	228.11	1.351670	0.743788	0.000072*
KAW 2710	103.19	194.67	1.539230	0.744988	0.000060
KAW 2711	112.59	194.85	1.678550	0.748610	0.000072
KAW 2712	109.31	188.34	1.685980	0.748640	0.000062
KAW 2713	111.98	188.32	1.727530	0.749582	0.000067
KAW 3329	119.59	159.92	2.174938	0.761320	0.000019
Metapelite					
KAW 2588	145.68	177.72	2.386250	0.770669	0.000011
KAW 2834	154.91	228.52	1.971190	0.759180	0.000077
KAW 2835	141.32	201.40	2.041060	0.762143	0.000071*
KAW 2836	164.20	172.62	2.771760	0.780879	0.000059
KAW 2838	146.03	202.12	2.101340	0.762732	0.000063
KAW 3458	147.97	312.93	1.372770	0.742926	0.000043

* data not used for isochron calculation

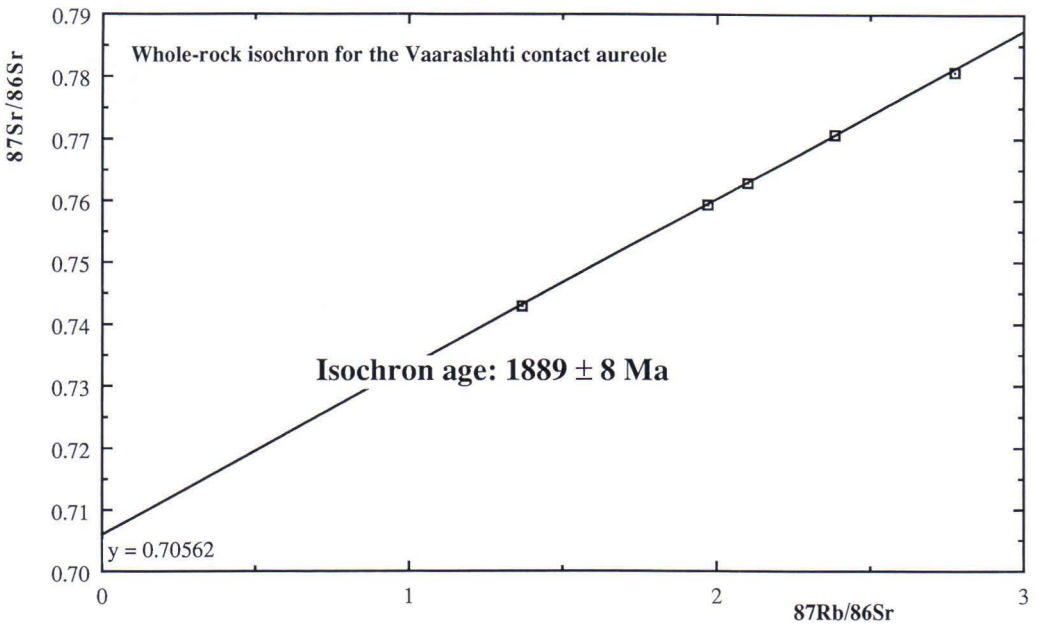


Fig. 2. Rb-Sr whole-rock isochron for five metapelite samples of the Vaaraslahti grt-crd-spl zone.

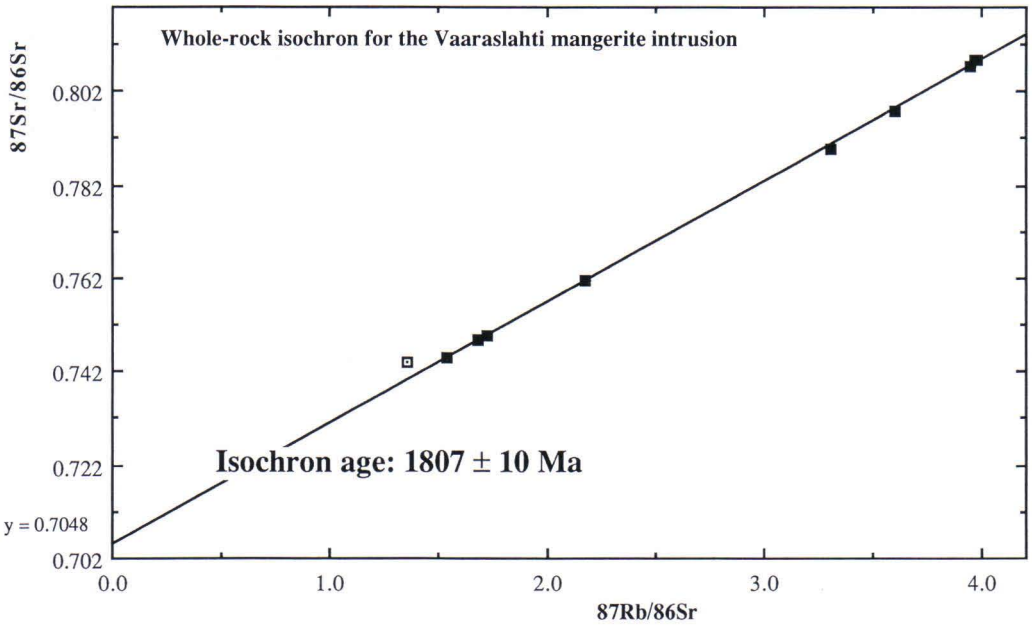


Fig. 3. Rb-Sr whole-rock isochron for ten out of eleven samples of the Vaaraslahti pyroxene granitoid intrusion. The sample marked by the open dot was not used for the isochron calculation.

age for the zircons of the intrusive (Salli 1983). The age is considered to represent the time of the high- grade metamorphism caused by the intrusion. The initial $^{87}\text{Sr}/^{86}\text{Sr}$ ratio is slightly lower than those calculated for similar rocks from the Pihtipudas (0.7072) and the Juva (0.7078) areas (Haudenschield 1990).

Eleven out of twelve samples of the pyroxene granitoid intrusion define a whole-rock isochron with an age of 1807 ± 10 Ma (Fig. 3). The initial $^{87}\text{Sr}/^{86}\text{Sr}$ ratio is 0.7048. The result can be interpreted as a) defining a mixture between a granitic and a monzonitic rock type with different $^{87}\text{Sr}/^{86}\text{Sr}$ initial ratios, b) metamorphic rehomogenisation, c) hydrothermal resetting of the Rb-Sr system. Interpretation "a" can be excluded for two reasons. The calculation of whole-rock isochrons from the granitic and the monzonitic samples separately, leaving out the intermediate data point of the overall isochron (Fig. 3), yielding geologically meaningless results. The apparent age of the granitic samples (1930 ± 30 Ma) is higher than the intrusion U-Pb zircon age, its initial $^{87}\text{Sr}/^{86}\text{Sr}$ ratio lower than the primordial mantle value. The monzonite samples yield an isochron age (1713 ± 50 Ma) below the biotite cooling age. 1884 Ma reference lines (representing the time of the intrusion) drawn through the highest and the lowest $^{87}\text{Rb}/^{86}\text{Sr}$ -values of

the whole-rock isochron intersect the y-axis at a lower initial ratio for the granite than for the monzonite. Concerning interpretation "b" a metamorphic overprint postdating the intrusion is inconsistent with the plutonic, unmetamorphosed texture of the rock. Only retrograde reactions were found to postdate the intrusion (Hölttä 1995). With respect to interpretation "c", oxygen isotope analyses of whole-rock and mineral samples (Haudenschield & Giletti 1991) show normal plutonic $\sigma^{18}\text{O}$ values. If hydrothermal processes had caused strontium rehomogenisation, the water involved would have had similar $\sigma^{18}\text{O}$ values to those of the whole rock system. Besides, a hydrothermal cycle cannot have affected the host-rock since its Rb-Sr whole-rock isochron still records the time of the contact metamorphic overprint. Fluids involved in the strontium homogenisation would have been derived from the intrusive itself. This interpretation is also supported by whole rock-plagioclase-potassium feldspar Rb-Sr isochrons (Haudenschield & Giletti 1991) which indicate ages of 1814 ± 12 Ma for the granitic and 1809 ± 4 Ma for the monzonitic samples. Postmagmatic strontium re-homogenisation took place at around 1810 Ma at moderate temperatures (see below), involving the intrusions own fluid system.

Potassium-Argon dating

Biotite

Biotite concentrates were separated from both the granitic and the monzonitic varieties of the Vaaraslahti intrusive. The analytical results are given in Table 2. The results of 1781 ± 14 Ma and 1783 ± 11 Ma are similar within the 1σ analytical error, which agrees well with the K-Ar age pattern determined for the surrounding host-rocks (Haudenschield 1988). The time of cooling of the Vaaraslahti area to about 300°C can be dated as 1780 Ma.

Hornblende

Hornblende was separated from pyroxene and biotite by hand picking and ground; magnetite inclusions were removed on a magnetic separator. Owing the symplectitic intergrowth of biotite, hornblende and pyroxene the hornblende concentrate may have a purity of about 98%. Potassium was mass-spectrometrically determined with 1.14%. The K-Ar age was calculated as 1847 ± 10 Ma. The analytical results are given in Table 2.

Table 2. K-Ar analytical data.

sample no.	grain size mm	%K	$^{40}\text{K} \times 10^{-8}$ mol/g	^{40}Ar rad. $\times 10^{-10}$ mol/g	^{36}Ar $\times 10^{-12}$ mol/g	$^{40}\text{Ar}/^{36}\text{Ar}$ $\times 10^3$	$^{40}\text{K}/^{36}\text{Ar}$ $\times 10^6$	% ^{40}Ar rad.	model age Ma ± 1 sigma
3328									
biotite	1 - 2	7.64	22.80	402.54	0.4323	93.408	0.5274	99.68	1781 \pm 14
3329									
hornblende	0.35-0.5	1.14	3.40	63.63	0.0179	355.930	1.9017	99.92	1847 \pm 10
biotite	0.35-0.5	6.73	20.09	354.73	0.3115	114.174	0.6444	99.74	1783 \pm 12

Interpretation of the isotopic data

Considering all available isotopic data, the following interpretation is possible: the pyroxene granitoid complex intruded around 1885 Ma into its host-rock, causing a re-equilibration of the Rb-Sr system in the metapelites and extensive contact metamorphism. A cooling rate of 15-20°C/Ma has been calculated for the first 10 Ma, on the assumption of a maximum temperature at the time of the intrusion of 850°C and a blocking temperature of 650-700°C for the monazite (Mezger et al. 1989). Increasing monazite ages with increasing distance from the contact (Vaasjoki & Sakko 1988) correspond with decreasing contact-metamorphic temperatures, reaching the blocking temperature of monazite at a distance of about 80 m. Hornblende and biotite

K-Ar ages indicate a decrease of the cooling rate of about 1°C/Ma around the 1850 Ma time mark (Fig. 4).

The Rb-Sr ages may be attributed to continuous re-equilibration of the Rb-Sr system of the feldspars during cooling to a temperature of about 400-450°C, although the possibility of a second thermal event resetting the Rb-Sr system at temperatures between the biotite and the hornblende blocking temperature cannot be excluded. Tectonic movements associated with the Rb-Sr resetting may have had a slight influence on the intrusion. Block movements leading to individual cooling of adjacent areas continued until 1640 Ma, as indicated by the youngest K-Ar and Rb-Sr mica ages in the area (Haudenschild 1988, 1990).

CONCLUSIONS

The 1890 Ma pyroxene granitoid intrusion has contact-metamorphically overprinted its pelitic host-rocks and reset its Rb-Sr system. A long-lasting cooling process in the medium to low temperature range (500-300°C) led to continuous re-equilibration of the Rb-Sr system within the pyroxene granitoid, while the metapelitic whole-rock system remained closed after the metamorphic peak. The difference in behaviour of the two rock types may be explained by their fluid budget, as well as their

different texture and mineralogy, affecting their susceptibility to secondary alteration. Reactions producing biotite at the expense of hornblende and pyroxene and myrmekitic feldspar-quartz intergrowths in the pyroxene granitoid are evidence of the post-intrusive re-equilibration process. The strontium exchange within the pyroxene granitoid body ceased at a temperature between the blocking of hornblende (550°C) and biotite (300°C), and can be estimated at 400-450°C.

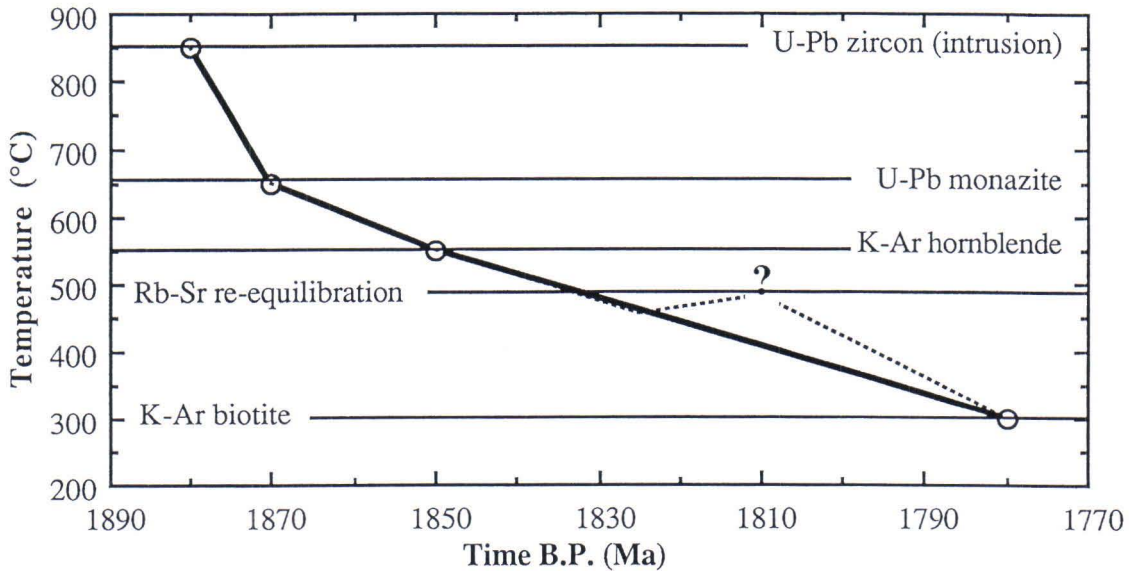


Fig. 4. Time vs. temperature evolution path for the Vaaraslahti block as indicated by the isotope results.

ACKNOWLEDGEMENTS

The author wishes to thank Prof. E. Jäger and Prof. B. Giletti for critical discussions concerning the data interpretation. Important contributions were also made by Dr. K. Korsman and P. Hölttä from the Geological Survey

of Finland. Help from members of the Berne Isotope Geology Laboratory was appreciated. Isotope studies were supported by a post-doctoral fellowship of the Swiss National Science Foundation (Schweizerischer Nationalfonds).

REFERENCES

- Dalrymple, G.B. & Lanphere, M.A. 1969.** Potassium argon dating. San Francisco: W. H. Freeman. 258 p.
- Flisch, M. 1982.** Potassium-argon analysis. In: Odin, G.S.(ed.) Numerical Stratigraphy. Chichester: John Wiley, 151–158.
- Flisch, M. 1986.** K-Ar dating of quaternary samples. In: Hurford, A., Jäger, E. & Ten Cate, J.A.M. (eds.) Dating young sediments. Bangkok, Thailand: CCOP technical secretariat, 299–323.
- Haudenschild, U. 1988.** K-Ar age determination on biotite and muscovite in the Pihtipudas-Iisalmi and Joroinen-Sulkava areas, Eastern Finland. In: Korsman, K. (ed.) Tectono-metamorphic evolution of the Raahe-Ladoga zone. Geological Survey of Finland, Bulletin 343, 33–50.
- Haudenschild, U. 1990.** Cooling history of the eastern Svecokareliides: whole-rock and mica Rb-Sr and hornblende K-Ar ages in the areas of Pihtipudas-Iisalmi and Joroinen-Sulkava, Finland. Bulletin of the Geological Society of Finland 62(1), 39–59.
- Haudenschild, U. & Giletti, B.J. 1991.** Rb-Sr and Oxygen Isotope Geochemistry on a Complex Proterozoic Intrusive, Vaaraslahti, Finland. Schweizerische Mineralogische und Petrographische Mitteilungen 71, 115–123.
- Hölttä, P. 1988.** Metamorphic zones and the evolution of granulite grade metamorphism in the early Proterozoic Pielavesi area, central Finland, Geological Survey of Finland, Bulletin 344. 49 p.
- Hölttä, P. 1995.** Contact metamorphism of the Vaa-

- raslahti pyroxene granitoid intrusion in Pielavesi, Central Finland. In: Hölttä, P. (ed.) Relationship of granitoids, structures and metamorphism at the eastern margin of the Central Finland Granitoid Complex. Geological Survey of Finland, Bulletin 382, 27–79. (this paper)
- Jäger, E. 1979.** Introduction to geochronology. In: Jäger, E. & Hunziker, J.C. (eds.) Lectures in isotope geology. Berlin, Heidelberg, New-York: Springer-Verlag, 1–12.
- Kirsten, T. 1966.** Determination of radiogenic argon. In: Schaeffer, O.A. & Zähringer, J. (eds.) Potassium argon dating. Heidelberg: Springer-Verlag, 7–39.
- Korsman, K. (ed.) 1986.** Development of deformation, metamorphism and metamorphic blocks in eastern and southern Finland. Geological Survey of Finland, Bulletin 339. 58 p.
- Korsman, K. (ed.) 1988.** Tectono-metamorphic evolution of the Raahe-Ladoga zone. Geological Survey of Finland, Bulletin 343. 96 p.
- Korsman, K., Hölttä, P., Hautala, T. & Wasenius, P. 1984.** Metamorphism as an indicator of evolution and structure of the crust in Eastern Finland. Geological Survey of Finland, Bulletin 328. 40 p.
- Lahti, S.I. 1995.** Mineralogy and geochemistry of the Vaaraslahti pyroxene granitoid in Pielavesi, Finland. In: Hölttä, P. (ed.) Relationship of granitoids, structures and metamorphism at the eastern margin of the Central Finland Granitoid Complex. Geological Survey of Finland, Bulletin 382, 5–25. (this paper)
- Marttila, E. 1976.** Evolution of the precambrian volcanic complex in the Kiuruvesi area, Finland. Geological Survey of Finland, Bulletin 283. 109p.
- Mezger, K., Hanson, G.N. & Bohlen, S.R. 1989.** U-Pb systematics of garnet: dating the growth of garnet in the Late Archean Pikwitonei granulite domain at Cauchon and Natawahunan Lakes, Manitoba, Canada. Contributions to Mineralogy and Petrology 101, 136–148.
- Salli, I. 1977.** Pielavesi. Geological Map of Finland 1 : 100 000, Pre-Quaternary Rocks, Sheet 3314. Espoo: Geological Survey of Finland.
- Salli, I. 1983.** Pielaveden kartta-alueen kallioperä. Summary: Pre-Quaternary rocks of the Pielavesi map-sheet area. Geological Map of Finland 1 : 100 000, Explanation to the Map of Pre-Quaternary Rocks, Sheet 3314. Espoo: Geological Survey of Finland. 29 p.
- Schumacher, E. 1975.** Herstellung von 99.9997 per cent ^{38}Ar für die $^{40}\text{K}/^{40}\text{Ar}$ Geochronologie. *Chimia* 29, 441–442.
- Steiger, R.H. & Jäger, E. 1977.** Subcommittee on geochronology: convention on the use of decay constants in geo- and cosmochronology. *Earth and Planetary Science Letters* 36, 359–362.
- Vaasjoki, M. & Sakko, M. 1988.** The evolution of the Raahe-Ladoga zone in Finland: isotopic constraints. In: Korsman, K. (ed.) Tectono-metamorphic evolution of the Raahe-Ladoga zone. Geological Survey of Finland, Bulletin 343, 7–32.
- Wetherill, G.W., Kouvo, O., Tilton, G.R., Gast, P.W. 1962.** Age measurements on rocks from the Finnish Precambrian. *Journal of Geology* 70 (1), 74–88.

BLOCK BOUNDARY AT THE SOUTHEASTERN MARGIN OF THE PALEOPROTEROZOIC CENTRAL FINLAND GRANITOID COMPLEX

by

MIKKO NIRONEN

Nironen, M. 1995. Block boundary at the southeastern margin of the Paleoproterozoic Central Finland Granitoid Complex. *Geological Survey of Finland, Bulletin 382, 91–115*. 13 figures and 3 tables.

The structural setting of igneous rocks near Mikkeli, at the southeastern margin of the Central Finland Granitoid Complex, was studied. The structures in tonalites/granodiorites, migmatitic volcanic-sedimentary gneisses and the coarse-porphyratic Puula Granite at the margin of the Complex (western domain) were compared with the structural-metamorphic sequence in K-feldspar-sillimanite and garnet-cordierite gneisses immediately to the east of the Complex (eastern domain). These results indicate that there is a shear zone, or block boundary, at the margin of the Central Finland Granitoid Complex, defined by anastomosing zones of mylonites and cataclasites. The sense of movement within the shear zone was essentially vertical, west-side-up.

In the western domain, high grade metamorphism of the country rock gneisses preceded the emplacement of the tonalites and granodiorites at 1906 Ma. There is no counterpart to this metamorphism in the eastern domain. The Puula Granite was emplaced 1875 Ma ago as the last expression of igneous activity by which time the surrounding granitoids had already cooled considerably. Shear zone activity at the boundary of the two domains started after 1875 Ma, remained active 1840–1830 Ma ago when metamorphism culminated in the eastern domain, and continued during subsequent retrograde metamorphism.

Keywords (GeoRef, Thesaurus AGI): structural geology, shear zones, block structures, granites, gneisses, metamorphism, deformation, absolute age, U/Pb, Paleoproterozoic, Mikkeli Province, Finland

Mikko Nironen, Geological Survey of Finland, FIN-02150 Espoo, Finland

INTRODUCTION

In the Paleoproterozoic Svecofennian Domain of southern Finland, the schists and gneisses, e.g. in the Tampere Schist Belt, have generally an E-W trending lithological layering and foliation, but around the extensive Central Finland Granitoid Complex (CFGC) they are gradually reoriented into the NW-SE trending gneisses of the Savo Schist Belt (Fig. 1). The present study area, at Otava, is located at the intersection of these two main structural trends. The rocks of the CFGC as well as the plutonic rocks in the central and southern Savo Schist Belt yield typical synkinematic Svecofennian ages (1.90-1.88 Ga; Aho 1979, Korsman et al. 1984, Huhma 1986, Nironen 1989, Nironen & Front 1992).

The Savo Schist Belt is known to consist of a block structure in which each block was subjected to a distinct tectonothermal history (Korsman et al. 1984). Korsman et al. (1988) delineated a block boundary at Otava between

the CFGC and adjacent gneisses. According to them, the western granitoids belong to the Kiuruvesi-Haukivesi complex in which metamorphism culminated before synkinematic plutonism. The Kiuruvesi-Haukivesi complex is characterized by retrograde metamorphic mineral assemblages. In contrast, the eastern gneisses are part of the Rantasalmi-Sulkava area in which prograde metamorphic features predominate. In this area, the emplacement of synkinematic granitoids preceded progressive metamorphism which culminated at Sulkava as late as 1.83-1.81 Ga ago.

There are still problems in understanding the evolutionary relationship between these two major structural zones of the Svecofennian supracrustal rocks, and between the synkinematic (1.88 Ga) and late-kinematic (1.83 Ga) magmatisms. In order to shed light to these problems, the structural setting of the granitoids around Otava was selected for study.

GEOLOGICAL SETTING

The southeastern margin of the CFGC comprises two granite batholiths and a complex of tonalites and granodiorites (Fig. 1). The northern batholith, the Puula Granite, is roughly 450 km² and the Suontee Granite is 250 km² in area. Both granites are coarse-porphyritic, with abundant K-feldspar megacrysts. The tonalites and granodiorites contain supracrustal rocks (migmatitic mica gneisses with amphibolite and quartz-feldspar gneiss intercalations) as xenoliths of highly variable size and abundance.

The supracrustal rocks outside the CFGC are K-feldspar-, sillimanite- and cordierite-bearing schists and gneisses. Similar rocks in the Savo Schist Belt have been interpreted as metaturbidites on the basis of well preserved sedimentary structures in low grade rocks (Gaál & Rauhamäki 1971). Biotite gneisses, biotite-hornblende gneisses and amphibolites occur as interlayers in the metaturbidites. Pillow lava structures have locally been preserved in the amphibolites (Gaál & Rauhamäki 1971, Kousa 1985).

ROCK TYPES

The study area was divided into two domains along the margin of the CFGC (Fig. 2).

Hence, the boundary roughly coincides with the block margin delineated by Korsman et al.

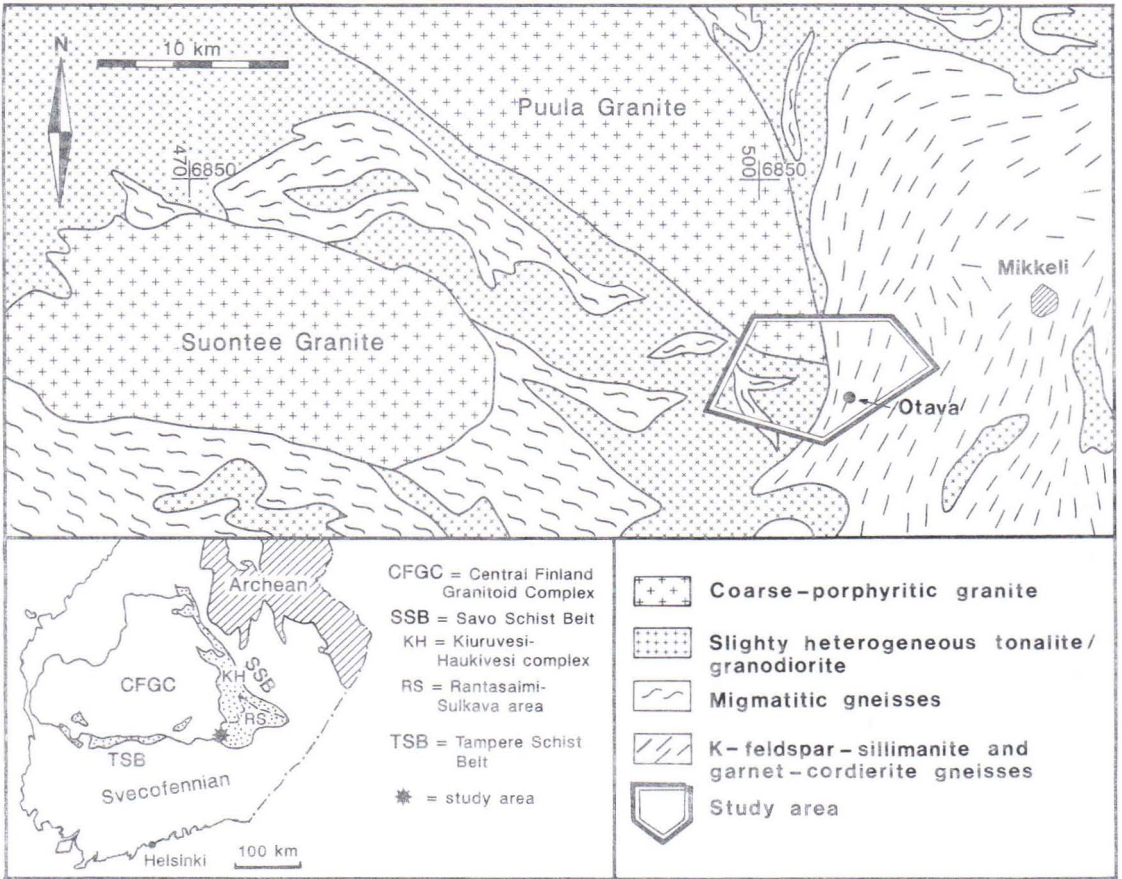


Fig. 1. Geological setting of the study area (modified from Kallio 1988 and Simonen & Niemelä 1980).

(1988). In the eastern domain, the grade of metamorphism in the metaturbidites increases eastwards from sillimanite schists and coarser K-feldspar-sillimanite gneisses into garnet-cordierite gneisses. The latter contain abundant garnet-bearing pegmatite dikes. Biotite schists and gneisses as well as hornblende-biotite gneisses, devoid of porphyroblasts and interpreted as metamorphosed tuffs or tuffites, occur as interlayers in the metaturbidites.

The trondhjemite stock in the eastern domain contains abundant pegmatitic dikes as well as xenoliths of mica gneiss and amphibolite. Pegmatites are most abundant at the mar-

gins of the stock.

The Puula Granite occupies the northern part of the western domain. It contains K-feldspar megacrysts, typically from 1-4 cm up to 7 cm in size, which usually comprise 40-60% of the rock by volume, although this value decreases into 20% in some marginal areas. The megacrysts are commonly anhedral to subhedral, but euhedral megacrysts also occur, especially where the overall abundance of megacrysts is lower (Fig. 3a). The groundmass consists of euhedral to subhedral, strongly zoned (An_{37-10}) plagioclase laths, 2-15 mm in length, together with biotite and interstitial

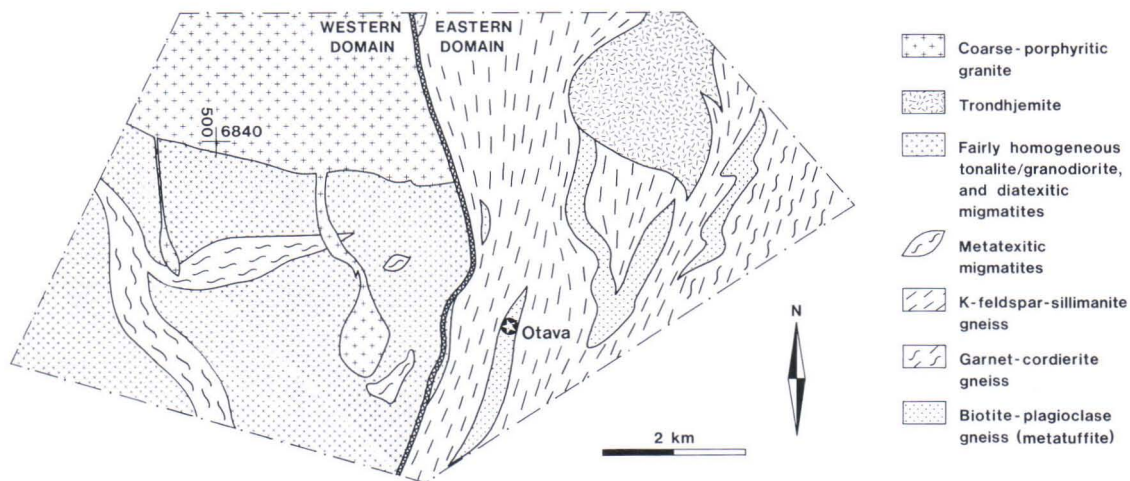


Fig. 2. Geological map of the study area. A shear zone separates the area into two domains.

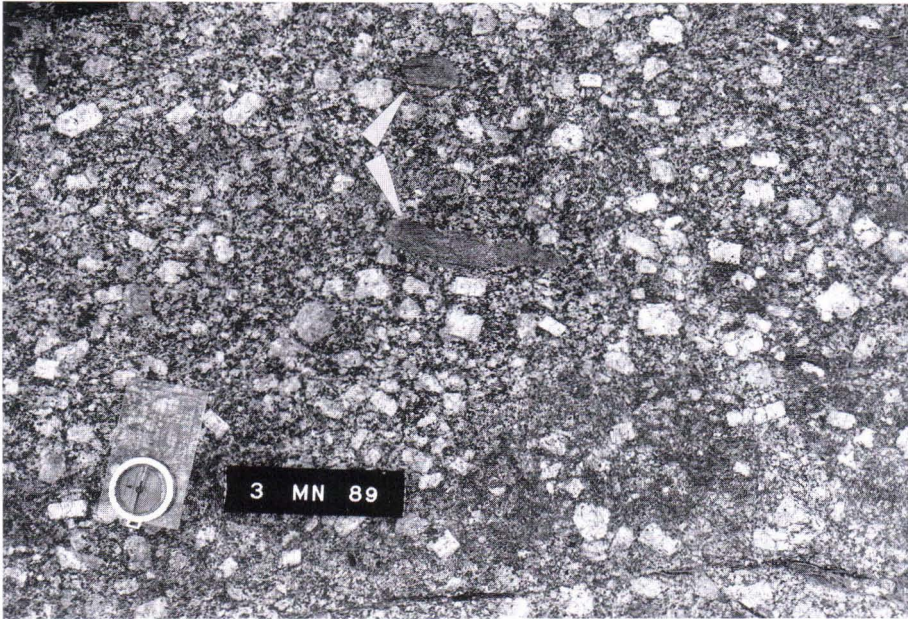
quartz. Hornblende, largely altered to actinolite near the contacts, is also a major constituent, although biotite is the predominant mafic mineral.

Two apophyses of coarse-porphyritic granite extend southwards from the Puula Granite. They truncate a variety of lithologies, including tonalites, granodiorites and minor granites as well as variably disrupted supracrustal rocks. The tonalites and granodiorites show a range of mineral compositions; some tonalites are fairly dark and hornblende-bearing while others contain only biotite as the mafic mineral. The mafic minerals are commonly retrogressed into chlorite. Other major constituents are plagioclase (An_{45-30} in tonalites, An_{35-30} in granodiorites), quartz, and K-feldspar in granodiorites. Homogeneous tonalites and granodiorites grade into diatexitic which contain amphibolite xenoliths and remnants of gneissic rocks, and further into extremely heterogeneous metatexitic rocks in which several intrusive phases, tonalitic to granitic in composition, have migmatized supracrustal rocks. The supracrustal rocks in the western domain are cummingtonite gneisses, biotite gneisses with garnet and K-feldspar porphyroblasts, biotite gneisses devoid of porphyroblasts (metatuffites), and amphibolites. Gneisses with alternating psammitic layers containing abundant concretions and pelitic, strongly migmatitic layers are probably turbiditic in origin.

PUULA GRANITE CONTACT PHENOMENA

In the southern part of the batholith, the contacts of the granite are either obscured by surficial deposits or lakes, or else intensely deformed. A non-mylonitic contact was however found at the southern contact against fine-grained granodiorite. Near the contact, the granite shows a weak preferred orientation

of K-feldspar megacryst long axes and mafic enclaves (Fig 3a). A preferred orientation of K-feldspar phenocrysts was observed at several sites near the contact of the batholith. Also the larger plagioclase laths in the matrix are preferentially oriented (Fig 3b). Deformation of the matrix minerals is minor, with



a)



b)

Fig. 3. a) Puula Granite near the southern contact. Note the weak preferred orientation in the matrix and of K-feldspar megacrysts and mafic enclaves (shown by arrows). Length of code bar 15 cm. $x=6839.46$, $y=3502.74$ b) Matrix at the site of Fig. 3a. Striped = biotite, heavily stippled = actinolite, lightly stippled = feldspar (plagioclase and K-feldspar), bright = quartz. Scale bar 3 mm.

weak bending of biotite flakes, and undulatory extinction of quartz together with subgrain formation at grain margins. Given the preferred orientation of feldspars and relatively low degree of strain in the matrix, the feldspar fabric is attributed to magmatic flow or "pre-full crystallization" deformation rather than solid-state deformation (cf. Hutton 1988, Paterson et al. 1989). Hence, the K-feldspar megacrysts may be considered as phenocrysts (megacrysts grown in melt). They rotated into subparallelism in viscous magma, and the rock was subsequently subjected to minor crystal

plastic deformation.

At the contact, the granodiorite contains numerous small, subangular xenoliths of supracrustal rocks. Tortuous apophyses of granite, a few centimeters in width, and a few isolated K-feldspar megacrysts occur in the granodiorite (Fig. 4). The mafic minerals in the granodiorite have been altered to chlorite. Evidently the granitic magma and fluids penetrated the already solidified and cooled granodiorite via fractures related to the emplacement of the Puula Granite.

STRUCTURAL SEQUENCE IN THE EASTERN DOMAIN

D_a deformation

In the metatuffites, the earliest recognizable tectonite fabric, defined as S_a , is parallel

to compositional layering. The original trend of S_a cannot be deduced because of later fold-

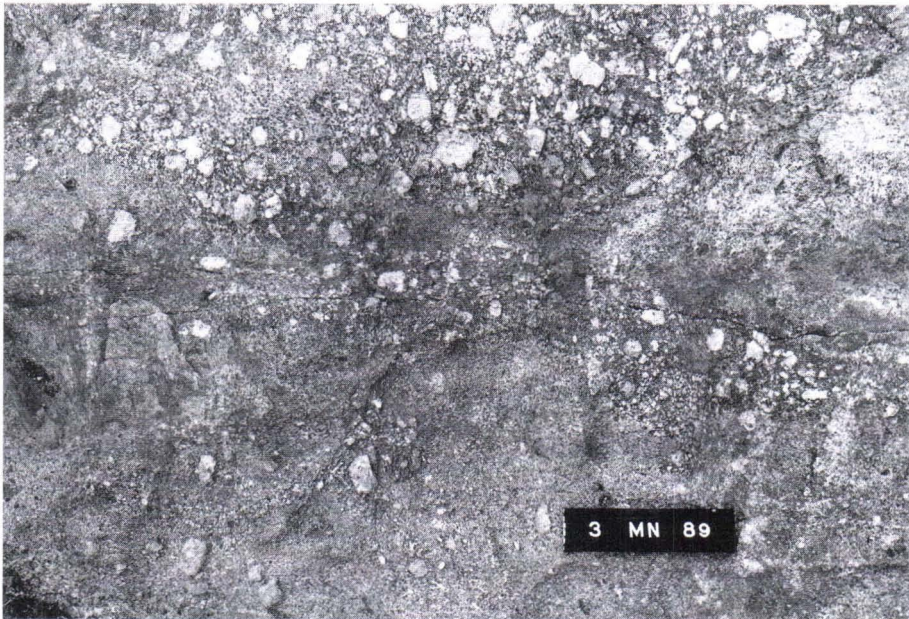


Fig. 4. Contact between the Puula Granite and the fine-grained tonalite. Length of code bar 15 cm. $x=6839.46, y=502.74$.

ing (Fig. 5). This foliation in the metatuffites is differentiated at microscopic scale, and is expressed as the preferred orientation of biotite flakes. Ubiquitous leucocratic veins in the metaturbidites, parallel to S_a , are the result either of subsolidus segregation or anatexis. Thicker pegmatitic dikes in K-feldspar-sillimanite gneisses and garnet-cordierite gneisses, slightly crosscutting S_a , are presumably anatectic in origin.

In the K-feldspar-sillimanite gneisses, the K-feldspar porphyroblasts contain small biotite inclusions with a weak preferred orienta-

tion at an angle to the S_a foliation in the matrix (Fig. 6a). This suggests that a tectonite fabric, older than S_a , is preserved in the porphyroblasts but was reactivated and decrenulated in the matrix during D_a (cf. Bell 1986). Alternatively, the porphyroblasts grew during an early stage of D_a and were transposed in the matrix during a later stage of D_a . Since the inclusion trails are rather vague and show no clear curvature, it is impossible to conclude whether the porphyroblasts grew before or during D_a deformation.

D_b deformation

A characteristic feature of D_b deformation is its heterogeneity. In places folding is open, and a fairly weak foliation has developed. Granitic and pegmatitic dikes have intruded along the axial plane (Fig. 6b). Coarse biotite flakes define the S_b foliation, and in mica-rich lithologies a differentiated crenulation cleavage with an intersection lineation has developed. In the K-feldspar-sillimanite gneisses, sillimanite fibres appear to have been micro-

folded at S_b fold hinges (Fig. 6c).

In a broad zone in the center of the study area (Fig. 5), extending northwards along the margin of the Puula Granite, D_b strain intensity is greater than elsewhere; F_b folds are isoclinal and older foliations have been transposed parallel to subvertical S_b . Quartz shows the effects of dynamic recovery and recrystallization (subgrains and new grains along the margins of larger grains), but even the new

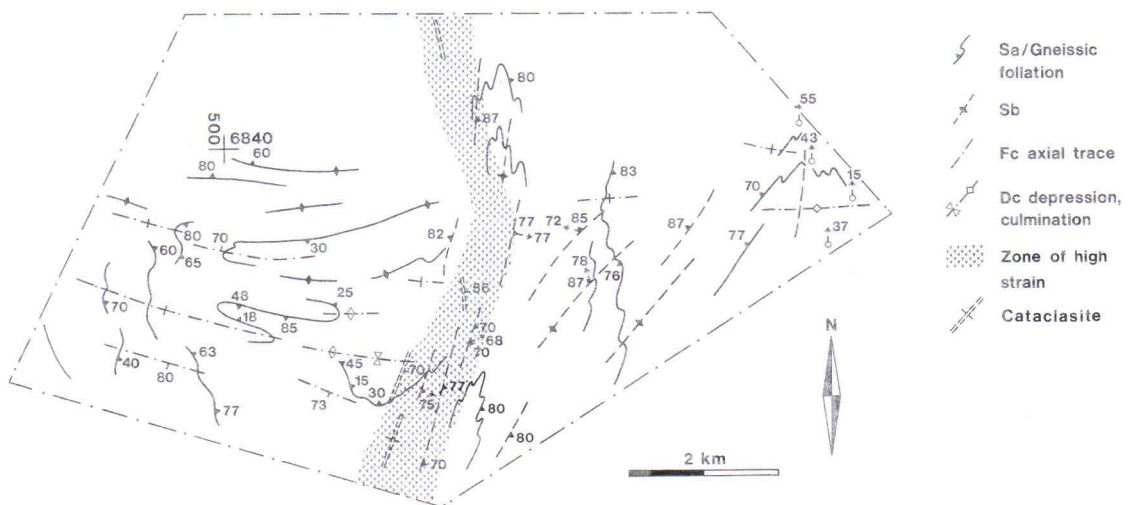
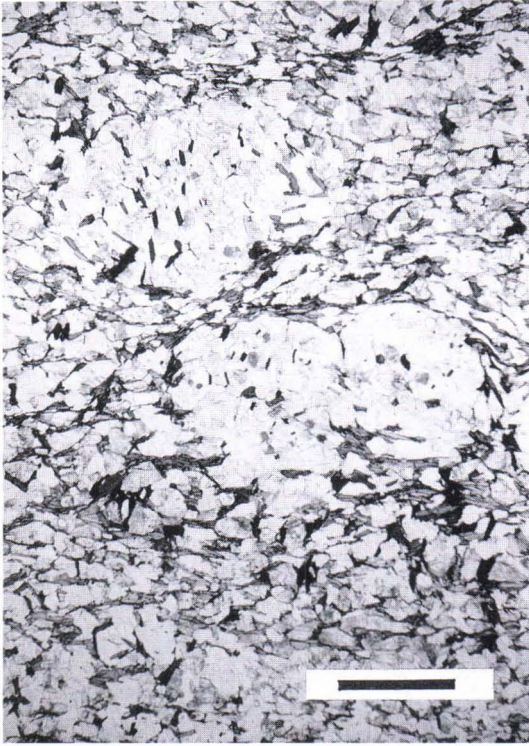


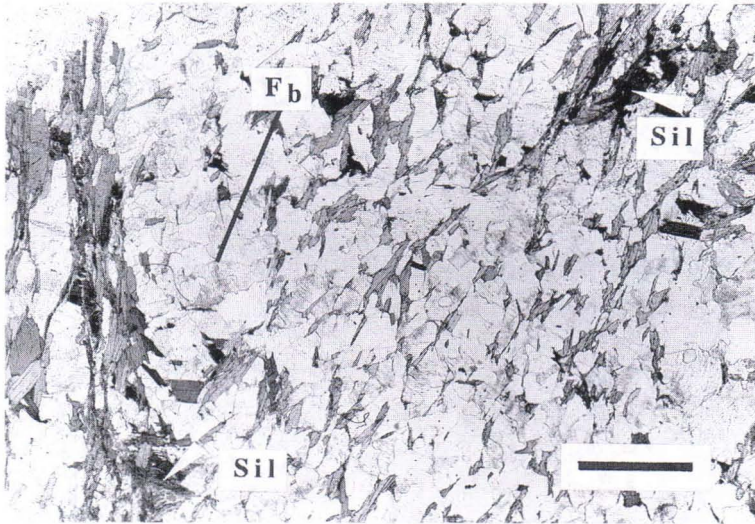
Fig. 5. Structural map of the study area.



a)



b)



c)

Fig. 6. K-feldspar-sillimanite gneiss. $x=6838.36$, $y=3505.12$. a) Small biotite flakes in K-feldspar, oriented at an angle to biotite foliation in the matrix. Plane polarized light. Scale bar 2 mm. b) F_b folding. Length of code bar 15 cm. c) Microfolded sillimanite fibres (Sil), partly decomposed into muscovite, at the hinge of F_b fold. Plane polarized light. Scale bar 2 mm.

grains are strained. Deformation twinning is common in plagioclase. Anastomosing dark seams, consisting of strained and kinked biotite flakes as well as recrystallized fine biotite, are probably the result of pressure solution processes along fractures.

In the garnet-cordierite gneisses, garnet-bearing pegmatite dikes are parallel to the differentiated S_b foliation. The dikes are probably anatectic, and the biotite-rich, garnet-bearing schlieren in them represent melanosome (restite?). The large garnet porphyroblasts in the mesosome, commonly 1-2 cm in length, are parallel to foliation, but in places the S_b biotite flakes wrap around garnet (Fig. 7a). Crenulated sillimanite fibres are preserved within cordierite (Fig. 7b and c). The elongate cordierite blasts as well as the crenulation axial planes are parallel to S_b in the matrix, defined by coarse biotite.

Shelley (1993, p. 295) suggested retrograde replacement of sillimanite by mica as an ex-

planation for microfolded sillimanite fibres in mica. However, the systematic array of the sillimanite microfolding within the cordierite porphyroblasts and the parallelism between axial planes of the microfolds and the S_b foliation suggests growth of cordierite over F_b microfolded sillimanite. The microstructure in Fig. 7c is similar to the one modelled by Bell (1981) for deformation partitioning during crenulation. Accordingly, the crenulated foliation within cordierite is interpreted as S_a . Sillimanite growth initiated before or during an early stage of D_b , and cordierite and garnet grew during a later stage of D_b deformation.

The mica gneiss xenoliths in the trondhjemite indicate that deformation and associated metamorphism preceded the emplacement. At the eastern contact the composite S_b foliation can be seen to continue into the igneous rock as fractures. Hence, the trondhjemite was emplaced before D_b deformation had ceased.

D_c deformation

A domal F_b - F_c fold interference structure is evident in the eastern part of the domain (Fig. 5). F_b fold axes steepen away from the culmination of the dome. F_c folding is seen at outcrops as open to tight, almost symmetric similar folding. The subvertical fold axial planes trend roughly E-W (Figs. 5 and 8). At microscopic scale, older foliations are crenulated, with biotite being strained and kinked in the microfold hinges. The effects of dynamic re-

covery can be seen in quartz, but even the subgrains are strained. Retrograde alteration of mafic minerals to green biotite, pale amphibole and chlorite is common. Few muscovite flakes have grown during D_c , but these are also strained. Some unstrained grains, crystallized in the hinges of F_c microfolds, show that muscovite growth continued after D_c deformation.

D_d deformation

Cataclastic D_d deformation is mostly seen in the zone of intense D_d strain, near the boundary of the two domains. It is expressed

as fractures and thin (2-5 mm) seams of microbreccia, subparallel to S_b .

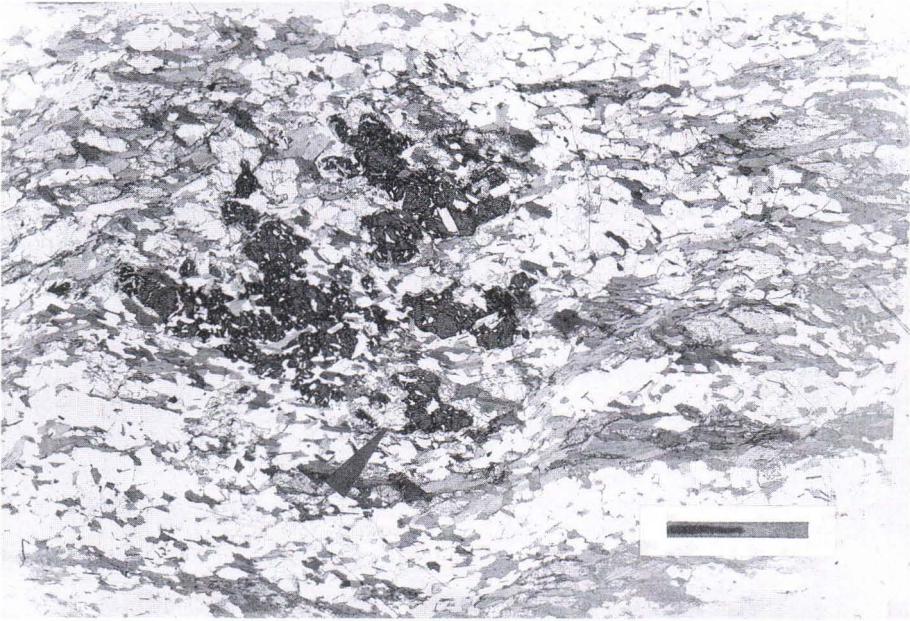


Fig. 7a)

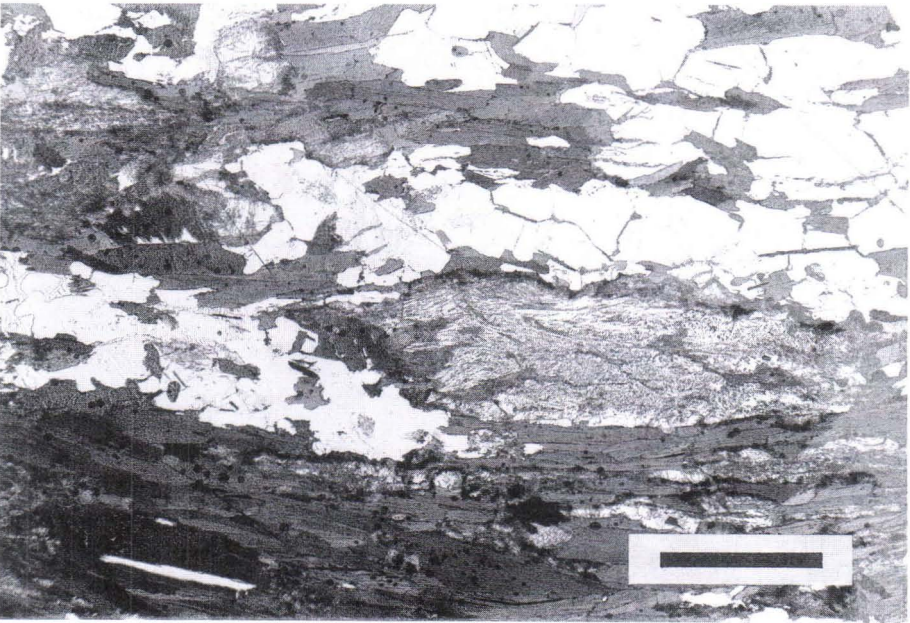


Fig. 7b)

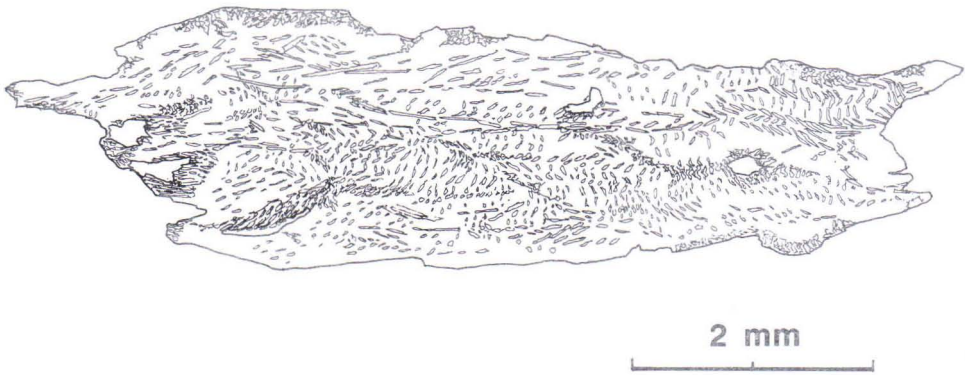


Fig. 7c)

Fig. 7. Garnet-cordierite gneiss. a) S_b biotite foliation wraps around garnet. Post- D_b cordierite (e.g. the grain shown by the arrow) overgrows biotite. Plane polarized light. Scale bar 5 mm. $x=6838.70$, $y=3507.98$. b) Microfolded sillimanite fibres in cordierite, axial plane is parallel to S_b in the matrix. Scale bar 2 mm. $x=6839.32$, $y=3508.32$. c) Sketch of the sillimanite microstructure in the cordierite porphyroblast in Fig. 7b.

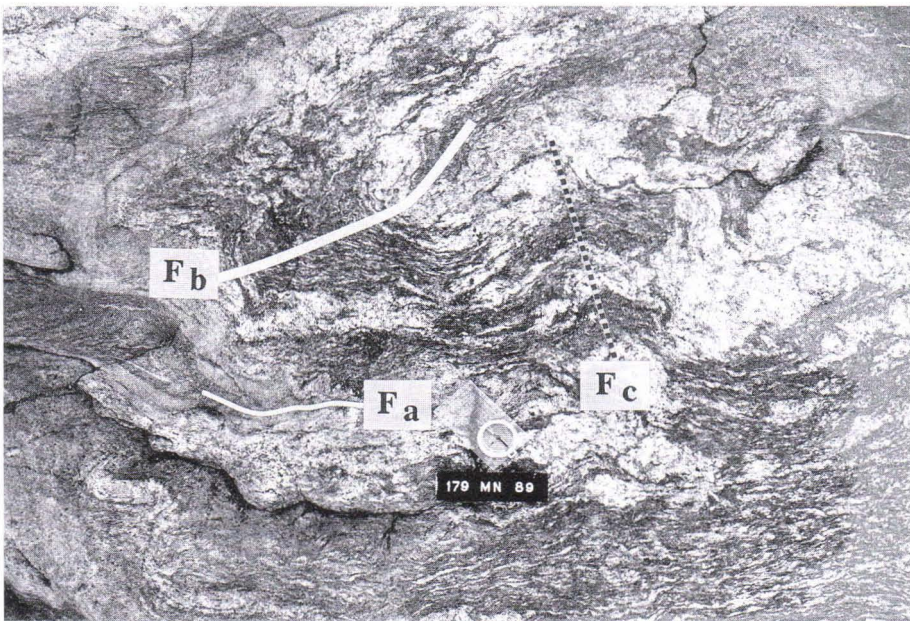


Fig. 8. Polyphase folding in garnet-cordierite gneiss. Length of code bar 15 cm. $x=6839.30$, $y=3508.36$.

IGNEOUS AND STRUCTURAL SEQUENCE IN THE WESTERN DOMAIN

Three types of tonalite/granodiorite were discerned in the field, based on differences in the character and amount of xenoliths and in the degree of foliation (Fig. 9). The oldest intrusive rock, occurring in a small area, is a distinctly foliated, medium-grained tonalite/granodiorite (Figs. 9a and 10a). The rock contains strongly elongated mafic enclaves and few inclusions of supracrustal rock parallel to the foliation.

Two successive phases of weakly foliated to unfoliated tonalitic/granodioritic rock occupy most of the area to the south of the Puula Granite. The older one is a gray, fine-grained rock (Fig. 9b) and the younger a more felsic, medium-grained rock (Fig. 9c). No contact was found between the distinctly foliated and the unfoliated to weakly foliated granitoids, but in addition to the difference in foliation intensity, the latter rocks contain abundant biotite gneiss and amphibolite xenoliths.

The trend of the gneissic foliation varies considerably (Fig. 5). It is fairly undifferentiated in homogeneous lithologies but migmatitic in mica-rich rock types. The gneissic foliation was subjected to folding with an E-W trending axial plane. In places the oldest, fine-grained granitoid rock has intruded the folded supracrustal rocks along the E-W trending axial plane (Fig. 10b). Some xenoliths in the fine-grained rock contain a folded migmatitic foliation similar to the foliation in the metatextitic migmatite areas. The foliation, expressed as preferred orientation of biotite flakes, is associated with foliation-parallel leucocratic veins. The foliation-parallelism and the mafic selvages adjacent to the veins (Fig. 10b) suggest subsolidus segregation (cf. Sawyer & Robin 1986). The veins are granitic in composition, which is characteristic of higher grade subsolidus veins, according to Sawyer and Robin (1986). Irrespective of whether the veins are the result of subsolidus segrega-

tion or anatexis, they indicate at least upper amphibolite facies metamorphic conditions. A weak biotite orientation can be seen in the axial plane of the folds. In some xenoliths, garnet has overgrown the older gneissic foliation but the straight inclusions trails differ from the microfolded pattern in the matrix. K-feldspar porphyroblasts with biotite inclusion trails differing in orientation from the external (gneissic) foliation were also observed.

The gneissic foliation and migmatization in the supracrustal rocks may be interpreted as the result of metamorphism and deformation predating the emplacement of the granitoids, or as the result of emplacement of the granitoids, i.e. contact metamorphism. The sequence of 1) migmatization, 2) growth of garnet porphyroblasts in some xenoliths, 3) folding and growth of new biotite, and 4) injection of the fine-grained granitoid type along the axial plane can be distinguished. The growth time of a garnet porphyroblast with ca. 1 mm diameter has been estimated to be less than 1 Ma, and a few Ma is required for the development of a penetrative foliation (see Barker 1994). These estimates are compatible with contact metamorphism caused by the emplacement of several granitoid pulses. However, considering that the oldest, distinctly foliated granitoid occurs only in a small area, the sequence presented above should have been caused by the emplacement of the fine-grained granitoid type. Since the sequence appears too complex for a single emplacement event, an interpretation of metamorphism predating the intrusion of at least the fine-grained granitoid is preferred.

The three tonalitic/granodioritic phases show evidence of decreasing intensity of deformation and associated recrystallization in their igneous microstructures (Fig. 9). The oldest, distinctly foliated rock probably intruded during the deformation associated with migmati-

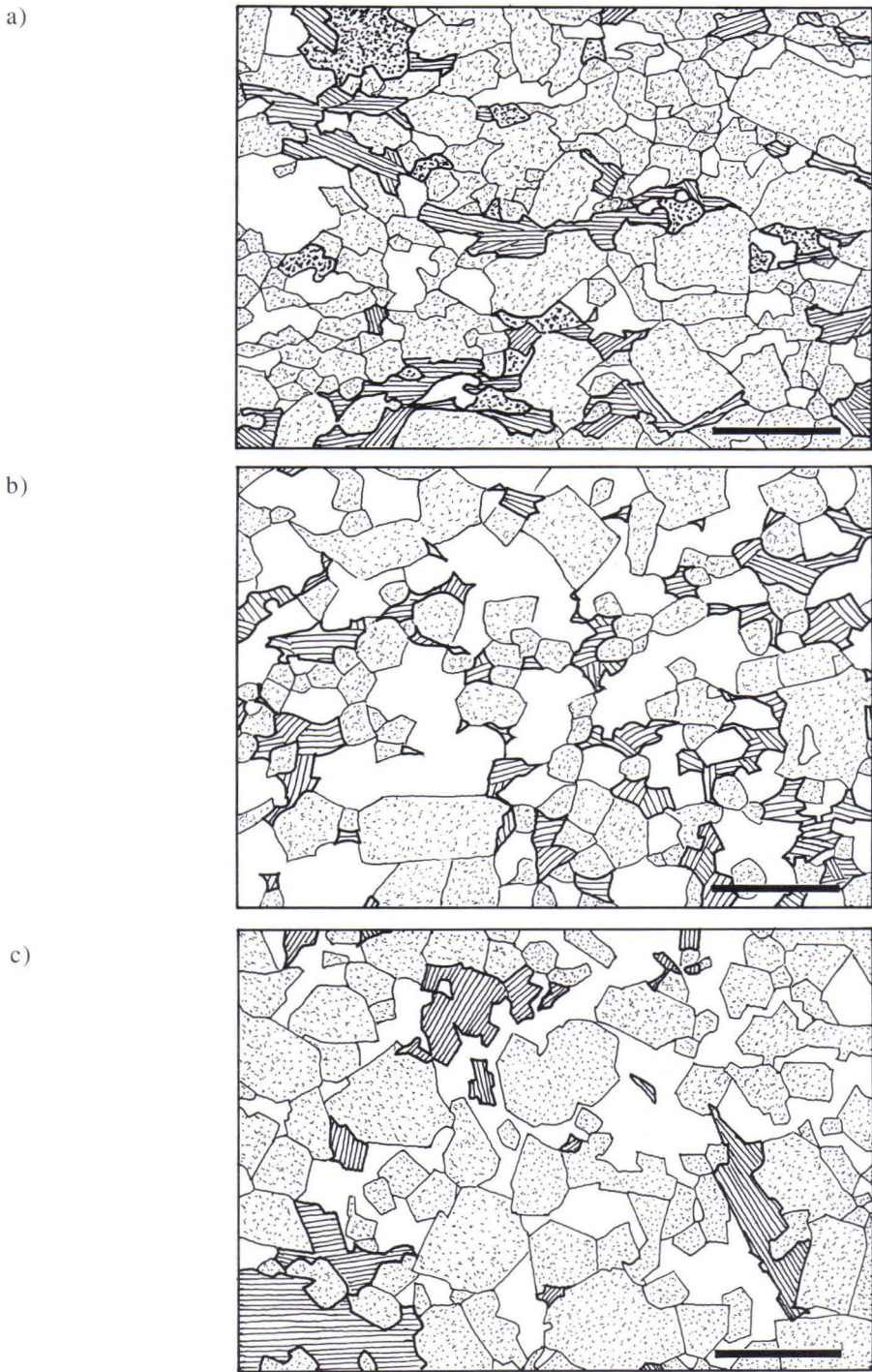
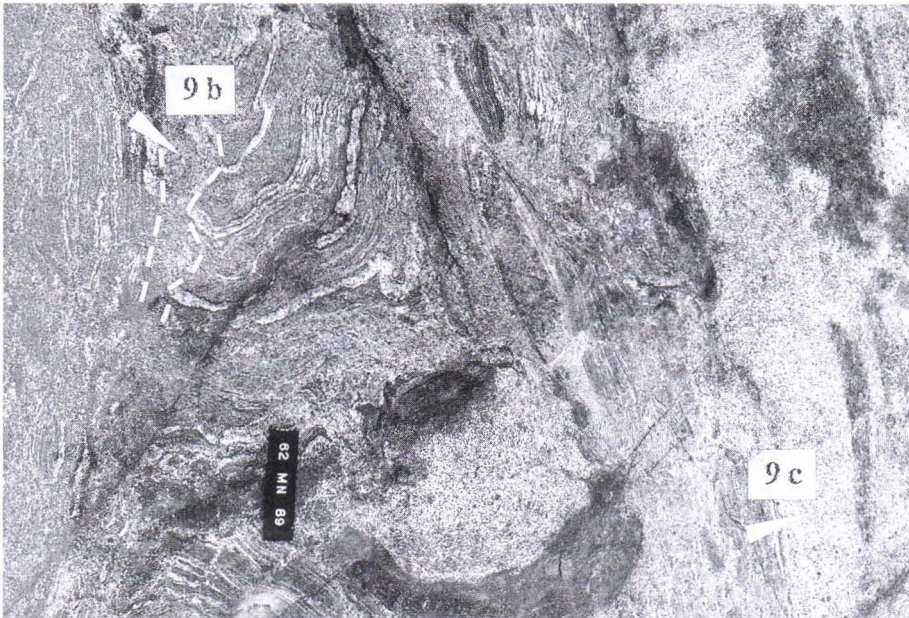


Fig. 9. Microstructures of tonalites and granodiorites in the western domain. a) Distinctly foliated granodiorite. b) Fine-grained, slightly foliated granodiorite. c) Medium-grained unfoliated tonalite. Striped = biotite, heavily stippled = epidote, lightly stippled = feldspar, bright = quartz. Scale bar 2 mm.



a)



b)

Fig. 10. a) A distinctly foliated tonalite/granodiorite containing xenoliths of supracrustal rock. The foliation is overprinted by a shear zone system. $x=6838.11$, $y=3501.90$ b) A fine-grained tonalite/granodiorite (Fig. 9b) and a younger, medium-grained tonalite (Fig. 9c) have intruded a migmatitic and folded mica gneiss. Note intrusion of the older rock subparallel to axial plane. Length of code bar 15 cm. $x=6838.74$, $y=3501.11$.

zation of the gneisses, or during an early stage of the deformation that generated the E-W trending foliation. The fairly homogeneous younger tonalites and granodiorites contain an E-W trending foliation albeit weaker than the one seen in the oldest tonalite. Hence, the younger plutonic rocks intruded the formerly migmatized supracrustal rocks during the deformation which generated the folding. During subsequent intrusion of a felsic, medium-grained tonalite, the gneisses were almost completely assimilated, and only the amphibolitic portions were preserved. The felsic tonalite contains some garnet as a hybrid contamination product or restitic mineral.

The two apophyses of the Puula Granite crosscut the tonalites/granodiorites and the foliations described above. Moreover, a small body of unfoliated, fine-grained granite brecciates the oldest tonalite/granodiorite. These granites represent the last episodes of igneous activity in the western domain.

A NNE-SSW trending foliation, overprinting the E-W trending foliation, is seen in the gneisses and the tonalites/granodiorites. The metatuffites are folded, and biotite has recrystallized along the axial planes. Foliation intensity increases eastwards to the zone of high strain (shown in Fig. 5). The zone is heterogeneously deformed, consisting of zones of mylonites and cataclasites anastomosing between areas of low strain. In less deformed granitoids, partly recrystallized biotite and hornblende/actinolite form thin, anastomosing seams. In the mylonitic granitoids, deformation is seen as reduction of grain size in dynamically recrystallized quartz and mica, and deformation twinning and fracturing of feldspar porphyroclasts with limited recrystallization along microcracks. These features suggest mylonitization near the amphibolite facies - greenschist facies transition (Simpson 1985). In the orthomylonitic igneous rocks, stretching lineations plunge steeply to vertically. In vertical sections S-C fabrics and fractured porphyroclasts with quartz tails in-

dicate west-side-up sense of shear (Fig. 11a). Quartz ribbons occur between K-feldspar and amphibole porphyroclasts, and plagioclase has neocrystallized into fine-grained white mica, quartz and epidote. Biotite grains are kinked and chlorite is a common alteration product of biotite. These features indicate greenschist facies metamorphism.

No signs of penetrative NNE-SSW trending foliation was observed in the Puula Granite, hence there is no direct evidence of the age relationship between this deformation and the emplacement of the granite. However, the emplacement probably predated deformation, because the foliation wraps around the southeastern termination of the granite. Moreover, the foliation is not visible in the tonalites and granodiorites immediately south of the southern contact (Fig. 3); this area probably was a strain shadow during deformation.

Open to tight folding and shearing of the NNE-SSW trending foliation, with roughly E-W striking crenulation, can be seen where the supracrustal rocks occupy large areas. No leucosome formation is associated with this folding. The orientation of the foliation in the gneisses around the eastern Puula Granite injection, which dips moderately towards the granite suggest that the southern part is a bowl-shaped body, in contrast to the general dike-like form. Probably this southern portion was deformed into bowl-shape due to fold interference contemporaneous with D_c doming in the eastern domain. Subhorizontal fold axes and axial traces were observed elsewhere in the western domain, but the difficulty in correlation of structures in strongly migmatitic areas makes it debatable whether these structures are the result of F_b - F_c fold interference or earlier deformation.

D_d cataclastic deformation can be seen in the igneous rocks as fracturing with highly variable orientations (also in the Puula Granite). The fracture surfaces are chloritized and often slickensided. Broader cataclastic zones, extending up to tens of meters and consisting



a)

b)

Fig. 11. a) Mylonitic granodiorite with S-C fabric at the boundary of the western domain. Vertical section (parallel to lineation, perpendicular to foliation), looking north. Sense of shear is west-up. K-feldspar porphyroclasts (with quartz ribbon tails) are bright, amphibole clasts with remnants of clinopyroxene are gray, strongly altered plagioclase and mica are dark. Plane polarized light. Scale bar 5 mm. $x=6838.65$, $y=3502.94$. b) Cataclastic microbreccia, overprinting mylonitic foliation in granodiorite at the boundary of the western domain. Cross-polarized light. Scale bar 2 mm. $x=6838.02$, $y=3503.19$.

of microbreccia, are confined to the D_d shear zone at the boundary of the two domains.

Cataclastic deformation overprints the mylonitic S_b foliation (Fig. 11b).

STRUCTURAL AND METAMORPHIC CORRELATION

When the structures in the metaturbidites and metatuffites (eastern domain) are compared with the structures in the plutonic sequence (western domain), one faces the problem that only the last three tectonothermal events can be correlated unequivocally (Table 1). There is no counterpart in the eastern domain to the migmatitic foliation and asso-

ciated high grade metamorphism in the supracrustal rocks of the western domain. The biotite inclusion trails in K-feldspar porphyroblasts may, however, express an early deformational event synchronous with migmatization in the western domain.

Because the original orientation of S_a in the eastern domain is not known, there is little

Table 1. Structural correlation between the western and eastern domains. Notations in parentheses in the eastern domain refer to the Rantasalmi-Sulkava area (cf. Korsman & Kilpeläinen 1986).

WESTERN DOMAIN		EASTERN DOMAIN	
	Gneissic foliation in metatexites		(Biotite inclusion trails in K-feldspar porphyroblasts)
	Folding in metatexites, E-W axial trace. Intrusion of tonalites/granodiorites	D _a (D ₂)	Penetrative foliation, growth of fibrous sillimanite and K-feldspar. Beginning of anatexis
	Intrusion of Puula granite		
D _b	Folding, NNE-SSW axial trace	D _b (D ₃)	Crenulation, NNE-SSW to NE-SW axial trace. Partial anatexis
D _c	Crenulation, E-W axial trace; dome & basin interference structures	D _c	Crenulation, E-W axial trace; dome & basin interference structures
D _d	Cataclastic zones	D _d	Cataclastic zones

basis for correlation between D_a and the folding with E-W axial trend in the western domain. Moreover, the style of deformation and associated metamorphism also differ, mainly due to lithological differences.

Correlation between S_b and the NNE-SSW trending foliation in the western domain is justified, because 1) the intensity of strain increases towards the center of the study area from both sides, 2) the style of deformation is similar, and 3) mineralogical changes suggest similar metamorphic conditions. Hence, the D_b ductile shear zone in the center of the study area is a boundary between two lithologies that had distinct earlier tectonothermal histories. The igneous rocks in the western domain had been emplaced before the two domains were juxtaposed by predominantly vertical movement (west-side-up) during and after D_b.

The microstructures in Fig. 7 (p. 101) show that the prograde metamorphic reactions in the eastern domain occurred mainly during D_b. The reaction biotite+sillimanite+quartz => cordierite+K-feldspar±garnet indicates increasing temperature.

The garnet in Fig. 7a has decomposed in its rims into cordierite which overgrows D_b biotite and is devoid of sillimanite. The reaction suggests decompression. In places fine-grained Al-silicate (mainly andalusite) and biotite borders the cordierite porphyroblasts (Fig. 12). These mineral assemblages indicate post-D_b retrogressive metamorphism in the garnet-cordierite gneisses. Similarly, sillimanite in the K-feldspar-sillimanite gneisses has commonly decomposed into muscovite.

Korsman et al. (1988) concluded that prograde reactions are characteristic of the Rantasalmi-Sulkava area whereas retrograde reactions are seen in the Kiuruvesi-Haukivesi complex. In the eastern domain, both types of reactions can be seen in the garnet-cordierite gneisses.

In the Rantasalmi-Sulkava area (Fig. 1), Korsman and Kilpeläinen (1986) discerned a penetrative S₂ foliation, overprinting an S₁ fabric that can be distinguished only in the northern part of the area. Growth of sillimanite fibres parallel to S₂ and preservation of early D₂ biotite in K-feldspar porphyroblasts



Fig. 12. Late retrograde andalusite (shown by the arrow) in the rim of cordierite. Scale bar 1 mm. $x=6839.32$, $y=3508.32$ (as in Fig. 7b).

are similar to the features associated with D_1 structures in the eastern domain. Moreover, D_3 deformation caused the block structure in the Rantasalmi-Sulkava area, like D_b deformation in the present study area. The main problem in correlation between these two areas is that the E-W trending metamorphic isograds in the Rantasalmi-Sulkava area, parallel to S_2 (Korsman et al. 1984), shift into NE-SW trending isograds towards the present study area (Korsman et al. 1988). Hence, S_2 appears to grade into S_b and not S_a . If this is true, then the E-W trending foliation in the western domain is older than the E-W trending S_2 foliation north of Sulkava.

Large scale dome-and-basin structures have

been identified in the Savo Schist Belt (Gaál & Rauhamäki 1971, Nironen 1989). In the eastern part of the belt, D_2 deformation produced penetrative S_2 foliation and D_3 faulting (ductile shear zones), and the dome-and-basin structures were the result of F_4 - F_5 fold interference during retrograde metamorphism (Nironen 1989). Correlation of the latter structures with the D_c structures in the study area merely on structural grounds may not be justified. However, the microstructures and mineral assemblages indicate that the metamorphic conditions were similar in these two areas when the dome-and-basin structures were generated.

U-PB ISOTOPIC DATA

U-Pb isotopic analyses were made on zircons from three igneous rock types (Tables 2

and 3). The ages were calculated using the decay constants of Jaffey et al. (1971), and the

Table 2. U-Pb isotopic data from the Otava area.

Sample Fraction ⁽¹⁾ (g/cm ³) / \varnothing = grain size (μ m) abr = grains abraded	Concentration (ppm)		Measured	Lead ratios, ²⁰⁶ Pb= 100		
	²³⁸ U	²⁰⁶ Pb	²⁰⁶ Pb/ ²⁰⁴ Pb	²⁰⁴ Pb	²⁰⁷ Pb	²⁰⁸ Pb
A16 - Uusi-Kolo, Puula Granite						
A >4.2/ \varnothing > 130	341.2	84.24	1397	.06856	12.421	13.237
B >4.2	372.6	88.38	1187	.08004	12.558	14.164
C 4.0-4.2	1111	197.37	619	.15903	13.306	16.031
D >4.6/ \varnothing >160	300.6	75.28	579.4	.17152	13.824	16.725
E >4.6/70< \varnothing < 160/abr 5 h (\varnothing >70 after abr)	280.7	77.27	1991	.04826	12.180	12.818
F >4.6/70< \varnothing < 160/abr 5 h (\varnothing <70 after abr)	250.0	70.41	3810	.02432	11.832	12.710
G titanite/3.5-3.6/ \varnothing > 160/abr	59.1	15.96	278.5	.3550	15.726	56.166
H >4.6/dark, short/abr 3 h	402.1	106.26	1933	.04960	12.281	11.674
I >4.6/dark, long/abr 90 min	314.9	87.05	2536	.03617	11.957	12.902
J >4.6/clear, long/abr	179.6	50.94	2046	.04241	12.026	15.315
K >4.6/clear, short/abr 3 h	169.6	47.54	1220	.07990	12.581	15.166
A922 - Hokka, Puula Granite						
A >4.6/ \varnothing >70/abr 3 h	162.8	47.09	6696	.01129	11.700	12.151
B monazite	717.1	205.32	3825	.009461	11.602	2146
A923 - Kärjäniemi, Puula Granite						
A >4.6/ \varnothing >70/abr 3 h	191.2	55.24	20706	.002853	11.613	11.752
B monazite	482.3	142.58	10469	.000773	11.474	2140
A924 - Tähtiniemi, Puula Granite						
A >4.6/ \varnothing >70/abr 3 h	231.1	66.84	21228	.003004	11.622	11.181
B >4.6/clear, long/abr 2 h	250.4	72.03	2640	.02541	11.879	13.922
C monazite	439.7	127.22	3277	.01648	11.689	2487
D 4.2-4.6/long/ \varnothing >70/abr 3 h	422.1	116.24	7418	.01193	11.644	12.285
E 4.2-4.6/clear, short/ \varnothing >70/abr	413.0	113.30	5064	.01693	11.733	11.059
F 4.2-4.6/dark/ \varnothing >70/abr 2 h	615.4	164.38	3866	.02219	11.973	11.068
G 4.0-4.2/dark/ \varnothing > 110/abr 2 h	1236	315.52	5144	.01615	11.743	9.662
A695 - Syväsmäki, granodiorite						
A >4.6	605.5	158.69	1876	.05286	12.258	6.880
B 4.2-4.6	405.4	107.37	2015	.04905	12.199	7.761
C 4.0-4.2	870.5	214.55	2536	.03908	12.086	6.148
D titanite	128.0	35.33	1311	.07505	12.480	6.767
E >4.6/ \varnothing >70/abr 5 h	554.0	161.82	18567	.004403	11.713	5.225
F 4.0-4.2/ \varnothing >70/abr 3 h	835.5	227.52	6267	.01485	11.848	5.028
All95 - Otava, granodiorite						
A 4.3-4.5/ \varnothing >70	506	147.8	10806	.00831	11.963	6.628
B 4.2-4.3/ \varnothing <70/abr 3 h	707	202.7	11112	.00811	11.728	5.915
C 4.2-4.3/ \varnothing >70	758	215.6	5782	.01635	12.056	6.435
D 4.3-4.5/ \varnothing <70	502	145.6	8355	.01112	11.876	6.989
E 4.2-4.3/ \varnothing <70	707	200.5	5564	.01738	11.876	6.510

⁽¹⁾ All fractions are zircon unless otherwise indicated. All data corrected for blank (0.88 ng Pb, 0.37 ng U).

Table 3. U/Pb ratios and apparent radiometric ages for zircons, monazites, and titanite from the Otava area.

Sample Fraction	Atomic ratios			Apparent ages (Ma)		
	$^{206}\text{Pb}/^{238}\text{U}$	$^{207}\text{Pb}/^{235}\text{U}$	$^{207}\text{Pb}/^{206}\text{Pb}$	$T(^{206}/^{238})$	$T(^{207}/^{235})$	$T(^{207}/^{206})$
A16 - Uusi-Kolo, Puula Granite						
A	.2854	4.522	.1149	1618	1735	1879
B	.2742	4.338	.1148	1562	1700	1876
C	.2054	3.157	.1115	1204	1446	1823
D	.2894	4.591	.1151	1638	1747	1880
E	.3181	5.056	.1153	1780	1828	1884
F	.3255	5.162	.1150	1816	1846	1880
G	.3118	4.681	.1089	1749	1763	1780
H	.3054	4.890	.1161	1718	1800	1897
I	.3195	5.052	.1147	1787	1828	1875
J	.3279	5.177	.1145	1827	1848	1872
K	.3239	5.136	.1150	1808	1841	1880
A922 - Hokka, Puula Granite						
A	.3343	5.323	.1155	1859	1872	1887
B	.3309	5.235	.1147	1842	1858	1875
A923 - Käräjaniemi, Puula Granite						
A	.3339	5.328	.1157	1857	1873	1891
B	.3417	5.401	.1146	1894	1884	1874
A924 - Tähtiniemi, Puula Granite						
A	.3343	5.338	.1158	1859	1875	1892
B	.3325	5.288	.1154	1850	1866	1885
C	.3344	5.287	.1147	1859	1866	1874
D	.3183	5.039	.1148	1781	1825	1877
E	.3171	5.029	.1150	1775	1824	1880
F	.3087	4.969	.1167	1734	1813	1907
G	.2950	4.687	.1153	1666	1764	1883
A695 - Syväsmäki, granodiorite						
A	.3029	4.821	.1154	1705	1788	1886
B	.3061	4.868	.1154	1721	1796	1885
C	.2849	4.539	.1156	1615	1738	1889
D	.3376	5.424	.1165	1875	1888	1903
E	.3148	5.055	.1165	1764	1828	1903
F	.3191	5.045	.1147	1785	1826	1874
All95 - Otava, granodiorite						
A	.3374	5.513	.1196			1934
B	.3311	5.303	.1173			1898
C	.3288	5.365	.1206			1931
D	.3352	5.420	.1188			1915
E	.3279	5.263	.1186			1902

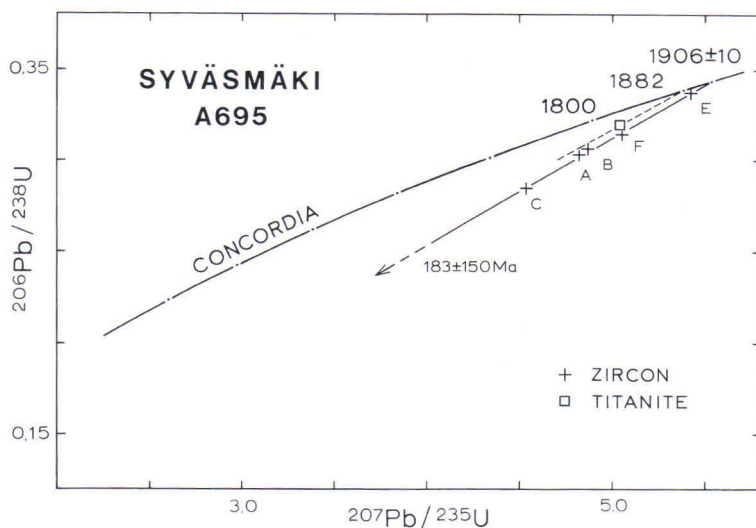
Atomic ratios corrected for common lead (see Doe & Stacey 1974)

method of York (1969) was used to fit the regression line. The age uncertainties of the concordia intersections are given at the 2-sigma level.

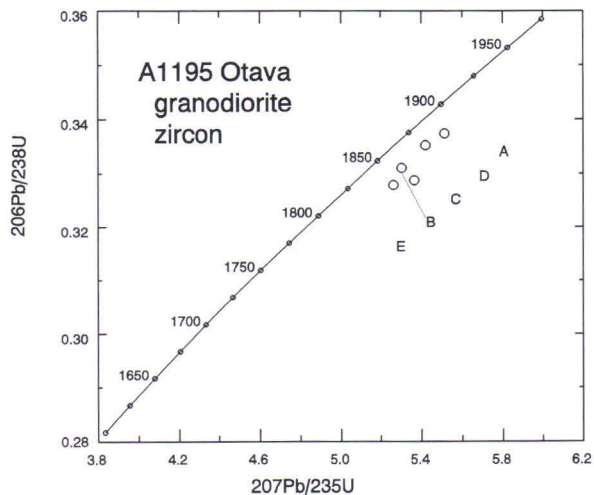
An age of 1906 ± 10 Ma (Fig. 13a) was obtained from a medium-grained granodiorite in

the western part of the study area. The granodiorite belongs to the youngest tonalitic/granodioritic phase (see p. 102). Titanite from the same sample yielded an age of 1882 Ma.

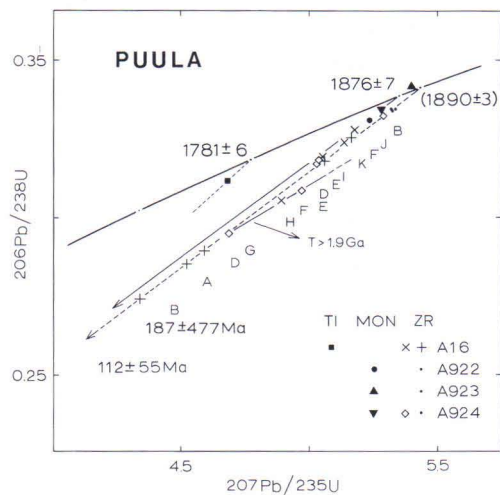
The distinctly foliated granitoid in the western domain gave an equivocal result (Fig.



a)



b)



c)

Fig. 13. Concordia diagrams of U-Pb isotopic data from igneous rocks in the Otava area. a) Unfoliated granodiorite. $x=6836.97$, $y=3497.23$. b) Distinctly foliated granodiorite. $x=6838.11$, $y=3501.90$. c) Puula Granite.

13b). The dispersion of the various fractions on the concordia plot suggests that the fractions consist of two zircon populations, one of about 1900 Ma and the other of at least 1930 Ma. The older zircons may be inherited from the source area; the younger ones would give the age of emplacement. However, it is uncertain whether zircons could persist in the rather high temperatures of granodioritic-tonalitic magma. Alternatively, the granitoid was emplaced about 1930 Ma ago, and the zircons were affected by an early metamorphism or the subsequent intrusion of the 1906 Ma old granitoids.

When the heavy mineral fractions of the four samples from different parts of the Puula Granite were analysed, it turned out that one sample (A16) contained abundant titanite but no monazite, whereas the other three samples contained monazite but titanite was rare or lacking. A total of 18 zircon fractions from the four samples show that also the Puula Granite contains more than one zircon population (Fig. 13c). When the most discordant fraction C (Table 3) is excluded, the density fractions yield a geologically dubious age of 1890 ± 3 Ma. The ratio points of long zircon crystals as well as the three monazites plot over the broken line defined by the density fractions. The monazite analyses give a very coherent age of 1874 Ma (the position of sample A923 above the concordia curve is probably due to analytical error). The addition of ratio points of (long) zircons to the monazite data is hazardous: an addition of a slightly

older zircon population may give an erroneous chord with only a slight change in the upper concordia intercept but a marked shift of the lower intercept towards the origin. Therefore, only two monazites (A922B and A924C) and one zircon fraction (A16J, long bright crystals) were used to define the younger population (1876 ± 7 Ma). If a chord is drawn through ratio points A16H, A924F and A924G, situated below the line of the density fractions, the upper intercept of concordia will give an age of 1968 ± 18 Ma. However, since the three ratio points form a relatively tight group and represent two samples, one should be cautious about the geological meaning of this age.

In a review of monazite U-Pb geochronology (Parrish 1990), the advantage of monazite dating was pointed out in determining the crystallization age of granitoids with inherited zircon. Inheritance in monazite U-Pb systematics is rare, but possible retrograde metamorphic growth of monazite in granitic rocks has to be taken in account. The coexistence of monazite and the coeval long, bright zircon crystals provide a strong evidence for crystallization of both minerals from a melt. Hence, these crystals date the crystallization of the Puula Granite about 1875 Ma ago.

The two titanite ages, 1882 Ma for the granodiorite and 1781 Ma for the Puula Granite, reflect cooling of the two granitoids. Thus the granodiorite had cooled below the closure temperature of titanite before the emplacement of the Puula Granite.

DISCUSSION

The age data indicate that the supracrustal rocks in the western domain are older than 1906 Ma, because they were folded and metamorphosed before the intrusion of the medium-grained tonalite/granodiorite. Ages around 1905 Ma have been obtained from magmatic rocks elsewhere in the Kiuruvesi-Haukivesi

complex (Huhma 1986, Vaasjoki & Sakko 1988). The distinctly foliated granitoid may be a counterpart of the 1.93-1.92 Ga orthogneisses, located further north in the Savo Schist Belt (see Lahtinen 1994). The equivocal U-Pb zircon data of the distinctly foliated granitoid shows the problems in interpreting

granitoids with discordant zircons. In this case the single zircon analysis method may provide a deeper insight into the history of the granitoid.

The age of the high grade metamorphism in the western domain is also ambiguous. Is the metamorphic episode only a few Ma older than the emplacement of the tonalites/granodiorites or considerably older, e.g. 1.92 Ga in age?

The metavolcanic rocks of the western domain are older than the metavolcanic rocks of the Tampere Schist Belt, dated between 1904 Ma and 1889 Ma (Kähkönen et al. 1989). If the E-W trending (fold axial planar) foliation in the western domain is considered part of the E-W structural trend of southern Finland, then this structure is certainly older than F_1 folding in the Tampere Schist Belt, dated around 1.88 Ga (Nironen 1989). The block boundary and other D_b structures in the eastern domain clearly overprint this structural trend.

The Puula Granite, the last magmatic pulse in the western domain, is undeformed except for the shear zone. A similarly coarse-porphyratic, apparently undeformed granite at the southern margin of the CFGC yielded an age of 1880 ± 16 Ma (Sjöblom 1990). Hence, a group of porphyritic granites, slightly younger than the typical synkinematic plutonic rocks, seem to exist at the southern margin of the CFGC.

Extensive retrogression is generally restricted to zones of deformation and/or hydrothermal activity (e.g. Etheridge et al. 1983). The mineral assemblages in the less deformed granitoids studied here suggest amphibolite facies conditions. The assemblages in the mylonitic rocks are apparently unstable, with both lower amphibolite facies and greenschist facies characteristics. The variety of mineral assemblages

as well as the shift from a regime of crystal-plastic deformation (mylonites) to cataclastic deformation suggests prolonged (continuous or repeated) deformation, facilitated by hydrothermal activity. Little can be said about the amount of uplift of the western block relative to the eastern one by the present retrograde mineral assemblages; the relative movement and the contemporaneous isostatic uplift of both blocks in the crust have contributed to the assemblages. Another problem is whether the supracrustal rocks of the eastern domain overlaid the high grade rocks of the western domain before erosion or whether the two areas were distinct until the juxtaposition.

The 1.88 Ga and 1.78 Ga ages of titanite in the granodiorite and the Puula Granite, respectively, imply that the western domain cooled relatively soon after magmatic activity. The age relationship between block movement and progressive metamorphism in the eastern domain is equivocal, because both occurred during a prolonged period. Apparently movement along the block boundary initiated during D_b deformation, and culmination of metamorphism in the eastern domain was roughly contemporaneous with D_b . Since the Puula Granite probably intruded before the initiation of D_b , the maximum age of D_b deformation is 1875 Ma.

The late folding, responsible for the dome-and-basin interference structures, occurred about 1.80 Ga ago in the Savonlinna area (Nironen 1989). The crust of the southeastern Savo Schist Belt was hot enough to deform in a ductile manner during D_c because of the late culmination of metamorphism and associated extensive granitic plutonism. The block boundary may have been active during this deformation, and it certainly was active afterwards, during cataclastic D_d deformation.

ACKNOWLEDGEMENTS

Kalevi Korsman introduced me into the problems of the area. Olavi Kouvo, Hannu Huhma and the staff of the Unit for Isotope Geology provided the age data. Pentti Hölttä helped in

understanding the metamorphic reactions. Leo Kriegsmann critically read the manuscript. Peter Sorjonen-Ward corrected the English. I appreciate the contribution of all these people.

REFERENCES


- Aho, L. 1979.** Petrological and geochemical studies of metavolcanics and associated granitoids in the Pihtipudas area, Central Finland. Geological Survey of Finland, Bulletin 300, 22 p.
- Barker, A. J. 1994.** Interpretation of porphyroblast inclusion trails: limitations imposed by growth kinetics and strain rates. *Journal of Metamorphic Geology* 12, 681–694.
- Bell, T.H. 1981.** Foliation development - the contribution, geometry and significance of progressive, bulk, inhomogeneous shortening. *Tectonophysics* 75, 273–296.
- Bell, T.H. 1986.** Foliation development and refraction in metamorphic rocks: reactivation of earlier foliations and decrenulation due to shifting patterns of deformation partitioning. *Journal of Metamorphic Geology* 4, 421–444.
- Doe, B.R. & Stacey, J.S. 1974.** The application of lead isotopes to the problems of ore genesis and ore prospect evaluation: A review. *Economic Geology* 69, 757–776.
- Etheridge, M.A., Wall, V.J. & Vernon, R.H. 1983.** The role of the fluid phase during regional metamorphism and deformation. *Journal of Metamorphic Geology* 1, 205–226.
- Gaál, G. & Rauhamäki, E. 1971.** Petrological and structural analysis in the Haukivesi area between Varkaus and Savonlinna, Finland. *Bulletin of the Geological Society of Finland* 43, 265–337.
- Huhma, H. 1986.** Sm-Nd, U-Pb and Pb-Pb isotopic evidence for the origin of the early Proterozoic Svecokarelian crust in Finland. Geological Survey of Finland, Bulletin 337, 48 p.
- Hutton, D.W. 1988.** Granite emplacement mechanisms and tectonic controls: inferences from deformation studies. *Transactions of the Royal Society of Edinburgh: Earth Sciences* 79, 245–255.
- Jaffey, A.H., Flynn, K.F., Glendenin, L.E., Bentley, W.C. & Essling, A.M. 1971.** Precision measurement of half-lives and specific activities of ^{235}U and ^{238}U . *Physical Reviews C* 4, 1889–1906.
- Kähkönen, Y., Huhma, H. & Aro, K. 1989.** U-Pb zircon ages and Rb-Sr whole-rock isotope studies of early Proterozoic volcanic and plutonic rocks near Tampere, southern Finland. *Precambrian Research* 45, 27–43.
- Kallio, J. 1988.** Hirvensalmi. Geological Map of Finland 1 : 100 000, Pre-Quaternary Rocks, Sheet 3124. Espoo: Geological Survey of Finland.
- Korsman, K. & Kilpeläinen, T. 1986.** Relationship between zonal metamorphism and deformation in the Rantasalmi-Sulkava area, southeastern Finland. In: Korsman, K. (ed.) *Development of deformation, metamorphism and metamorphic blocks in eastern and southern Finland*. Geological Survey of Finland, Bulletin 339, 33–42.
- Korsman, K., Niemelä, R. & Wasenius, P. 1988.** Multistage evolution of the Proterozoic crust in the Savo schist belt, eastern Finland. In: Korsman, K. (ed.) *Tectono-metamorphic evolution of the Raahe-Ladoga zone*. Geological Survey of Finland, Bulletin 343, 89–96.
- Korsman, K., Hölttä, P., Hautala, T. & Wasenius, P. 1984.** Metamorphism as an indicator of evolution and structure of the crust in Eastern Finland. Geological Survey of Finland, Bulletin 328, 40 p.
- Kousa, J. 1985.** Rantasalmen tholeiiteista ja komatiititista vulkaniiteista. Summary: The tholeiitic and komatiitic metavolcanics in Rantasalmi, Southeastern Finland. *Geologi* 37, 17–22.
- Lahtinen, R. 1994.** Crustal evolution of the Svecofennian and Karelian domains during 2.1–1.79 Ga, with special emphasis on the geochemistry and origin of 1.93–1.91 Ga gneissic tonalites and associated supracrustal rocks in the Rautalampi area, central Finland. Geological Survey of Finland, Bulletin 378, 128 p.
- Nironen, M. 1989.** Emplacement and structural setting of granitoids in the early Proterozoic Tampere and Savo Schist Belts, Finland - implications for contrasting crustal evolution. Geological Survey of Finland, Bulletin 346, 83 p.
- Nironen, M. & Front, K. 1992.** The 1.88 Ga old Mäntylä complex, central Finland: emplacement and deformation of mafic to felsic plutonic rocks and associated Mo mineralization. *Bulletin of the*

- Geological Society of Finland 64, 75–90.
- Parrish, R.R. 1990.** U-Pb dating of monazite and its application to geological problems. *Canadian Journal of Earth Sciences* 27, 1431–1450.
- Paterson, S.R., Vernon, R.H. & Tobisch, O. T. 1989.** A review of criteria for the identification of magmatic and tectonic foliations in granitoids. *Journal of Structural Geology* 11, 349–363.
- Sawyer, E.W. & Robin, P.-Y. F. 1986.** The sub-solidus segregation of layer-parallel quartz-feldspar veins in greenschist to upper amphibolite facies metasediments. *Journal of Metamorphic Geology* 4, 237–260.
- Shelley, D. 1993.** *Igneous and Metamorphic Rocks under the Microscope*. London: Chapman & Hall. 445 p.
- Simonen, A. & Niemelä, R. 1980.** Mikkeli. Geological Map of Finland 1 : 100 000, Pre-Quaternary Rocks, Sheet 3142. Espoo: Geological Survey of Finland.
- Simpson, C. 1985.** Deformation of granitic rocks across the brittle-ductile transition. *Journal of Structural Geology* 7, 503–511.
- Sjöblom, B. 1990.** Mäntän kartta-alueen kallioperä. Summary: Pre-Quaternary rocks of the Mänttä map-sheet area. Geological Map of Finland 1 : 100 000, Explanation to the Maps of Pre-Quaternary Rocks, Sheet 2231. Espoo: Geological Survey of Finland. 64 p.
- Vaasjoki, M. & Sakko, M. 1988.** The evolution of the Raahe-Ladoga zone in Finland: isotopic constraints. In: Korsman, K. (ed.) *Tectonometamorphic evolution of the Raahe-Ladoga zone*. Geological Survey of Finland, Bulletin 343, 7–32.
- York, D. 1969.** Least squares fitting of a straight line with correlated errors. *Earth and Planetary Science Letters* 5, 320–324.




Tätä julkaisua myy

**GEOLOGIAN
TUTKIMUSKESKUS (GTK)**
Julkaisumyynti
02150 Espoo

 (90) 46 931


Teleksi: 123185 geolo fi
Telekopio: (90) 462 205

**GTK, Väli-Suomen
aluetoimisto**
Kirjasto
PL 1237
70211 Kuopio

 (971) 205 111

Telekopio: (971) 205 215


**GTK, Pohjois-Suomen
aluetoimisto**
Kirjasto
PL 77
96101 Rovaniemi

 (960) 3297 111

Teleksi: 37295 geolo fi
Telekopio: (960) 3297 289


Denna publikation säljes av

**GEOLOGISKA
FORSKNINGSCENTRALEN (GFC)**
Publikationsförsäljning
02150 Esbo

 (90) 46 931


Telex: 123185 geolo fi
Telefax: (90) 462 205

**GFC, Distriktsbyrån för
Mellersta Finland**
Biblioteket
PB 1237
70211 Kuopio

 (971) 205 111


Telefax: (971) 205 215

**GFC, Distriktsbyrån för
Norra Finland**
Biblioteket
PB 77
96101 Rovaniemi

 (960) 3297 111


Telex: 37295 geolo fi
Telefax: (960) 3297 289

This publication can be
obtained from
**GEOLOGICAL SURVEY
OF FINLAND (GSF)**
Publication sales
FIN-02150 Espoo, Finland

 +358 0 46 931


Telex: 123185 geolo fi
Telefax: +358 0 462 205

**GSF, Regional office for
Mid-Finland**
Library
P.O. Box 1237
FIN-70211 Kuopio, Finland

 +358 71 205 111

Telefax: +358 71 205 215

**GSF, Regional office for
Northern Finland**
Library
P.O. Box 77
FIN-96101 Rovaniemi, Finland

 +358 60 3297 111

Telex: 37295 geolo fi
Telefax: +358 60 3297 289